AD-A153 583 FURTHER STUDIES OF THE NRL COLLECTIVE PARTICLE ACCELERATOR VIA NUMERICAL.. (U) MISSION RESEARCH CORP ALEXANDRIA VA R J BARKER AUG 84 MRC/WDC-R-086 1/2

UNCLASSIFIED N00014-84-C-2136 F/G 9/2 NL

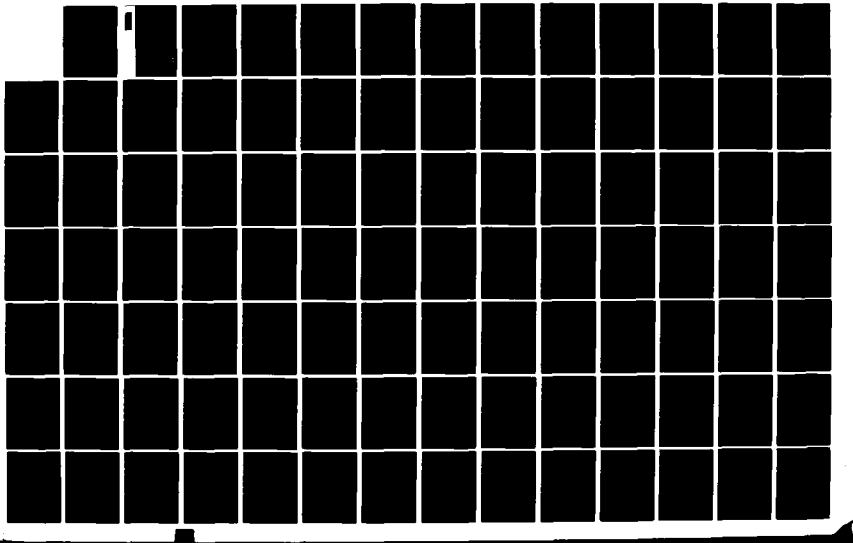

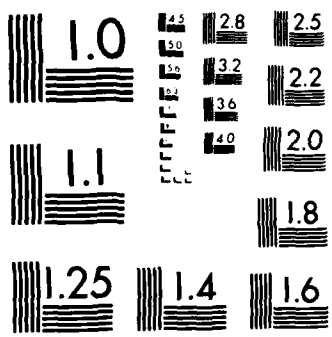

(12)

FURTHER STUDIES OF THE NRL COLLECTIVE PARTICLE ACCELERATOR VIA NUMERICAL MODELING WITH THE MAGIC CODE

Robert J. Barker

August 1984

Final Report for Period 1 April 1984 - 30 September 1984

Prepared for: Scientific Officer
Geophysical and Plasma Dynamics Branch
Plasma Physics Division
Naval Research Laboratory
4555 Overlook Avenue, S.W.
Washington, DC 20375

Attention: Dr. Peter J. Palmadesso

Contract No. N00014-84-C-2136

MISSION RESEARCH CORPORATION
5503 Cherokee Avenue, Suite 201
Alexandria, Virginia 22312
(703) 750-3556

COPY 4

FURTHER STUDIES OF THE NRL COLLECTIVE PARTICLE ACCELERATOR VIA NUMERICAL MODELING WITH THE MAGIC CODE

Robert J. Barker

August 1984

Final Report for Period 1 April 1984 - 30 September 1984

Prepared for: Scientific Officer
Geophysical and Plasma Dynamics Branch
Plasma Physics Division
Naval Research Laboratory
4555 Overlook Avenue, S.W.
Washington, DC 20375

Attention: Dr. Peter J. Palmadesso

Contract No. N00014-84-C-2136

MISSION RESEARCH CORPORATION
5503 Cherokee Avenue, Suite 201
Alexandria, Virginia 22312
(703) 750-3556

Unclassified

SECURITY CLASSIFICATION OF THIS PAGE (When Data Entered)

REPORT DOCUMENTATION PAGE	READ INSTRUCTIONS BEFORE COMPLETING FORM
1. REPORT NUMBER	2. GOVT ACCESSION NO. AD-A153583 3. RECIPIENT'S CATALOG NUMBER
4. TITLE (and Subtitle) Further Studies of the NRL Collective Particle Accelerator VIA Numerical Modeling with MAGIC Code.	5. TYPE OF REPORT & PERIOD COVERED Final Report April 1 - September 30, 1984
	6. PERFORMING ORG. REPORT NUMBER MRC/WDC-R-086
7. AUTHOR(s) Robert J. Barker	8. CONTRACT OR GRANT NUMBER(s) N00014-84-C-2136
9. PERFORMING ORGANIZATION NAME AND ADDRESS Mission Research Corporation 5503 Cherokee Avenue Alexandria, VA 22312	10. PROGRAM ELEMENT, PROJECT, TASK AREA & WORK UNIT NUMBERS
11. CONTROLLING OFFICE NAME AND ADDRESS Naval Reasearch Laboratory 4555 Overlook Avenue, S. W. Washington, D. C. 20375	12. REPORT DATE August 1984
	13. NUMBER OF PAGES 90
14. MONITORING AGENCY NAME & ADDRESS(if different from Controlling Office)	15. SECURITY CLASS (of this report) Unclassified
	15a. DECLASSIFICATION DOWNGRADING SCHEDULE
16. DISTRIBUTION STATEMENT (of this Report) DISTRIBUTION STATEMENT A Approved for public release; Distribution Unlimited	
17. DISTRIBUTION STATEMENT (of the abstract entered in Block 20, if different from Report)	
18. SUPPLEMENTARY NOTES	
19. KEY WORDS (Continue on reverse side if necessary and identify by block number) Collective Acceleration Numerical Simulation Foilless Diode Relativistic Electron Beams	

20. ABSTRACT (Continue on reverse side if necessary and identify by block number)

The 2-D, electromagnetic, relativistic simulation code, MAGIC, was used to investigate the detailed physics associated with the operation of the NRL CPA testbed experiment. Code results contradicted the original conclusions drawn from the experimental diagnostics in that the central beam always propagated with a current of 1-2kA in the simulations while the experimental probes failed to detect that beam's presence in dual-beam mode of operation. Since 1-2kA was on the sensitivity threshold of the instruments used in the experi-

DD FORM 1 JAN 73 1473 EDITION OF 1 NOV 65 IS OBSOLETE

Unclassified

SECURITY CLASSIFICATION OF THIS PAGE (When Data Entered)

20. ABSTRACT

ment, there is no reason to disbelieve the MAGIC results. This work argues in favor of a renewed CPA effect with improved diagnostics.

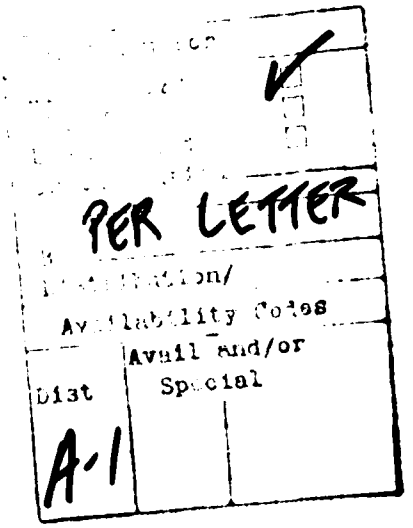

TABLE OF CONTENTS

LIST OF FIGURES

LIST OF FIGURES (Cont'd)

LIST OF FIGURES (Cont'd)

LIST OF FIGURES (Concluded)

LIST OF TABLES

SECTION 1

INTRODUCTION

The Plasma Physics Division of the Naval Research Laboratory has long played a leading role in advancing the physical understanding of intense charged particle beam generation and acceleration. A particularly noteworthy example of NRL's contribution to the field is presented by the series of innovative techniques proposed by the Lab to accomplish the acceleration of multi-kiloamp electron beams to energies well above 100 MeV. Among these suggested schemes is the Collective Particle Accelerator (CPA) concept introduced by Dr. Moshe Friedman (References 1 and 2) in 1977 and experimentally investigated by him for about 3 years thereafter. Although initial results were negative, they were not conclusive. Given the potential significance of such an accelerator to various programs underway in the Navy, it is highly desirable to resolve the question of the CPA's feasibility. Reconstructing the now dismantled experiment is still an option only if the previous negative results can be explained and a plausable method of correcting the results can be offered. For this purpose, Mission Research Corporation (MRC) has been conducting two-dimensional, relativistic, electromagnetic, particle-in-cell simulations using a model of the CPA with realistic operating parameters.

The first phase of this research was concluded late last year. The major findings of that work were summarized in the Mission Research Corporation Report, MRC/WDC-R-073, entitled "Numerical Simulations of the NRL Collective Particle Accelerator" (Reference 3). Those results confirmed the experimental observations that both the hollow electron beam as well as the central, pencil, electron beam were able to propagate freely down the full length of the drift tube when the device was in a single-beam mode of operation. The numerical findings also confirmed the empirical evidence that the hollow beam propagates undisturbed even when the device is in dual-beam operation (i.e., even when the central beam is present). Disagreement arose, however, between the numerical and

experimental conclusions regarding the behavior of the central beam in the dual-beam mode of operation. The experiment was unable to detect any propagation of the central beam, even over short distances in the presence of the outer, hollow beam. The previous simulations, on the other hand, found a central beam propagating down the length of the drift tube even in dual-beam operation. The current carried by that central beam, however, was found to be approximately one-third of the value observed for that beam in the absence of the outer hollow beam.

This apparent disagreement between simulation and experiment is crucially significant. If the simulation is correct, the experiment could still have been conducted on the existing CPA device because the central beam electron current was still appreciable. As it turns out, there is a possibility that the simulation does not disagree with the experiment, but rather disagrees only with the interpretation of the experimental diagnostics. It has been conceded that the B-detectors used in the experiment were probably not sensitive enough to pick up a central beam current of under a kiloamp in the presence of the outer 20-25 kA hollow beam (Reference 4). If the simulation results stand, they argue in favor of a renewed electron beam CPA experimental effort.

It was the objective of this second and final phase of the MRC/CPA simulation effort to modify the previously used simulation model in a number of important ways in order to either confirm or to contradict the previous results in a more conclusive fashion. To accomplish this, several reasonable criticisms of the previous model were addressed head-on. The main points to be satisfied were as follows:

1) The hollow electron beam used in the experiments had a peak current of 20-25 kA. The previous simulation used a hollow beam of almost 50 kA.

2) The voltage pulse for the rod cathode had a rise time of 5-10 nsec in the experiments but only 0.1 nsec in the

simulation. Perhaps a longer rise time dumps additional electrons from its low-energy leading edge into the virtual cathode, thus further inhibiting emission.

3) In the actual experiments, the applied axial magnetic field strength was maintained at a uniform 10-20 kG. The previous simulations used a 25 kG field. Perhaps that added a critical increment of extra stability to the central beam.

In the technical discussion that follows, the general research topic is described and the specific objective of this work is delineated. The discussion begins with a brief review of the experimental CPA device in question. The underlying, general theory is spelled out and the fundamental operative equations are listed. Thereafter follows a detailed picture of the actual experimental apparatus constructed at NRL to test the feasibility of the concept. The observed negative results are then described. At that point, the specifics of this effort are initiated with a reduction of the actual physical device to a numerical model which is both physically valid and computationally tractable. Particular attention is paid to the assumptions which are made to arrive at the model. These assumptions determine which phenomena can or cannot manifest themselves in the simulations. For this work MRC used its 2-1/2-D, electromagnetic, relativistic MAGIC code. A complete description of the code's capabilities and limitations is given in the Appendix. Then, Section 4 presents the detailed results of the major simulation runs conducted with MAGIC to diagnose the CPA device. Numerous figures are included to provide as complete as possible a picture of the various physical phenomena at work. Clear conclusions are drawn in Section 5.

SECTION 2

THE EXPERIMENTAL DEVICE

Mission Research Corporation has applied its MAGIC simulation code to examine specific, critical physics questions involving the technical feasibility of NRL's Collective Particle Accelerator (CPA). These simulations now provide critical additional information to the parties concerned at NRL to determine the possible future of a revived CPA experimental effort. If the CPA is again brought to life, MRC proposes to continue its computational support of that program to optimize its performance. This section of the report reviews the NRL-CPA experiment and its chief results.

An approximate drawing of the CPA device experimentally tested at NRL by Dr. Moshe Friedman appears in Figure 1. The essential elements consisted of two opposing e-beam, foilless diodes installed at opposite ends of a 5-meter-long, 4.76 cm diameter metal drift tube. Both diodes were fed from the same 1.0 MV, 100 nsec pulsed power generator. However, a transformer installed in the feed-line branch leading to the hollow cathode diode boosted the effective diode voltage at that end to 1.5 MV compared with the 1.0 MV of the opposing rod diode. The hollow-beam diode consisted of a 4.0 cm diameter tapered graphite cathode inserted into the flared anode structure at one end of the drift tube. The anode diameter increased from 4.76 to 15.24 cm over an axial distance of 12.7 cm. This flaring was accomplished in two parts: first, a diameter increase from 4.76 to 7.0 cm over a 5.1 cm axial distance, and then, an increase from 7.0 to 15.24 cm over the remaining 7.6 cm. This two-staged anode flaring was exactly repeated on the opposite end of the drift tube where the rod diode was placed. The axial positioning of the cathodes was not a fixed parameter in the experiments. The electron beam produced by the hollow cathode had an outside diameter of about 4.0 cm and a radial beam thickness of about 0.2 cm. It carried a peak average current of about 20-25 kA. The tip of the rod cathode typically projected 1 or 2 cm into the drift tube. A graphite ring about 1.0 cm in cross-section hugged the

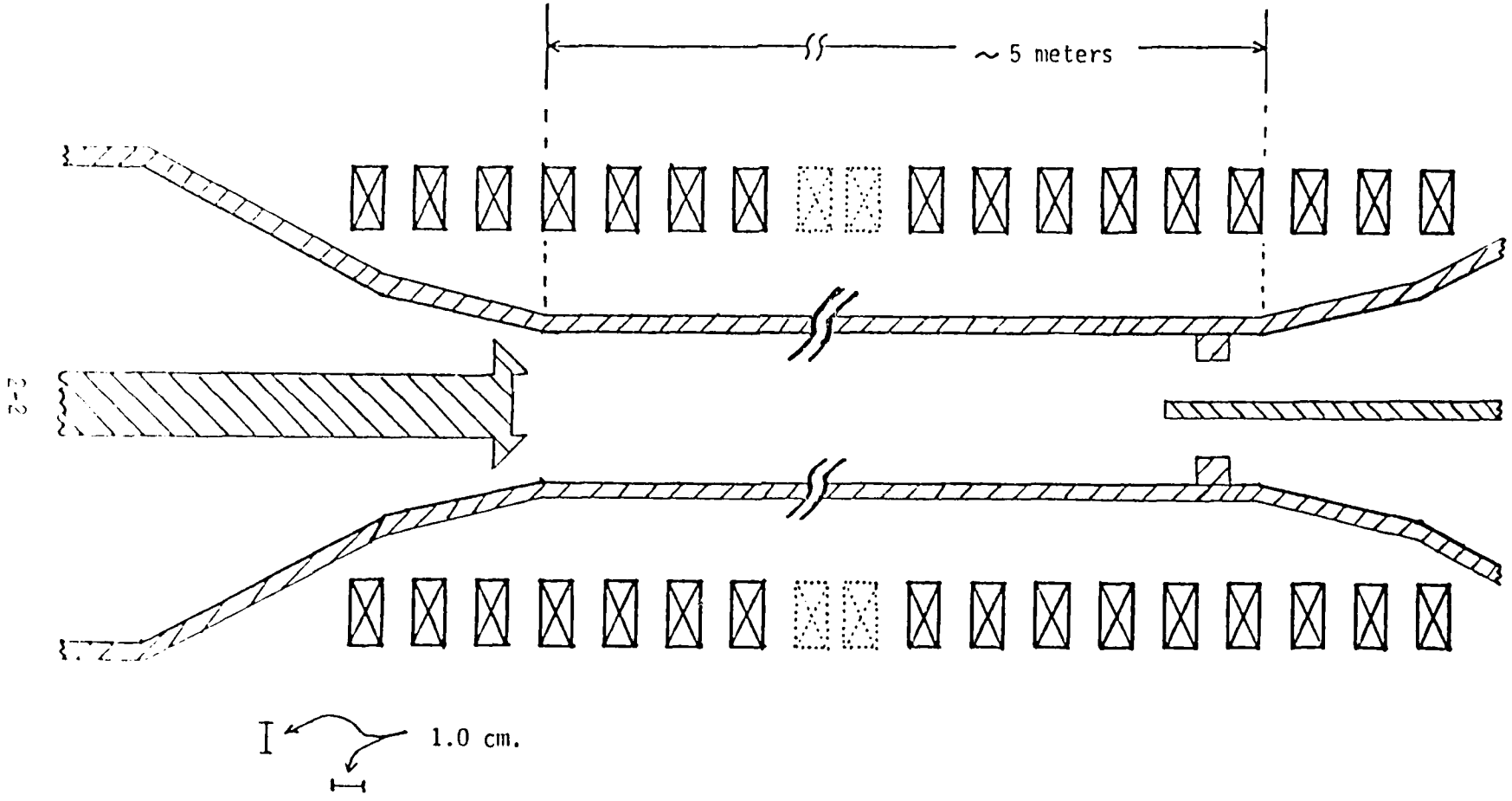

Figure 1. The Experimental CPA Device.

inner drift tube wall in the vicinity of the rod tip to act as a beam stop for the hollow electron beam. The axial position of this graphite beam-stop was again not a fixed experimental parameter. In some cases it was placed a short distance in front of, and in some cases a short distance behind the rod cathode tip. The rod cathode emitted a pencil e-beam of diameter 0.5 cm with a peak current of 2 kA and a current and voltage rise time of about 5.0 nsec. In the actual CPA, the hollow electron beam would experience a density modulation sinusoidally to zero at a predetermined frequency. Uniformly positioned several centimeters apart down the entire external length of the drift tube were a series of magnetic field coils which could create either a constant 15 kG B_z or an axially-rippled B-field consisting of an average 22.5 kG component to which is added a ripple of the form $B_1 \cdot \cos\left(\frac{2\pi z}{L}\right)$ where $B_1 \approx 7.5$ kG and $L = 60.0$ cm. (Note that the uniform field coil spacing was compressed for the last several coils at both ends of the tube to provide intensified B_z-fields behind the respective diodes.)

To describe the physics of the CPA device, we rely on excerpts from Reference 1. In that report, it is pointed out that the axial electric field component at r=0, produced by an annular, unneutralized, magnetically-focused intense relativistic electron beam (IREB) propagating through a drift tube of radius R can be approximated by

$$E_z \approx -\left[\frac{1}{2\pi\varepsilon_o}\right]\frac{\partial Q}{\partial z}\ln\frac{R}{r_b} - \left[\frac{\mu}{2\pi}\frac{\partial I}{\partial t}\right]\ln\frac{R}{r_b} + \frac{Q}{2\pi\varepsilon_o}\frac{1}{r_b}\frac{\partial r_b}{\partial z} \qquad (1)$$

where Q is the beam's charge per unit length ($Q = I/v_b$), I is the beam current, r_b is the beam radius, and v is the electron velocity. If the drift tube walls are covered with a thin dielectric layer of thickness, δR, and permeability, ε, one finds

$$E_z \approx -\frac{\mu}{2\pi}\frac{1}{\varepsilon^2-1}\frac{\partial I}{\partial t}\ln\frac{R}{r_b} + \frac{\mu}{2\pi\varepsilon^2}\frac{\varepsilon}{\varepsilon-1}\frac{\delta R}{R}\frac{\partial I}{\partial t} + \frac{Q}{2\pi\varepsilon_o}\frac{1}{r_b}\frac{\partial r_b}{\partial z}. \qquad (2)$$

Furthermore, by choosing

$$\frac{\delta R}{R} \approx \frac{\varepsilon}{\varepsilon - 1} \frac{1}{\gamma^2} \ln \frac{R}{r_b} \tag{3}$$

Equation (2) reduces to

$$E_z \approx \frac{Q}{2\pi\varepsilon_o} \frac{1}{r_b} \frac{\partial r_b}{\partial z} \quad . \tag{4}$$

Now assume a charge density modulation of the IREB of frequency and wavelength, f and λ respectively, such that $\lambda f = v$ and

$$Q\,(z,\,t) \approx \frac{Q_o}{2} \left[1 + \sin\left(\frac{2\pi}{\lambda} z - 2\pi f t\right)\right] \tag{5}$$

If an axially, sinusoidally rippled magnetic field with ripple wavelength, L, is now imposed in the drift tube, the annular beam will follow the B-field lines and have an axially varying radius of

$$r_b \approx r_o + r_1 \cos\frac{2\pi z}{L} \; ; \quad r_1 < r_o \tag{6}$$

where r_o is the mean IREB radius and r_1 is the amplitude of the radial ripples. Inserting (5) and (6) into (4) along with the assumption that the beam velocity, v, is approximately equal to the speed of light, c, yields

$$E_z \approx -\frac{1}{4} \frac{Q_o}{\varepsilon_o} \frac{r_1}{r_o L} \left\{\cos\left[2\pi z\left(\frac{1}{\lambda} + \frac{1}{L}\right) - 2\pi f t\right]\right.$$

$$\left. -\cos\left[2\pi z\left(\frac{1}{L} - \frac{1}{\lambda}\right) + 2\pi f t\right] + 2\sin\frac{2\pi z}{L}\right\} . \tag{7}$$

Thus, there are two "waves" with phase velocities

$$v_{\phi 1} = v \frac{L}{\lambda + L} \quad \text{, for the forward wave, and}$$

$$v_{\phi 2} = -v \frac{L}{\lambda - L} \quad \text{, for the backward wave.} \tag{8}$$

The amplitude of these "waves" is given by

$$E_{zo} \approx \frac{Q}{4\varepsilon_o} \left(\frac{r_1}{r_o L}\right) \quad . \tag{9}$$

Since only the backward wave can have a phase velocity approaching c, only the backward wave can accelerate electrons. Note that both waves can accelerate ions but ion acceleration is beyond the scope of this proposed research.

In the experiments conducted to date with the device in Figure 1, the hollow beam density was not modulated so acceleration could not be tested. However, for the beam and B_z that was in place, $L = 0.60$ meter, $r_1/r_o = 0.17$, and $Q = I/c = 2\times10^4/3\times10^8 = 6.67\times10^{-5}$ coulomb/meter. Assuming that the hollow beam could be density modulated with $\lambda \approx 2L$, then Equation (8) predicts a phase velocity of c for the backward wave which, with this value for Q inserted into Equation (9) yields 530 kV/meter as the effective axial acceleration field. Over the full 5 meter length, this amounts to a 2.5 MV energy gain which should be easily observable experimentally. It is worth noting as well that an IREB propagating through a rippled magnetic field can produce significant microwave radiation if the field strength is below a critical value given by

$$B_c \approx \frac{2\pi}{L} \frac{mc}{e} \gamma \quad . \tag{10}$$

For the experimental parameters of $L = 0.6$ and $\gamma = 1 + 1.5/.511 = 3.9$, B_c becomes about 0.7 kG which is far below the average 15 kG baseline axial guide field. It is also important to note the axial and temporal scale lengths in the experiment. The relativistic electron gyroradius is given by

$$r_G = 1.7 \times 10^3 \left(\gamma^2 - 1\right)^{1/2} B^{-1} \text{ cm} \qquad (11)$$

so that in the peak axial field of 30 kG, $r_G \approx 0.22$ cm. Similarly, the relativistic electron gyroperiod is found to be about 5×10^{-11} second.

In the actual experiments that were run at NRL, the hollow beam was not density modulated and the central pencil beam apparently did not propagate down the full length of the tube (Reference 4). Thus, the experiment never proceeded to the point of testing the acceleration concept itself. Specifically, with the 20 kA hollow beam in steady state propagation down the full length of the 5-meter tube (confirmed by damage patterns) the pencil diode voltage was ramped up from 0 to 1.0 MV over about 5 nsec. The pencil diode current rose likewise from 0 to 2.0 kA over about the same 5 nsec. The pencil beam was never observed to reach the other end of the tube in the presence of the hollow beam. In fact, magnetic field probe measurements made just 50 cm downstream from the pencil diode failed to detect the presence of the pencil beam. Therefore, the most significant immediate question addressed by these numerical simulations of the device was the simple one of survivability of the central beam. This report documents the numerical duplication of all of the above experimental observations. In addition, it was found that the central beam does, in fact, propagate down the axis of the tube but that its current is drastically reduced due to the formation of an effective virtual cathode right next to the emitting tip of the central rod cathode.

Before describing these results in Section 4, the following section first details the numerical model of the CPA which was used in this effort.

SECTION 3

THE NUMERICAL MODEL

From the start of this project, it was clearly out of the question to attempt a simulation of the full 5 meter length of the NRL Collective Particle Accelerator (CPA) drift tube. Far too many computational cells and particles would be required to model the full physical system. Such a model would be impractical for running on the available VAX-11/780 computer. (A Cray-compatible version of MAGIC exists, but no Cray-1 machine time was available for this work.) With this in mind, the previously reported first phase of this research was conducted using a numerical grid model whose radial dimensions were very close to that of the actual CPA, but which was only one-quarter of a meter long instead of the actual 5 meters. This previous model is depicted in Figure 2. It served very well in carrying out the initial analysis of the CPA system. Having an axial length about five times its diameter (see Figure 3) insured an adequate separation of the two opposing diodes to guarantee decoupling for several nanoseconds. This proved quite adequate for obtaining initial insights into the physics of the device's operation.

There were only two major drawbacks to that previous model. This first involved the representation of the hollow e-beam diode. To limit the number of numerical cells, the radial "flaring" at that end of the CPA tube was ignored. Instead, a simple cylindrical, hollow cathode was inserted into the end of the tube, and was allowed to field emit an e-beam in accordance with the normal Guassian prescription. However, since the spacing between the hollow cathode and the anode tube was now much smaller than that in the actual physical device (about 0.4 cm, as compared to an actual 1.0 cm), the electric field at the surface of the cathode was significantly more intense, resulting in a hollow beam current of almost 50 kA, compared with the experimentally observed 20-25 kA. The second objection to the previous numerical model was directly related to its grossly shortened length and to the fact that the hollow cathode potential was ramped to -1.5 MV, compared to -1.0 MV for the rod cathode. This voltage difference mandated that the pencil beam electrons would be

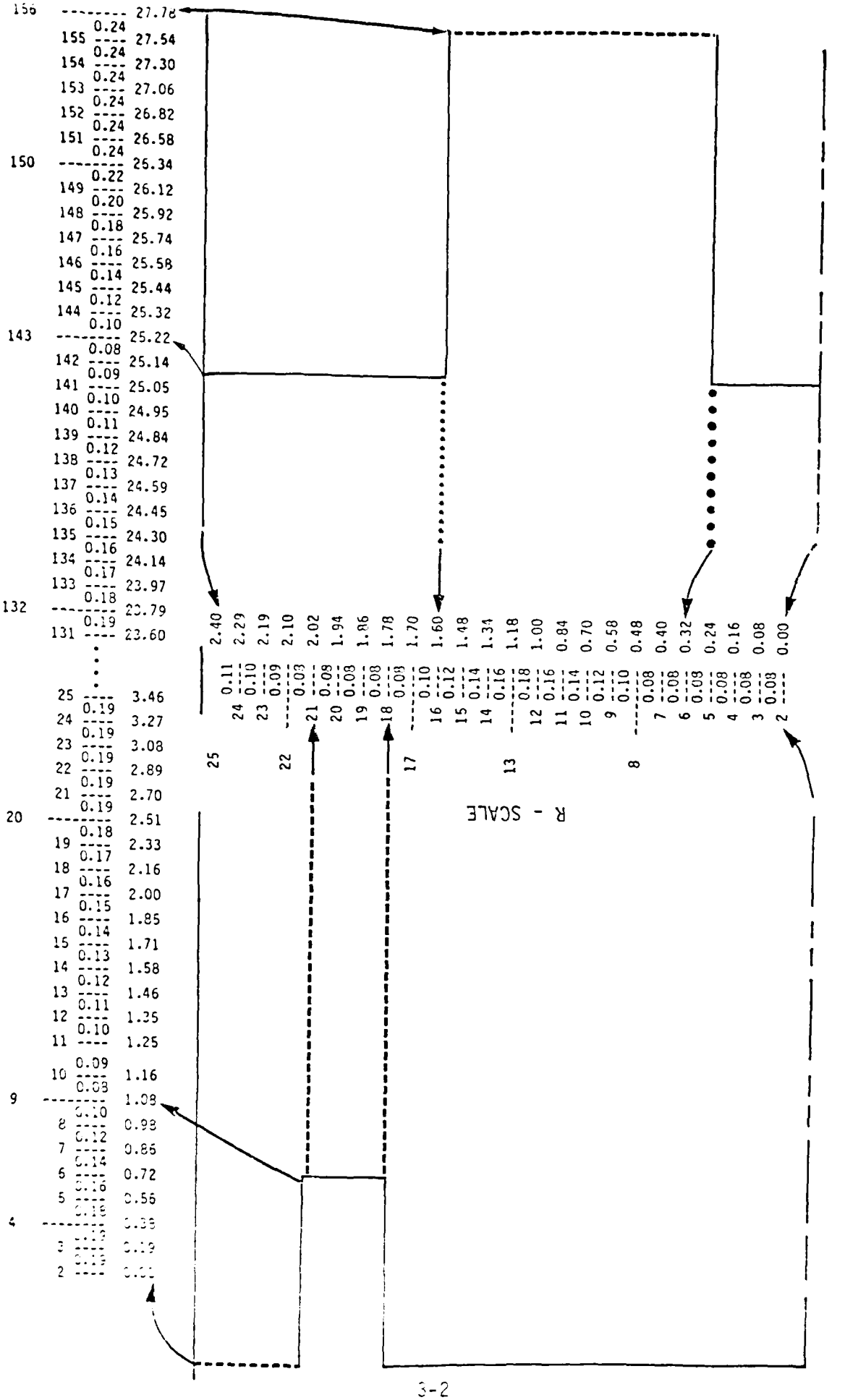

Figure 2. The Previous Simulation Grid.

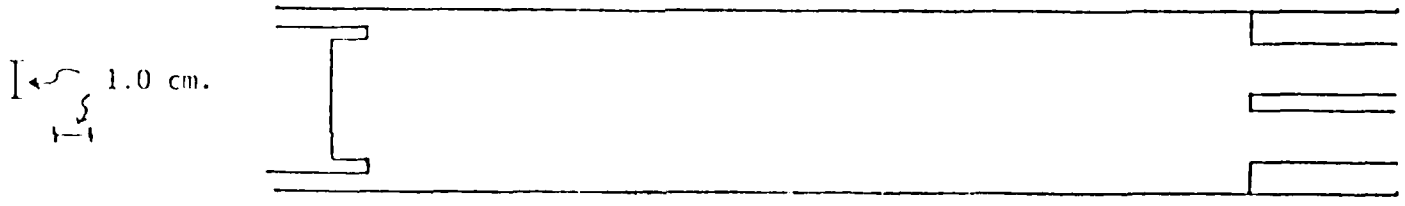

Figure 3. Scale Drawing of the Previous Numerical Model.

reflected back toward their point of origin as soon as they reached the hollow cathode end of the tube. Therefore, since the total drift length between cathodes was only 25.22 cm, it was possible for reflected electrons to complete a round trip back to the rod cathode in about 1.75 nsec. This made it impractical to simulate rod cathode voltage rise times of longer than about 1 nsec. In fact, fear of interference from reflected electrons before achieving equilibrium, encouraged the use of exclusively 0.1 nsec rise times in the previous work. It has since been suggested that the use of a much longer rise time, closer to the 5-10 nsec used in the experiments, would inject many more low energy electrons into the region near the tip of the rod cathode, and would thus permit the formation of a much denser negative space charge cloud (i.e., virtual cathode) there. If present, this effect could conceivably lower the pencil beam current much more than that observed in the previous simulations.

To correct these two shortcomings, a new numerical model was devised. The number of computational cells was practically doubled from the previous 4,000 to 7,500 cells. If all else were left the same, the peak number of particles in the simulation would double from 40,000 to about 80,000. The results would be catastrophic with regard to simulation run time on the VAX. To ease the strain on the computer, two significant steps were taken. First, the particle density of the central beam was cut approximately in half. Second, the outer, hollow beam was replaced by a pseudobeam of gradually imposed axial current density all along the cells spanning the former hollow beam radius.

The radial and axial cell spacing for the new model which emerged are shown in Figures 4 and 5, respectively. Note also from the figures that simple, hollow cathode at one end of the tube has been modified to include a "pencil beam dump" in its interior. This dump consists of a metal rod, centered on-axis which may be connected to the cathode, connected to the anode (via some convolute outside the simulation volume), or simply left "floating." This extra electrode thereby opens up possibilities for absorbing instead of reflecting central beam electrons, if so desired. The model is shown, drawn to scale, in Figure 6. The new

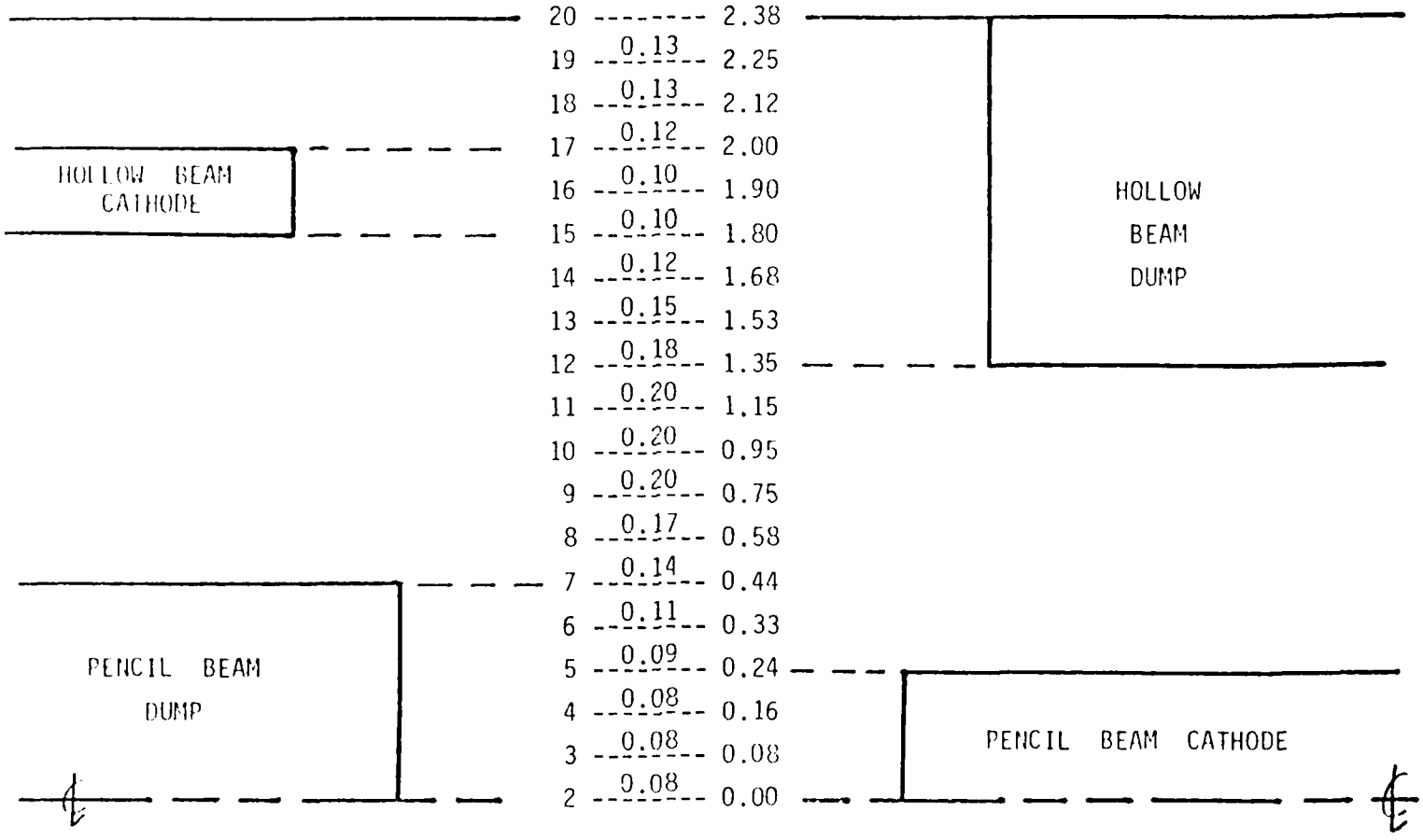

Figure 4. Radial Cell Spacing in the New Model.

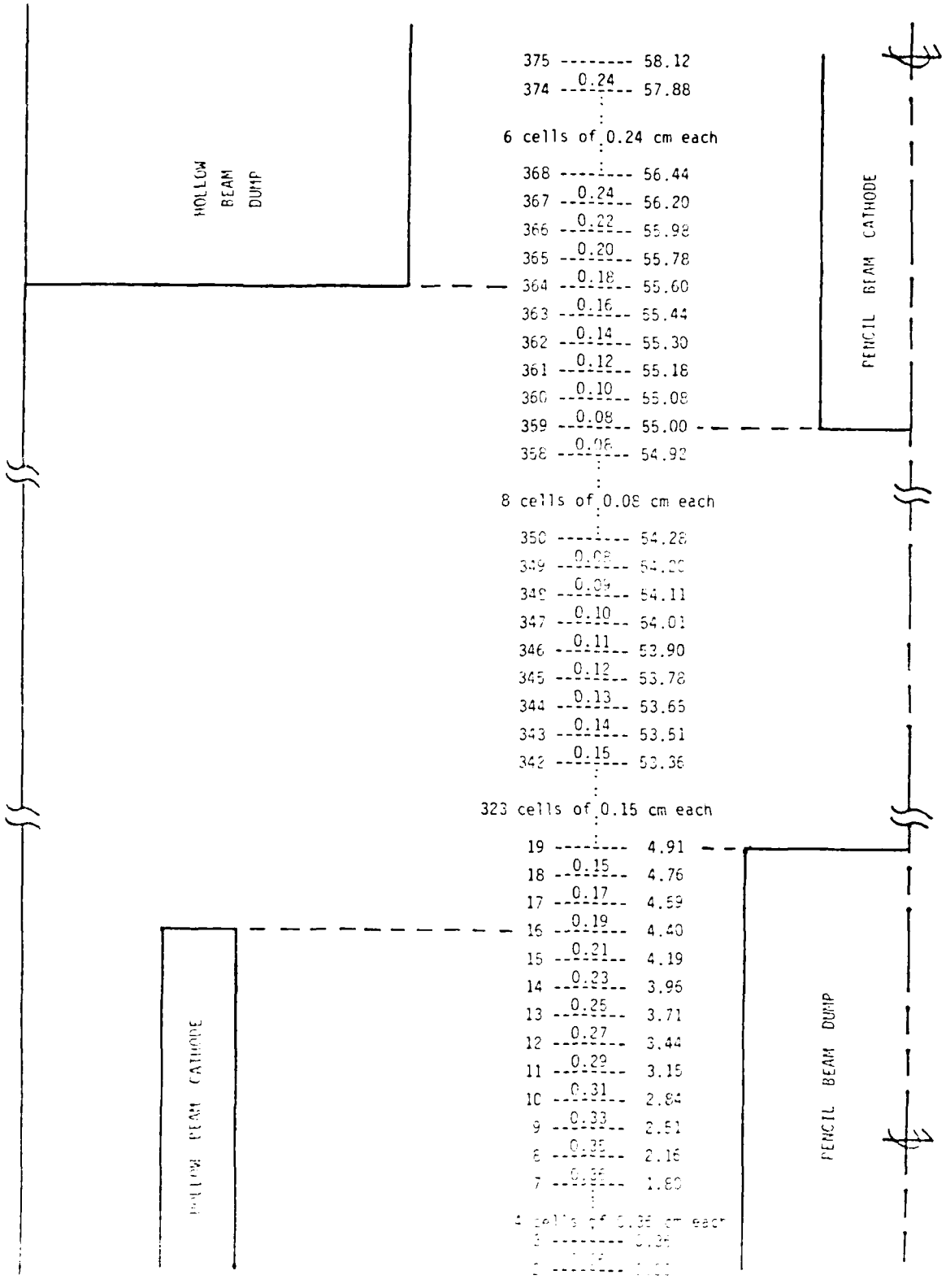

Figure 5. Axial Cell Spacing in the New Model.

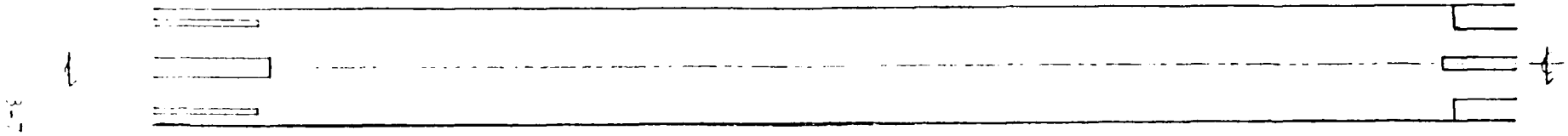

Figure 6. Scale Drawing of the New Numerical Model.

pencil beam drift distance is 50.09 cm instead of the previous 25.22 cm. In addition, six other model dimensions were improved in the sense that they were brought closer to those of the actual experiment. These are shown in Table 1. The final major difference between the old and new models lies in their imposed axial magnetic field strengths. The previous model imposed a uniform B_z of 25 kG down the entire length of the tube. The present model uses 15 kG instead, and this corresponds much more exactly to the value of B_z typically used in the experiment.

TABLE 1

COMPARISON OF MODEL DIMENSIONS
(In Centimeters)

	Previous Model	New Model	Actual Experiment
Drift Tube Radius	2.40	2.38	2.38
Hollow Cathode Thickness	0.24	0.20	0.20
Hollow Cathode Radius	2.02	2.00	2.00
Rod Cathode Radius	0.32	0.24	0.25
Dump Ring Thickness	0.80	1.03	1.00
Dump Ring Recess	0.00	0.60	-1.0 to 1.00

SECTION 4

RESULTS

In presenting the findings of this second phase of the NRL CPA modeling effort, it is only proper to begin by recapitulating the major results from the first phase. Only the bare essentials are provided, and the reader is referred to Reference 3 for more detailed information. In this second phase effort, the previous numerical model was used one last time to examine the changes in the physics when a particulate, low-current, hollow beam is substituted for the previous 50 kA beam. This step was necessary to benchmark the hollow beam characteristics before mimicking it with a pseudo beam.

The final three parts of this section deal only with results obtained using the new, longer numerical model system. First, there is a brief presentation showing the benchmark run of the single-beam case. The long system is shown to correspond closely to the previous short system. The last two runs are of the long model with central beam voltage rise times of 1.5 and 2.5 nsec, respectively. They test the hypothesized effects of greater numbers of early-time, low-energy electrons in exaggerating the magnitude of the virtual cathode opposite the rod cathode tip.

4.1 SUMMARY OF PREVIOUS RESULTS

Two key results must be cited from the prior phase of this research effort. They provide a convenient reference against which the new results may be gauged. The specific cases which must be recalled are the single-beam benchmark run and the dual-beam, reduced central current run. Both runs used the numerical model depicted in Figures 2 and 3. Both runs assumed an applied axial magnetic field strength of 25 kG.

For the single-beam case, a fast rise-time (about 0.1 nsec) voltage pulse of 1.0 MV was applied to the rod cathode. The time history

of that pulse is shown in Figure 7. For this run, no voltage was applied to the hollow cathode. The rod cathode was allowed to field-emit electrons from its axial face, with the resultant formation of a very well behaved and well collimated pencil beam traveling down the axis of the CPA tube, as shown in Figure 8. (Note that Figure 8 is not drawn to scale. The axial dimension is compressed approximately by a factor of ten with respect to the radial.) To measure the current flowing in this central beam, the same technique as was used in the experiment is also used in the simulation. Namely, the magnitude of the azimuthal component of the magnetic field is monitered as a function of time at predetermined points inside the drift tube. The time history of B_θ as read from one such "probe" is shown in Figure 9. This particular measurement is taken 2.2 mm axially downstream of the rod cathode tip and at a radius of about 1.413 cm from the tube centerline. After a very rapid rise, the azimuthal B-field strength mildly oscillates about a mean value of about 0.034 Wb/m^2. This translates to an axial current in the central beam of about 2.4 kA. This compares quite well to the experimentally observed central beam current of about 2 kA in a single-beam operation.

The highlight of the previous effort was a complete simulation of the CPA operating with both beams present. To achieve this configuration, 0.1 nsec rise time voltage pulses of 1.5 MV and 1.0 MV were applied to the hollow cathode and rod cathode respectively, with a 1.5 nsec time delay between them. These two voltage pulses are depicted in Figures 10 and 11. The hollow cathode pulse is observed to remain true to the 1.5 MV plateau, but the rod cathode pulse is not so well behaved. Instead of plateauing at a steady 1.0 MV, it rises first to about 1.05 MV and stays there for about 0.5 nsec, then rises slightly to 1.1 MV and stays at that value for about 1.0 nsec until finally rising to about 1.2 MV, where it stays until the end of the simulation run. These changing voltages are indicative of variations in the rod cathode beam current, which give rise to different beam-line impedances, whose mismatch with the transmission line impedance cause voltage pulse reflections and measured voltage changes. A complete round trip for a relativistic

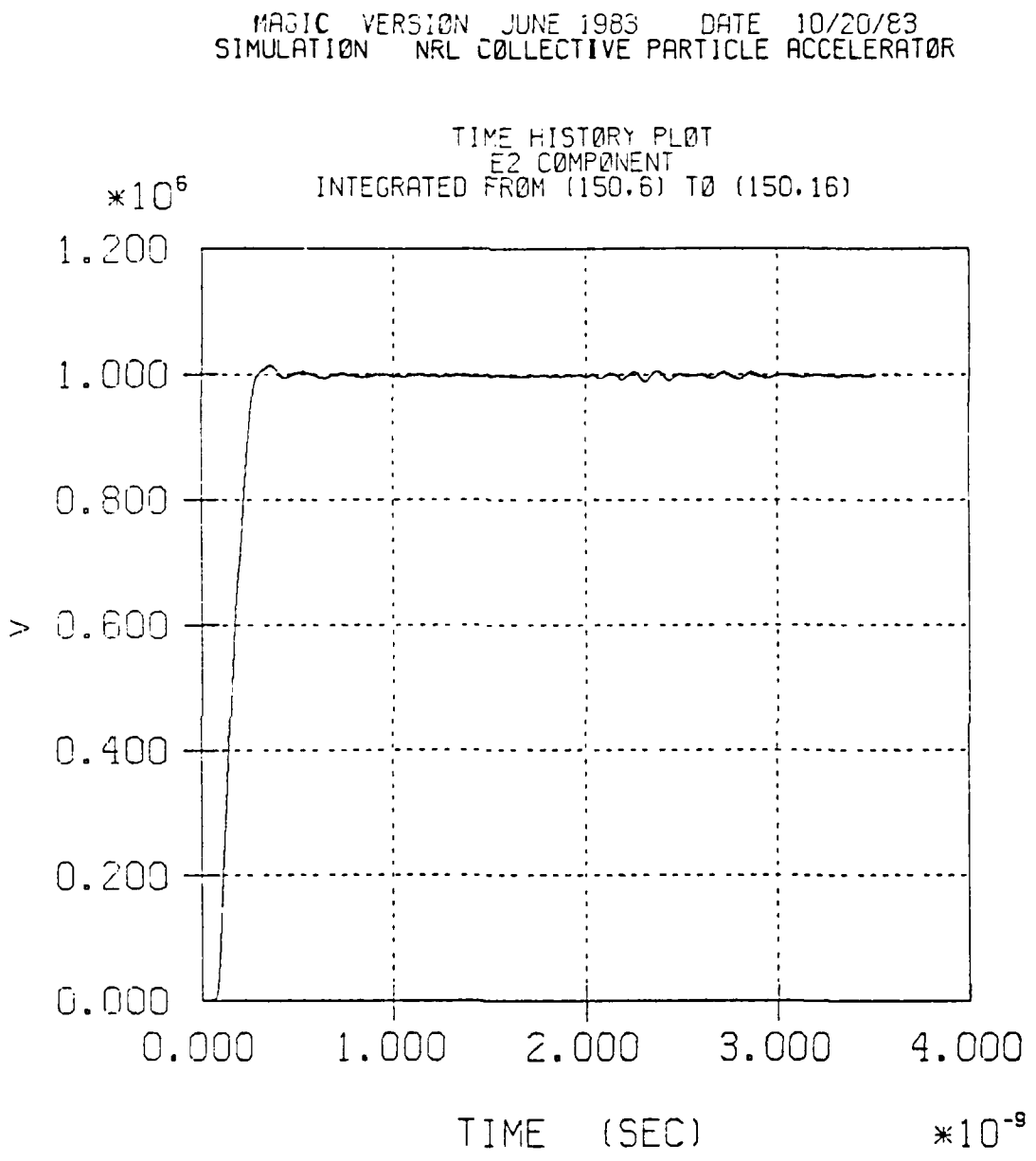

Figure 7. Rod Cathode Voltage Pulse for Previous Single-Beam Simulation.

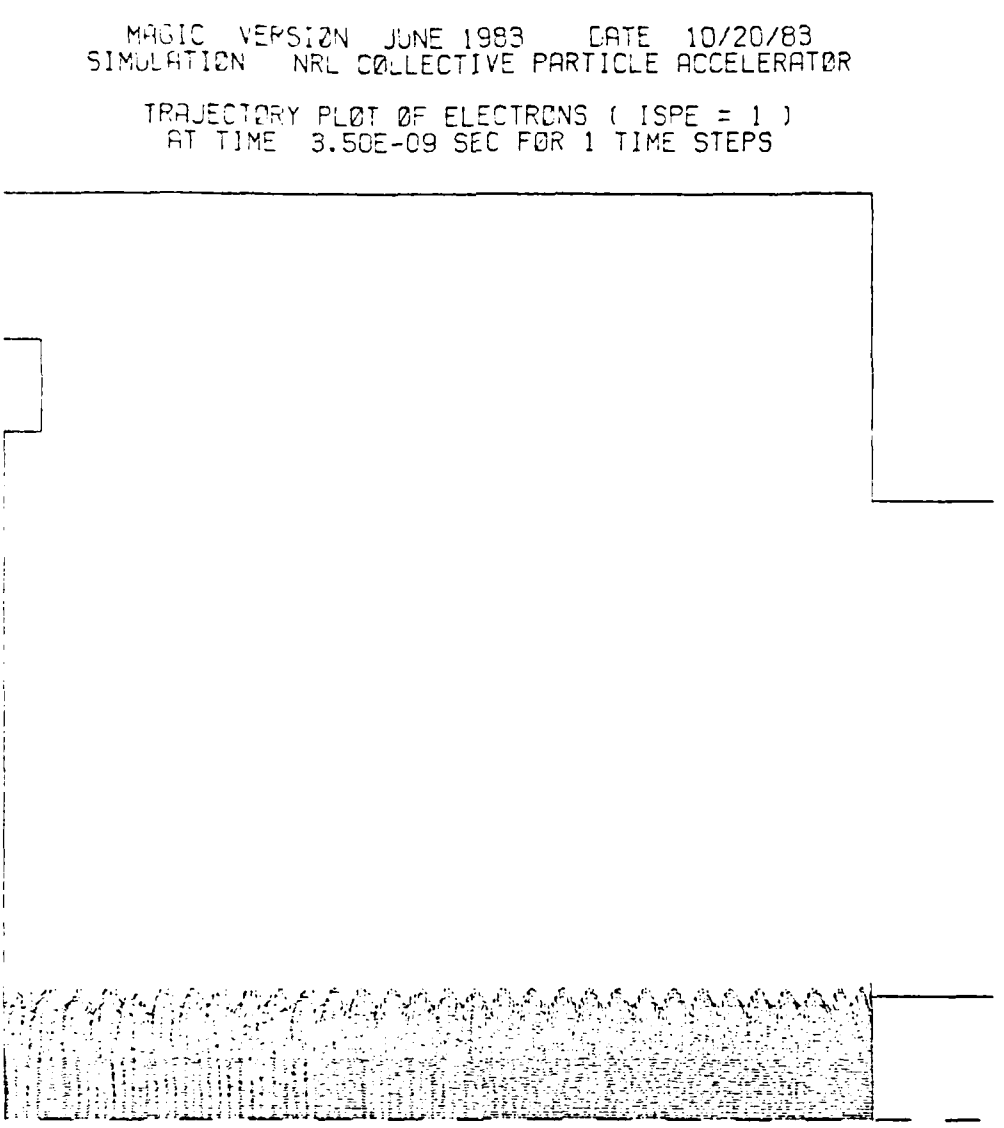

Figure 5. Sample Electron Position Plot for Previous Single-Beam Simulation.

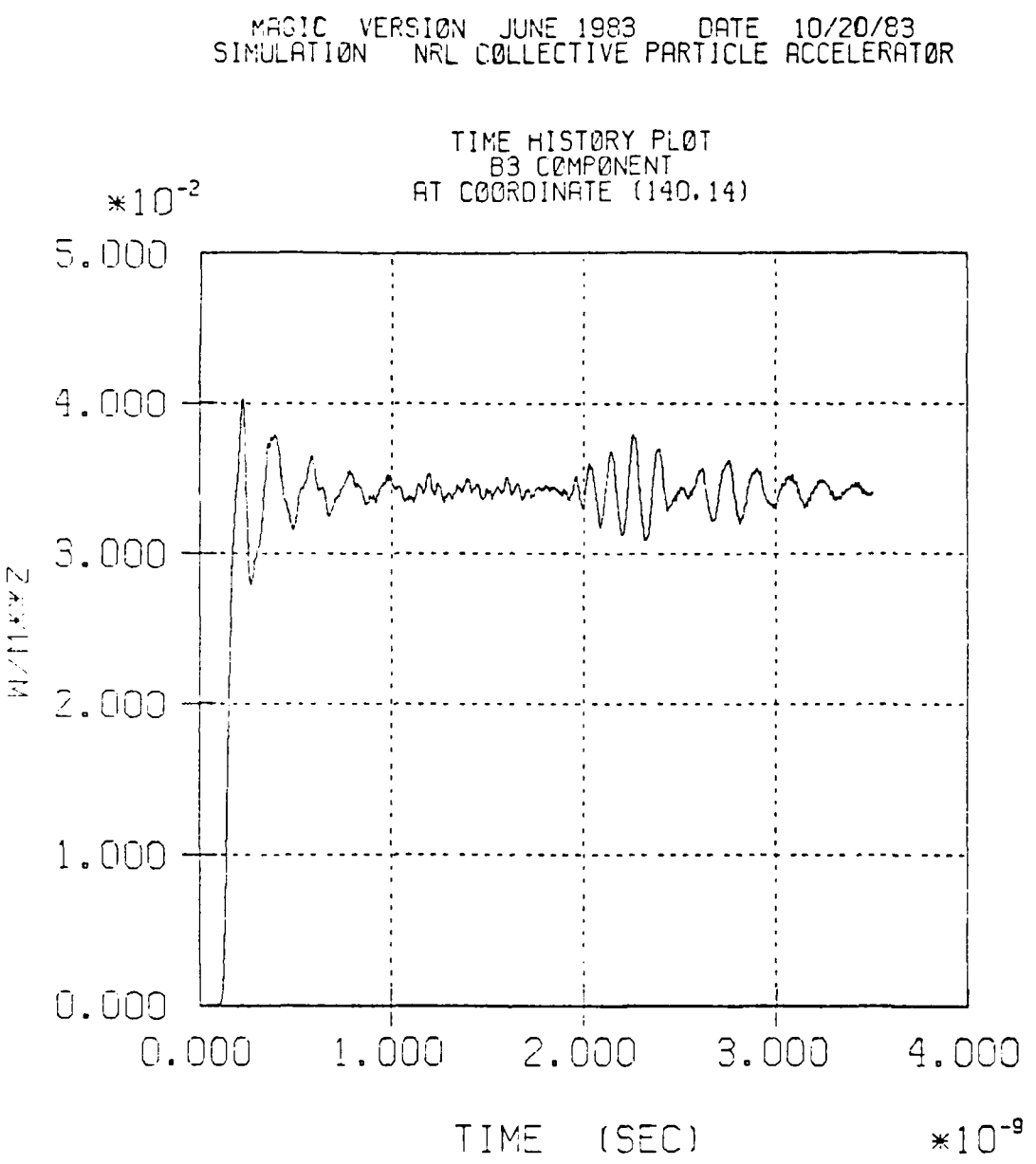

Figure 9. Time History of B_θ at a Radius of 1.413 cm for Previous Single-Beam Simulation.

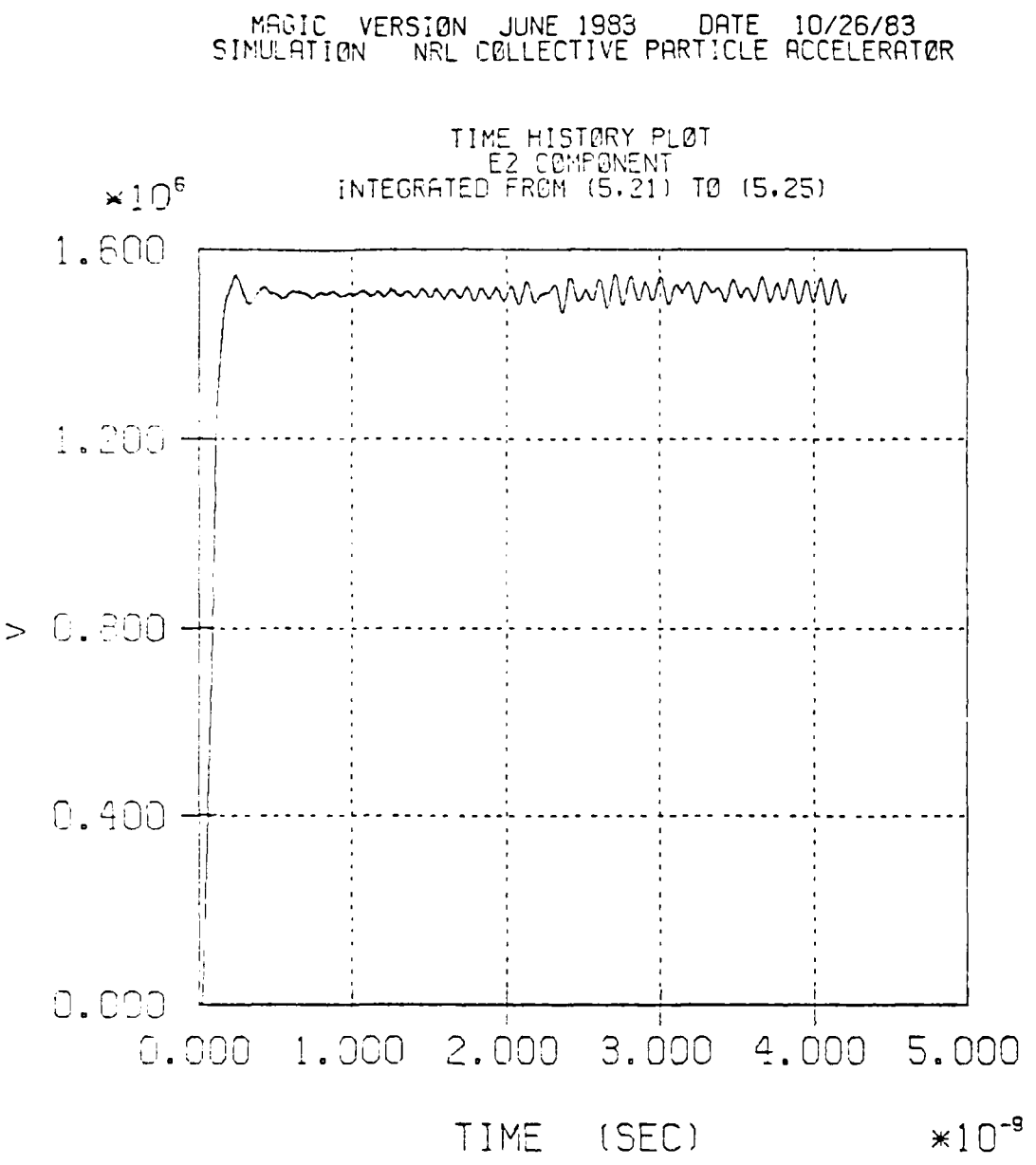

Figure 10. Hollow Cathode Voltage Pulse for Previous Dual-Beam Simulation.

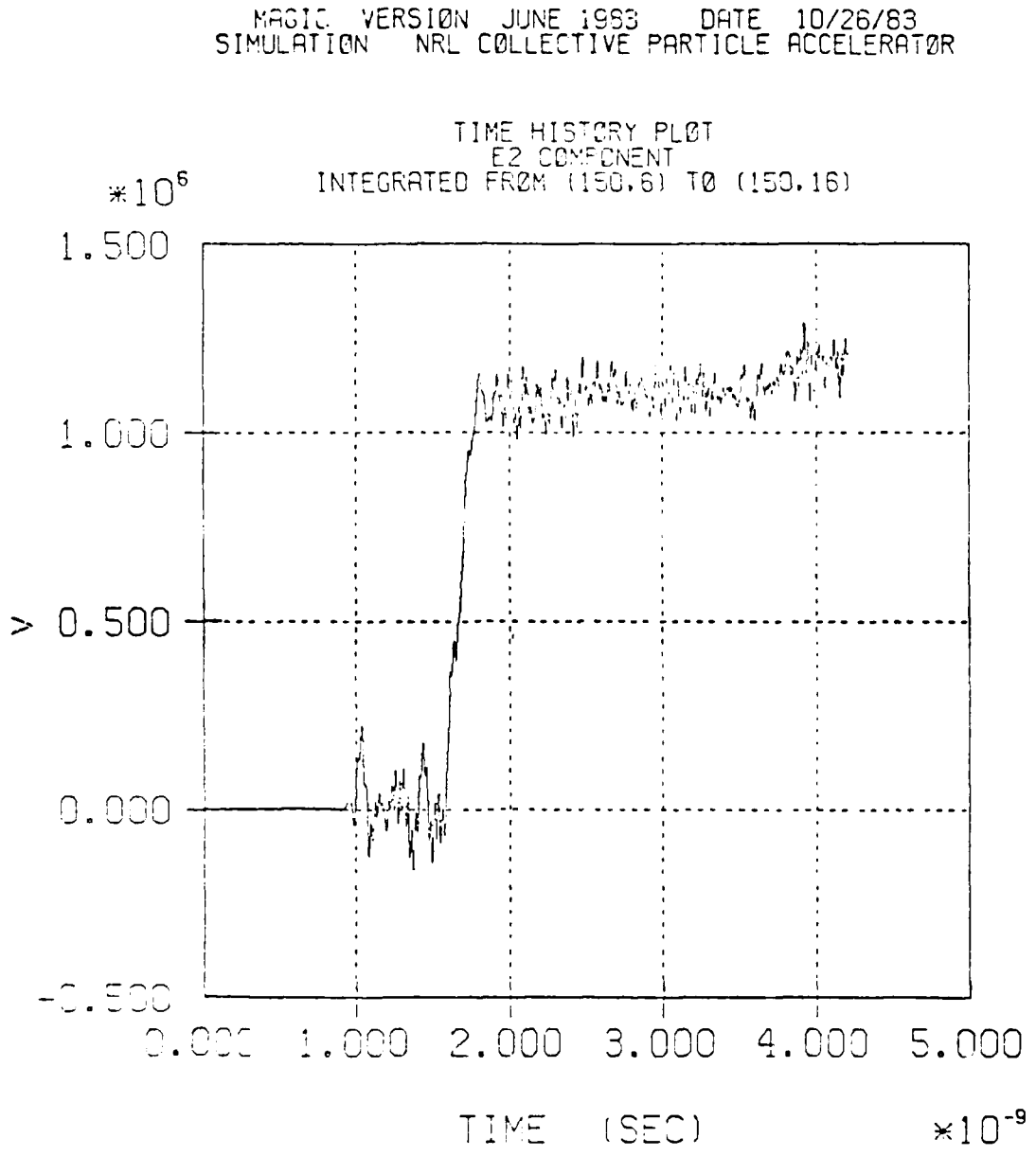

Figure 11. Rod Cathode Voltage Pulse for Previous Dual-Beam Simulation.

electron down the tube and back is about 1.75 nsec. Thus, the final rise to 1.2 MV can be attributed to current reduction due to such reflected electrons. The first step up from 1.05 to about 1.1 is probably a manifestation of the maturation of a virtual cathode opposite the rod cathode tip.

To better appreciate what is physically happening in the collective particle accelerator device, it is instructive to examine a sample electron position plot and representative phase-space plots for the two beams. Figure 12 shows the real-space distribution of sample electron macroparticles at 3.5 nsec into the simulation. It shows that both beams are established, with the central beam thinning due to reflections at the hollow cathode interior surface while, at the same time, thickening due to virtual cathode formation near the rod cathode tip. No significant disturbances, aside from the normal phase-mixing of radial ripples, is apparent in the hollow beam. The well behaved nature of the hollow beam is further confirmed by the phase-space plot of its constituent electrons, as shown in Figure 13. This plot also shows that the mean drift "momentum" of the beam's electrons is about 7.0×10^{8} m/sec, implying a relativistic drift gamma factor of about 2.33. This value of gamma translates to a mean drift energy for the electrons in the hollow beam of about 0.65 MeV.

The situation is quite different for the electrons in the central beam. Their phase-space plot is shown in Figure 14. The previously noted reflection of central beam electrons near the hollow cathode can be clearly seen on the left-hand side of the plot. Much more important to this work, however, is the oval shaped pattern on the right. It shows electrons experiencing a sharp acceleration gradient immediately following their emission from the rod cathode. That part is to be expected. What is noteworthy here is the sharp deceleration gradient the electrons see immediately thereafter. This deceleration is so strong that it appears to reflect a fraction of the electron stream right back toward the cathode tip. This deceleration is evidence for the existence of a virtual cathode of electron space-charge within 3 mm of the rod cathode

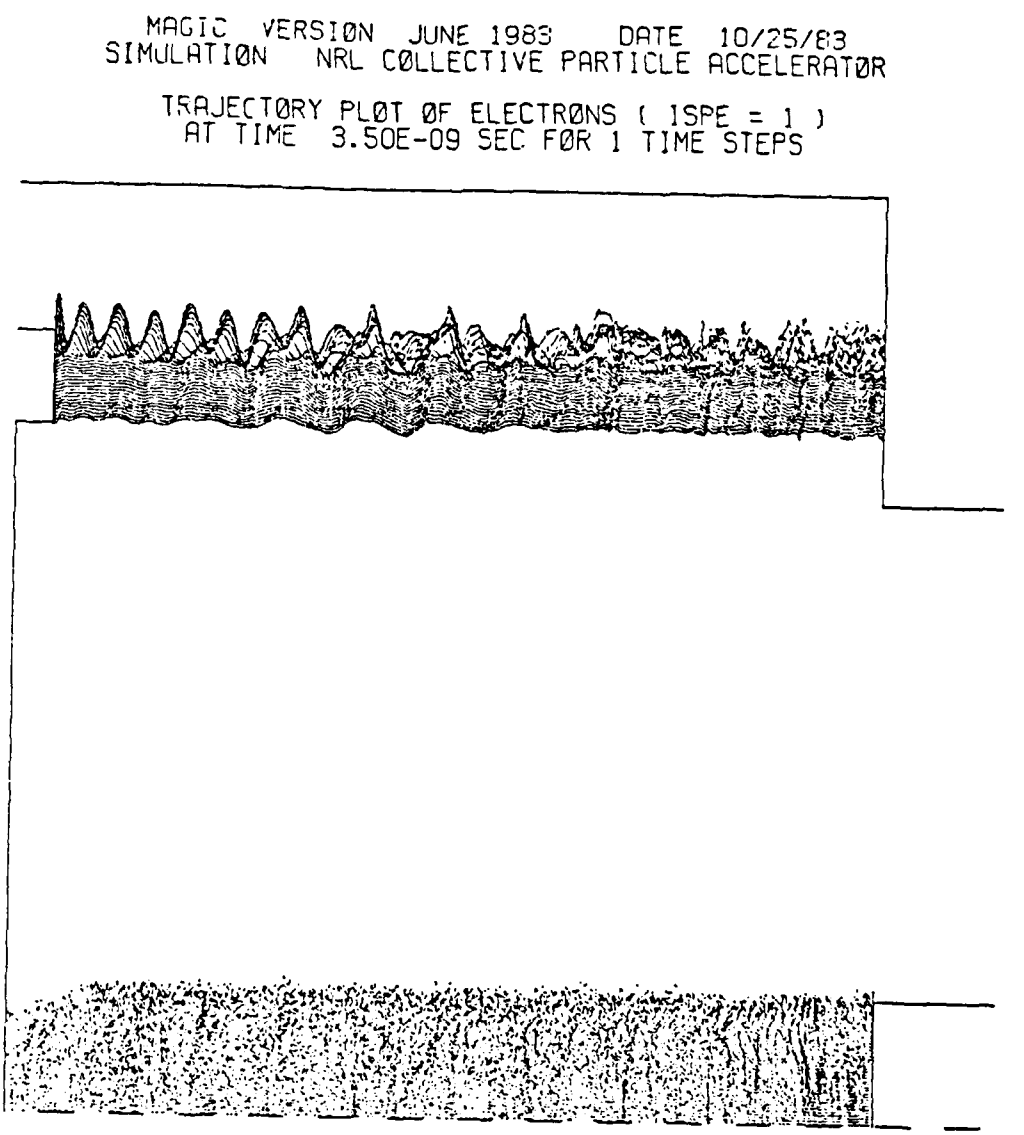

Figure 12. Sample Electron Position Plot for Previous Dual-Beam Simulation.

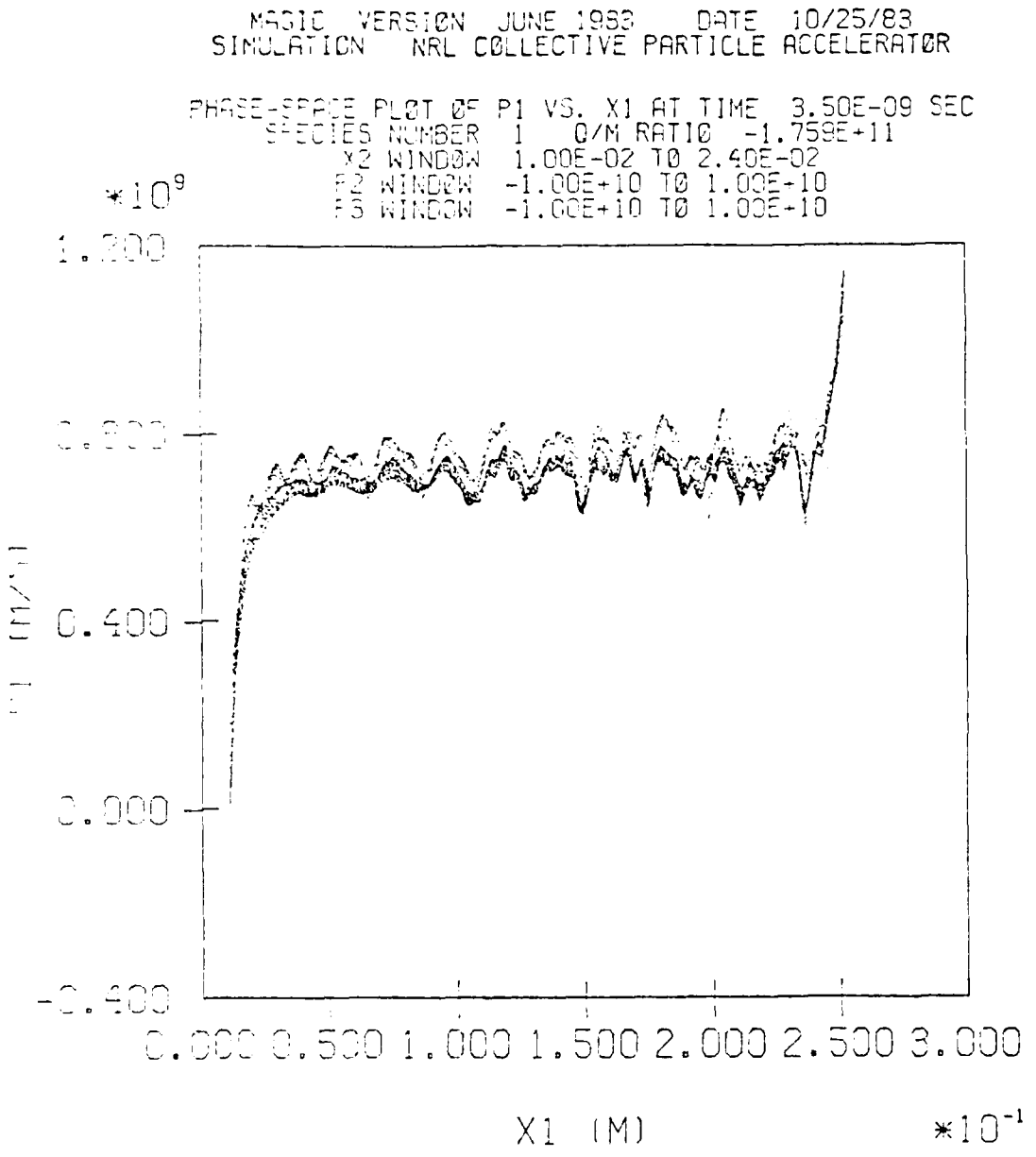

Figure 13. Phase-Space Plot of Hollow Beam Electrons in Previous Dual-Beam Simulation.

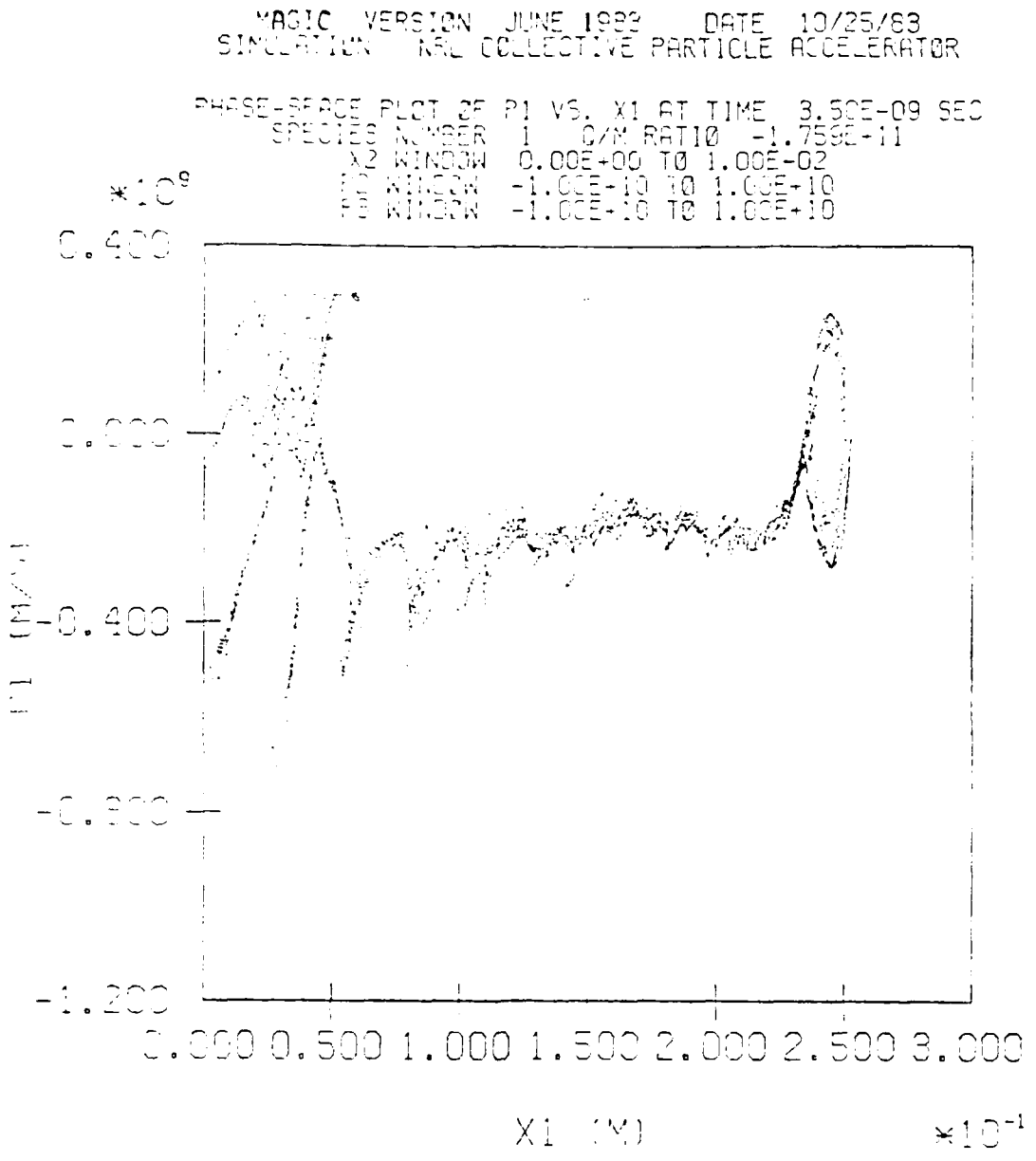

Figure 14. Phase-Space Plot of Central Beam Electrons in Previous Dual-Beam Simulation.

tip. The manifestation of such a phenomenon can only lead to a significant decrease in the net current carried by the central beam.

To measure beam currents in this simulation, the azimuthal component of the magnetic field was once again monitered at various locations in the drift tube. Figure 15 shows the time history of B_θ as read by a "probe" located almost 2 cm downstream of the rod cathode tip and at a radius of 2.345 cm from the tube centerline. At that radius, B_θ will track the <u>total</u> current of both beams at that axial position. Since no significant deviation from a plateau field strength of about 0.4 Wb/m^2 is visable, one can conclude that the central beam current is <u>much</u> smaller than that of the hollow beam, and that the hollow beam current is approximately 46.9 kA.

Figure 16 conveys the corresponding current information for the central beam. It traces the time history of B_θ at an axial position about 2 mm downstream of the rod cathode and at a radius of 1.413 cm. Although the "signal-to-background" ratio clearly leaves much to be desired, it is not difficult to estimate a mean field strength of about 0.015 Wb/m^2 between 2 and 3 nsec into the run. This gives a peak central beam current value of about 1.05 kA. This is down by a factor of almost 2.5 from the single-beam case and could easily go unnoticed in the actual experiment.

4.2 PREVIOUS MODEL WITH LOW OUTER BEAM CURRENT

The first phase of this research effort ended with the conclusions just stated in Section 4.1. The implications of that work argued in favor of a renewed experimental effort since the actual central beam current, although much reduced, was still substantial enough to use in testing the acceleration concept. Before pronouncing a final verdict, however, it was necessary to address the two major differences between the simulations and the experiment, namely the much higher hollow beam current and the artificially short voltage rise time on the rod cathode.

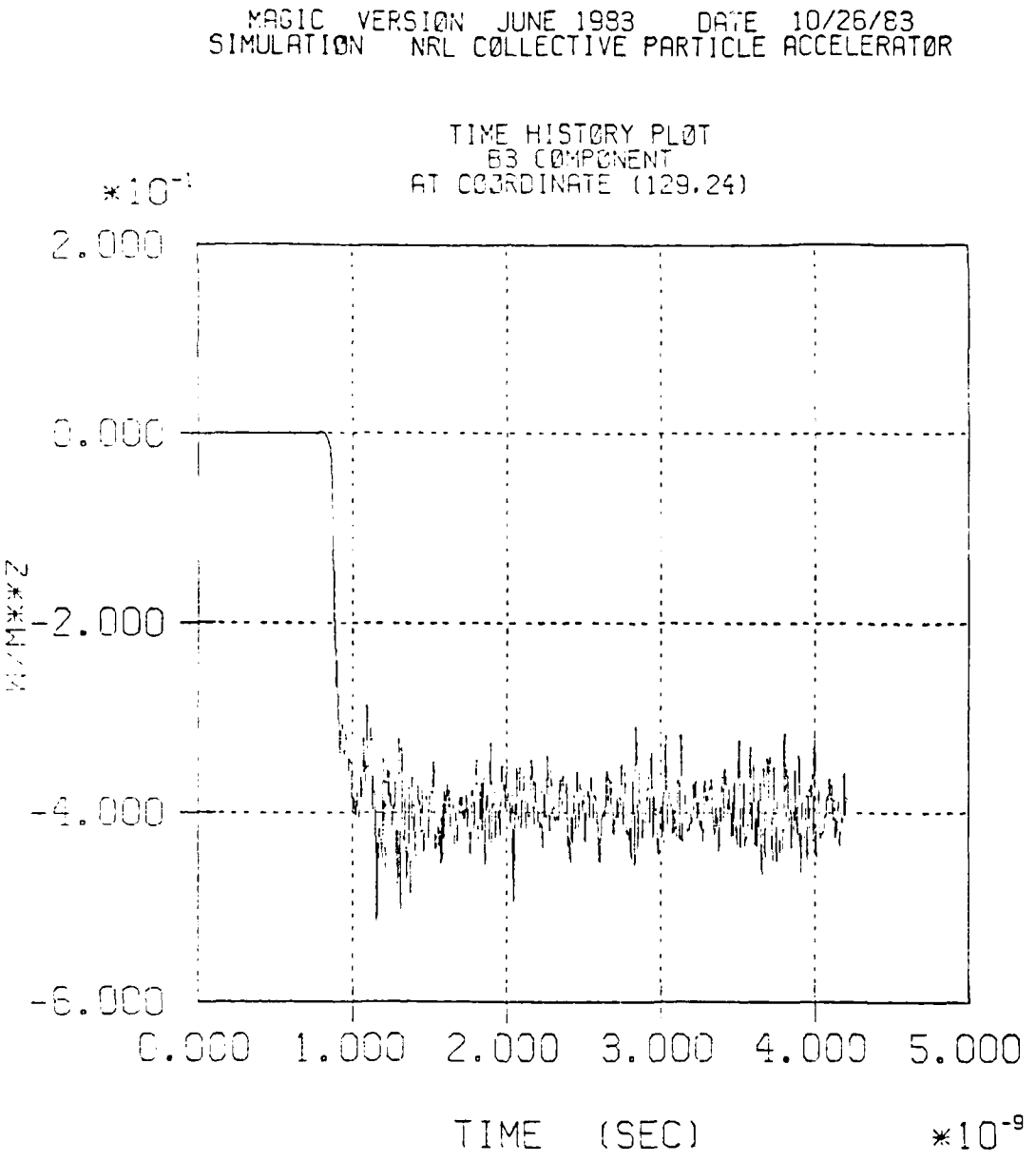

Figure 15. Time History of B_θ at a Radius of 2.345 cm for Previous Dual-Beam Simulation.

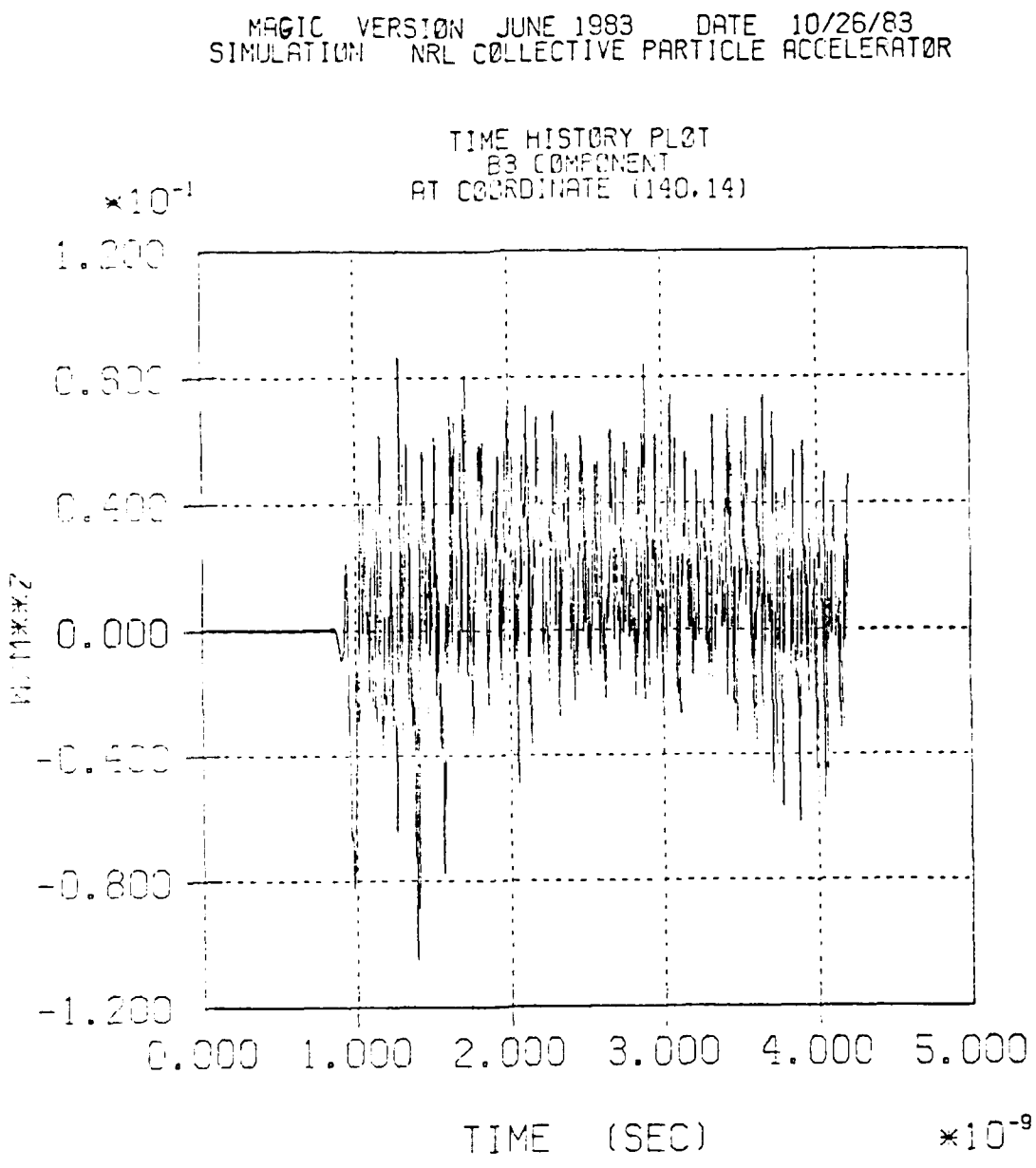

Figure 16. Time History of B_θ at a Radius of 1.413 cm for Previous Dual-Beam Simulation.

The problem of lowering the hollow beam current was relatively straightforward to solve. In fact, there were two avenues of solution open. One possibility would have been to modify the physical dimensions of the electrode system in such a way as to mimic the radial flaring of the tube and the cathode at the hollow beam diode end. By increasing the effective anode-cathode gap there, the electric field at the hollow cathode surface would have been reduced and the field emission algorithm would have yielded a proportionately lower emitted current. The price for such a "fix" would have been the addition of several extra layers of cells in the radial dimension. Three extra radial cells equate to almost 500 extra 2-D cells in the simulation. Such a waste of computational storage could not be easily defended, particularly given the more pressing demand to add cells to increase the axial length of the system.

A far more agreeable solution consisted of shutting off the Gaussian-field emission on the hollow cathode tip and replacing it with an artificially imposed, injected electron beam. Physically speaking, it was as if the solid cathode tip were replaced by a transparent, conducting foil through which a monoenergetic beam of electrons was injected. Specifically, for this simulation, the electrons were introduced with a near zero energy and with a radially uniform current density of 8.376×10^7 A/m^2 (=8.376 kA/cm^2).

The results from this simulation offered no surprises. Figure 17 shows a time history of the voltage pulse applied to the hollow cathode diode. It differs only slightly from the 1.5 MV plateau previously exhibited in Figure 10. More interesting are the electron trajectory plots of Figures 18 and 19. They depict the hollow electron beam in two separate, intermediate stages of development. A clear distinction can be drawn between the nose of the beam and its main body. The physical nature of the distinction is clarified by examining the phase-space plot for the hollow beam electrons at the exact same instant in time (t = 0.7 nsec) as that of Figure 19. This is shown in Figure 20.

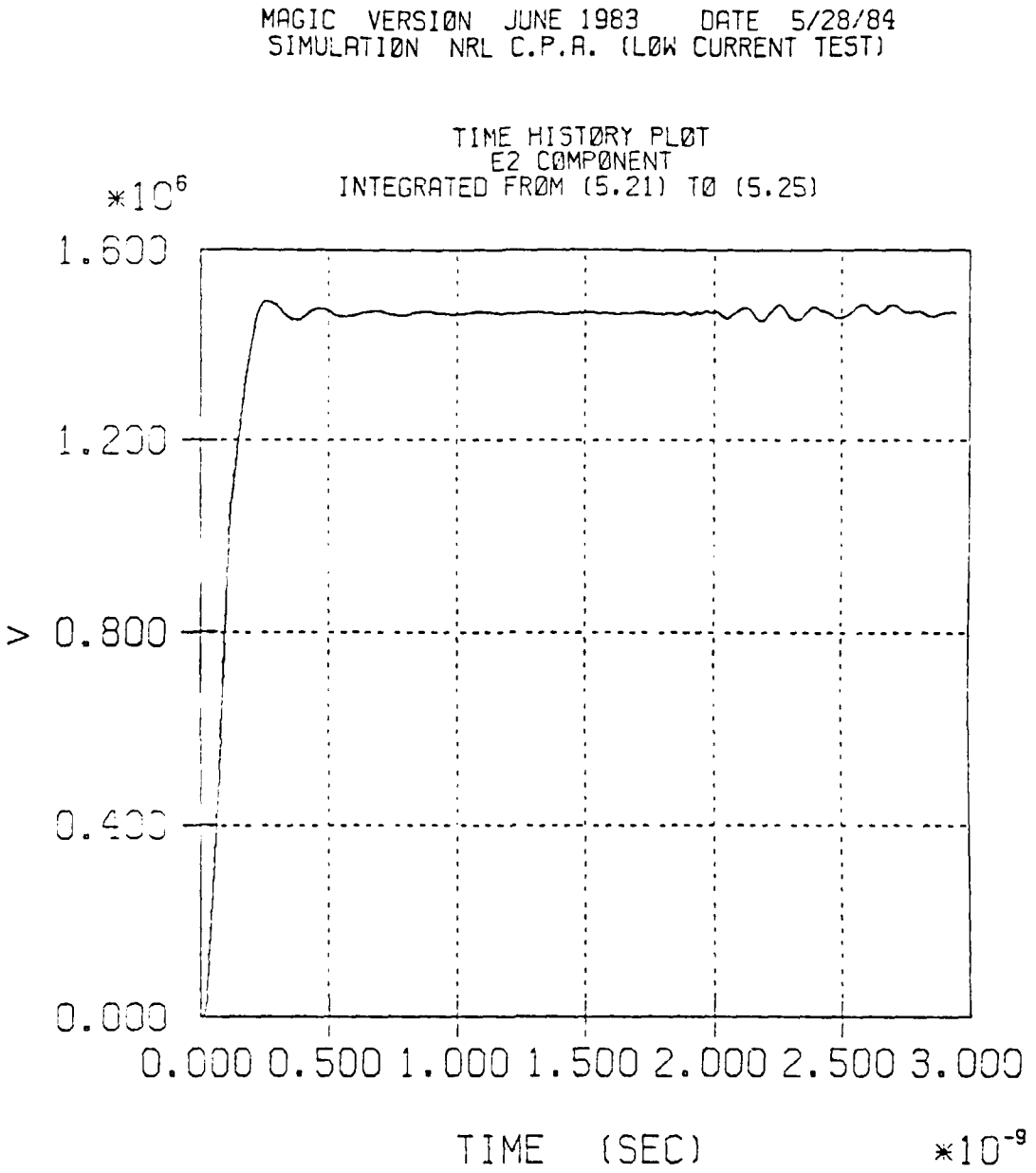

Figure 17. Hollow Cathode Voltage Pulse for Low Current Test on Previous Model.

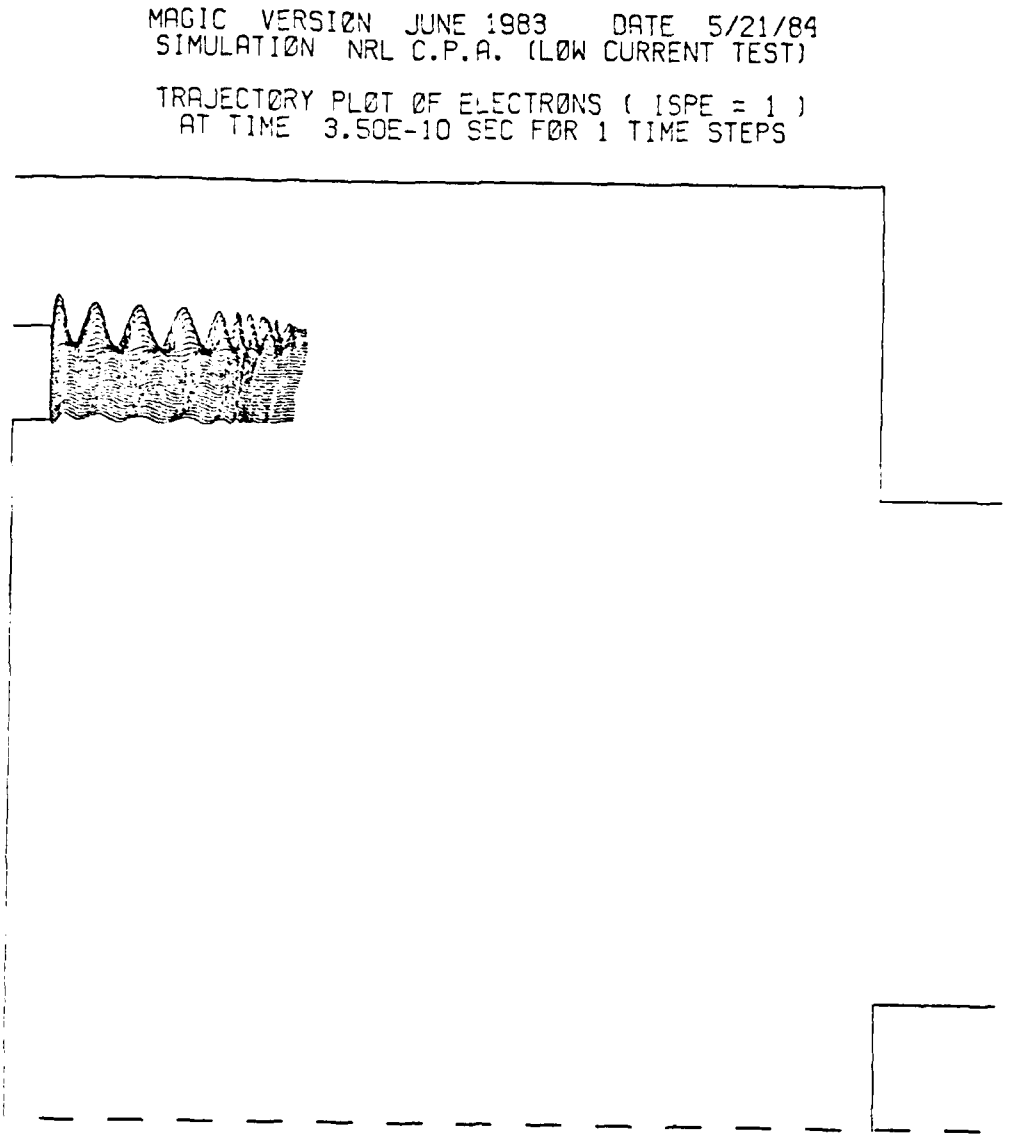

Figure 15. Electron Position Plot for Low Current Test at t = 0.35 nsec.

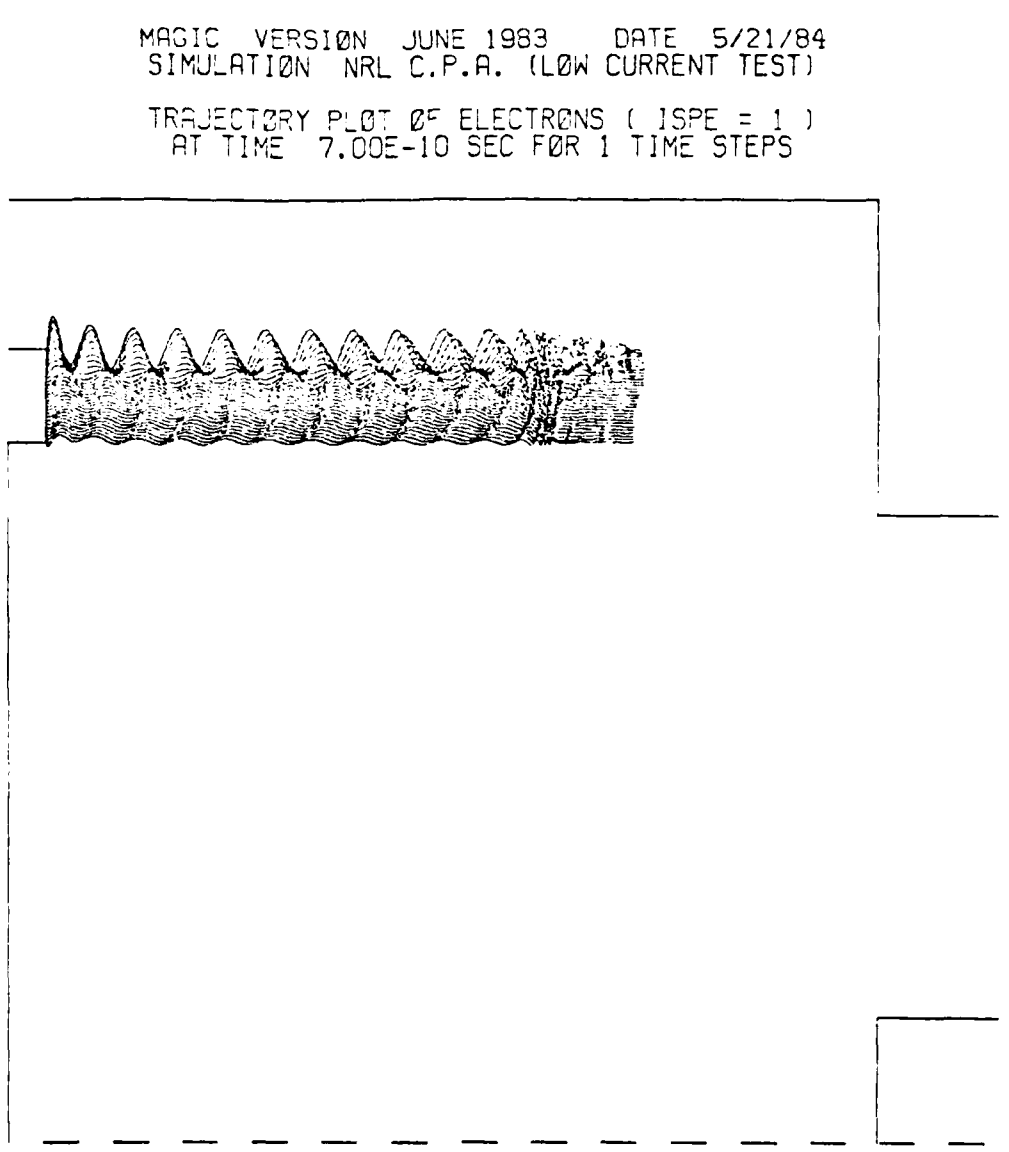

Figure 19. Electron Position Plot for Low Current Test at t = 0.70 nsec.

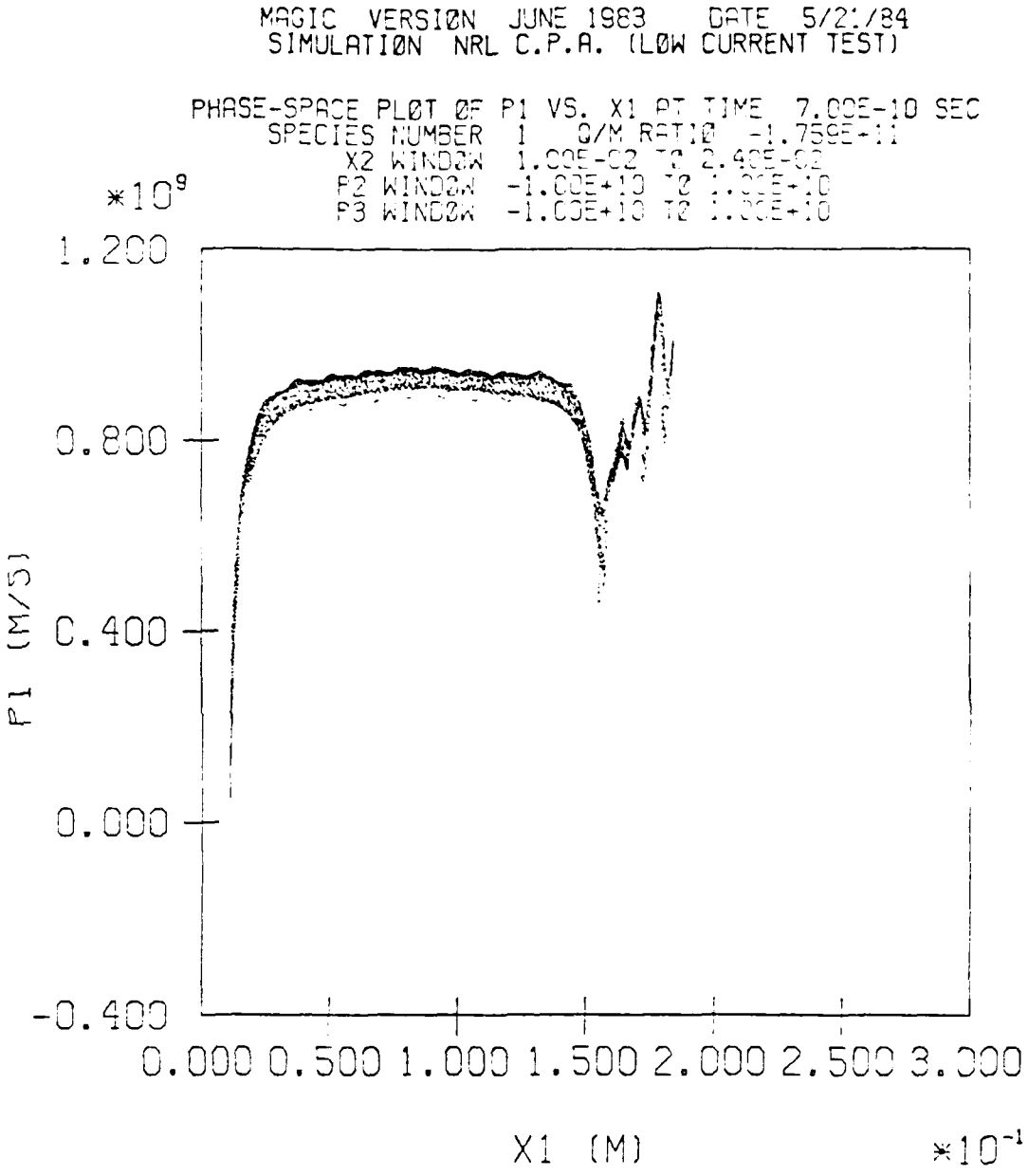

Figure 20. Phase-Space Plot of Hollow Beam Electrons for Low Current Test at t = 0.7 nsec.

As in the previous runs, the hollow beam was allowed to equilibrate for about 1.5 nsec before the rod cathode voltage pulse was turned on. This can be seen in Figure 21. The voltage plateaus at approximately 1.05 MV, which is close enough to the desired 1.0 MV. Figure 22 shows not only the established, well behaved hollow electron beam, but also an intermediate stage (at t = 2.1 nsec) of the development of the central beam. As can be seen from the phase-space plot of Figure 23, this low current hollow beam has a considerably higher value for the relativistic gamma factor. Here, γ equals 3.0 compared with about 2.4 for the previous 50 kA beam. The different current and the different beam drift velocity would lead one to expect that the hollow beam would have a substantially different effect on the physics of the central beam. Such was indeed the case. The central beam phase-space plot of Figure 24 shows very little evidence regarding the formation of any substantial virtual cathode space-charge well in the vicinity of the rod cathode tip. Instead, it displays the standard textbook attributes of an initial, sharp acceleration region, a plateau drift region, and a final, sharp acceleration region. The hollow beam is having only a marginal effect on the physics of the central beam.

To quantify the net effect, there remains only to measure the central beam current via the B_θ monitors. Figure 25 shows a time history plot of the azimuthal magnetic field strength at a radius of 2.345 cm and an axial position of Z = 23.22 cm for this case. At this radius, it encompasses both beams. Thus, at early time, it measures a B_θ of about 2.05 kG, which corresponds to a hollow beam current of 24.04 kA. The field strength begins to experience a distinct change shortly after the rod cathode is pulsed at 1.5 nsec. By t = 1.75 nsec, the presence of the central beam's reverse current is clearly seen. The precise magnitude of the central beam's current is best quantified by temporally sampling B_θ inside the radius of the hollow beam. This is shown in Figure 26 for an axial position of Z = 19.3 cm and a radius of R = 1.413 cm. The plateau field strength is about 2.74 kG, which corresponds to a central beam current of 2.12 kA.

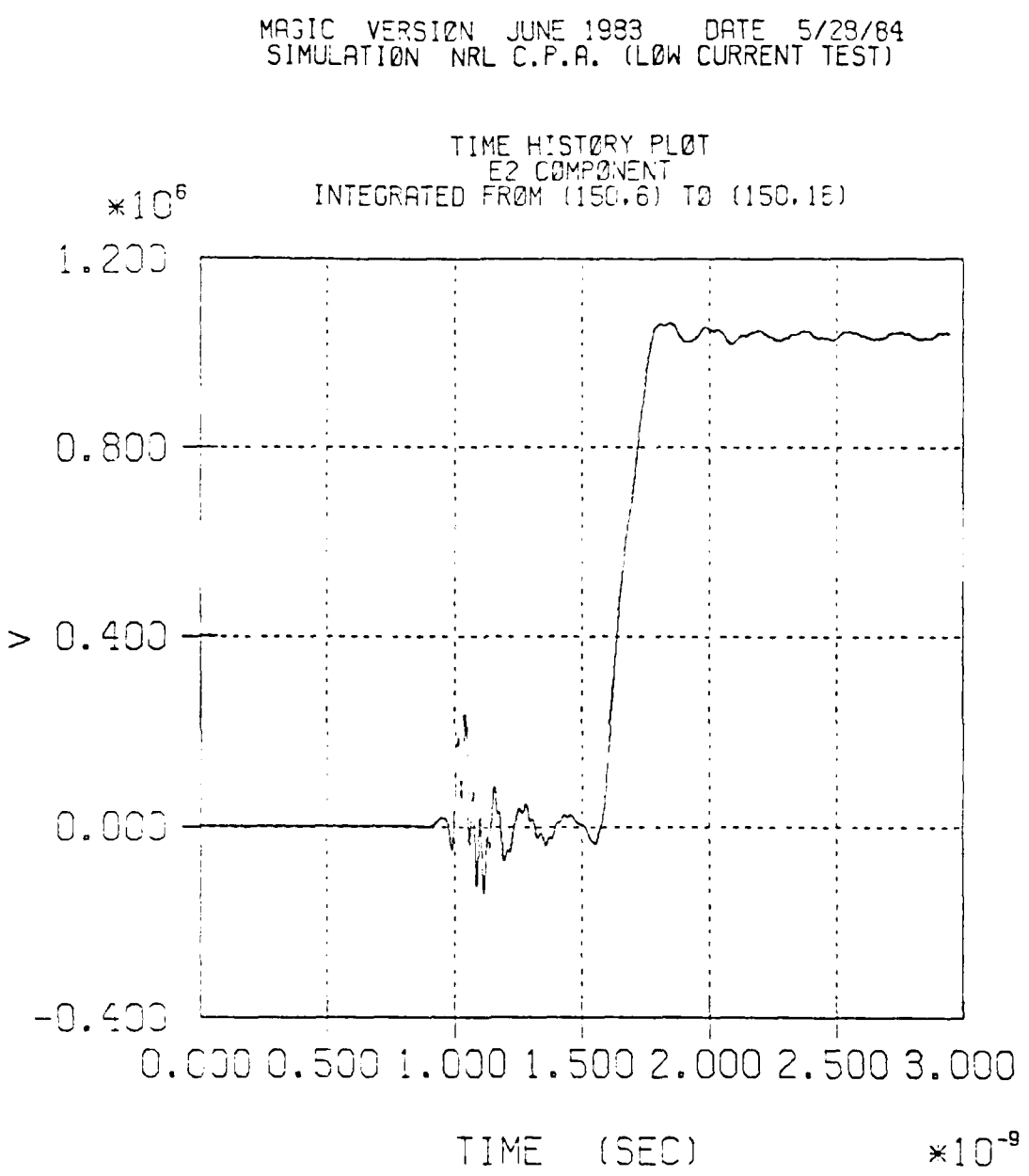

Figure 21. Rod Cathode Voltage Pulse for Low Current Test on Previous Model.

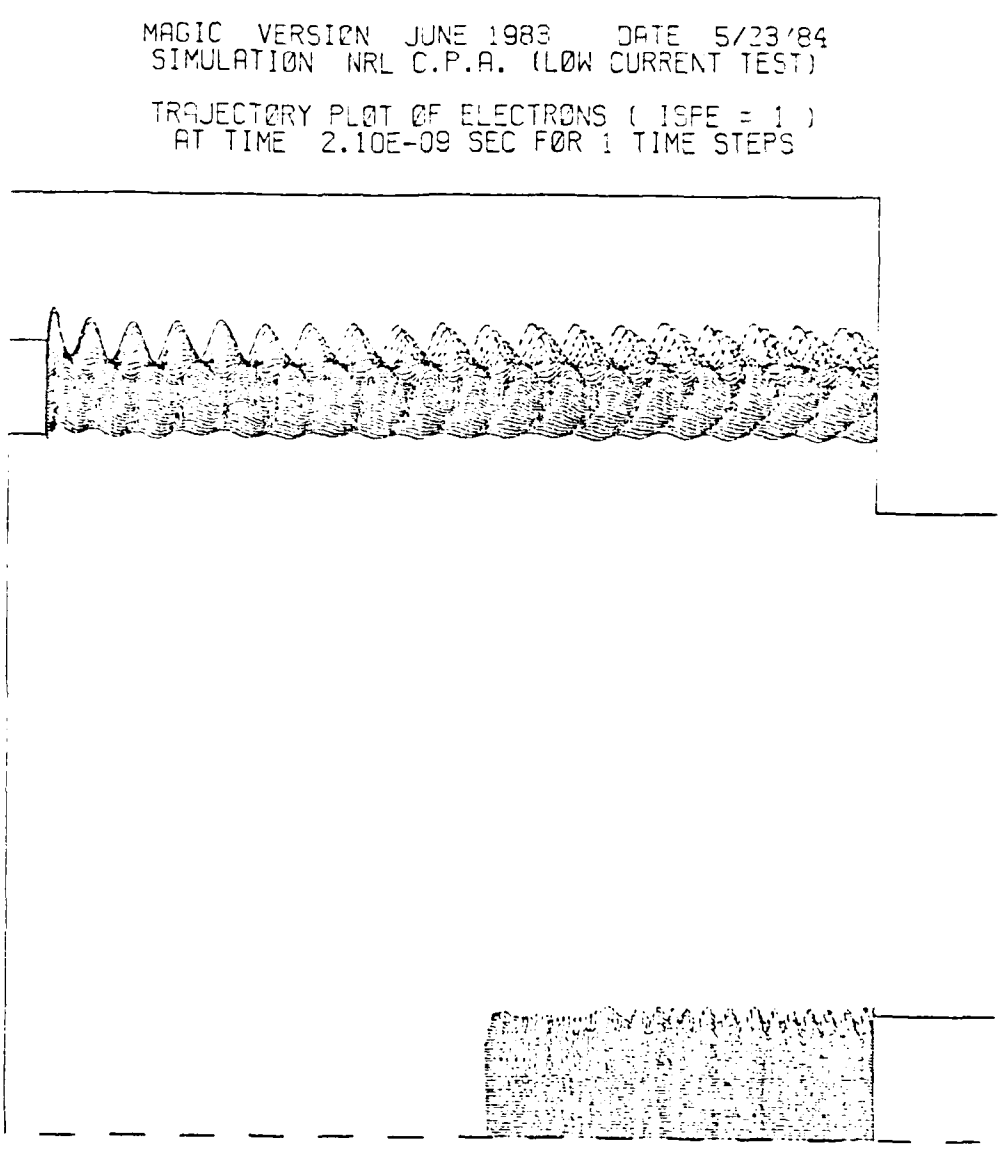

Figure 22. Electron Position Plot for Low Current Test at t = 2.1 nsec.

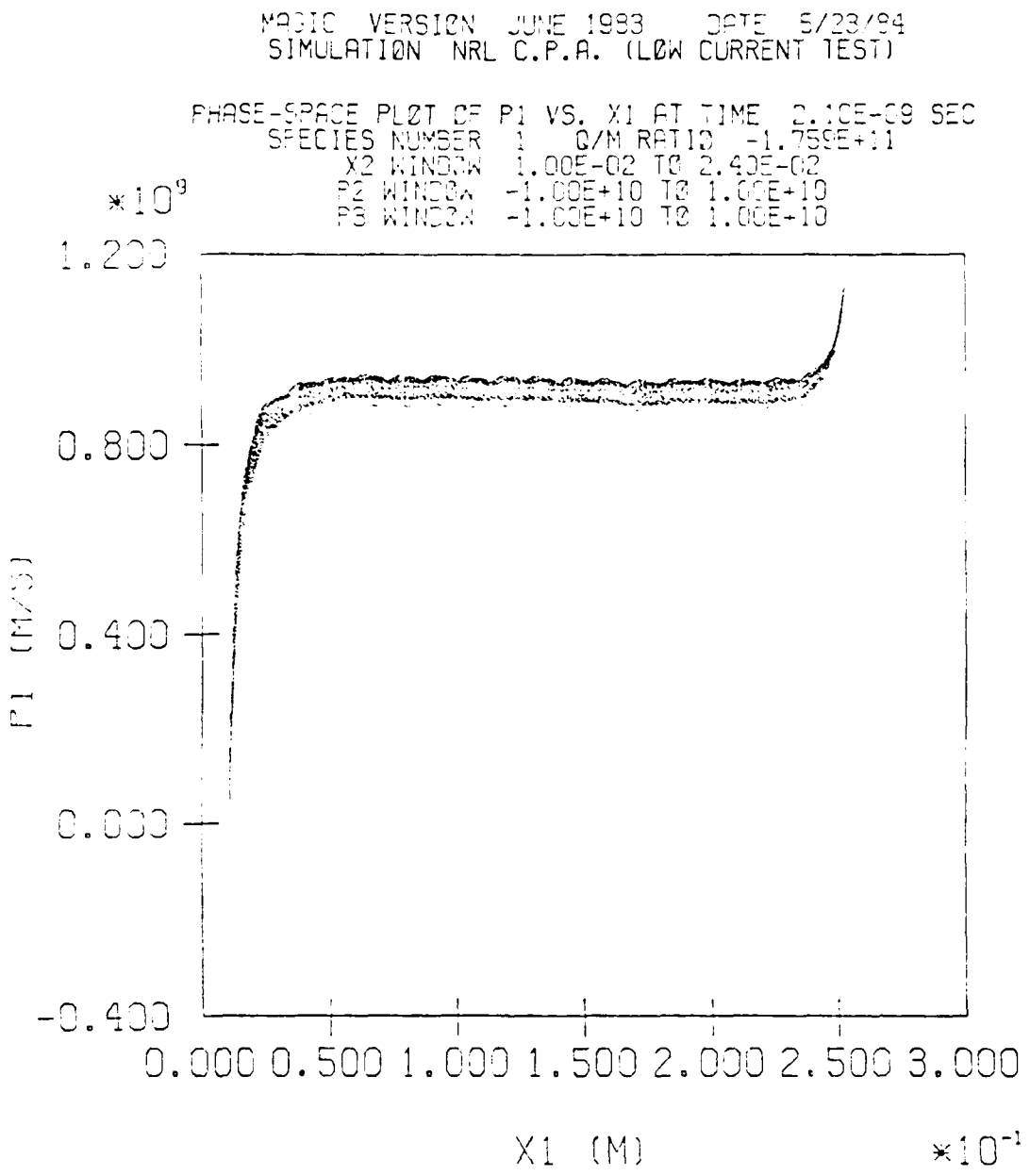

Figure 23. Phase-Space Plot of Hollow Beam Electrons for Low Current Test at t = 2.1 nsec.

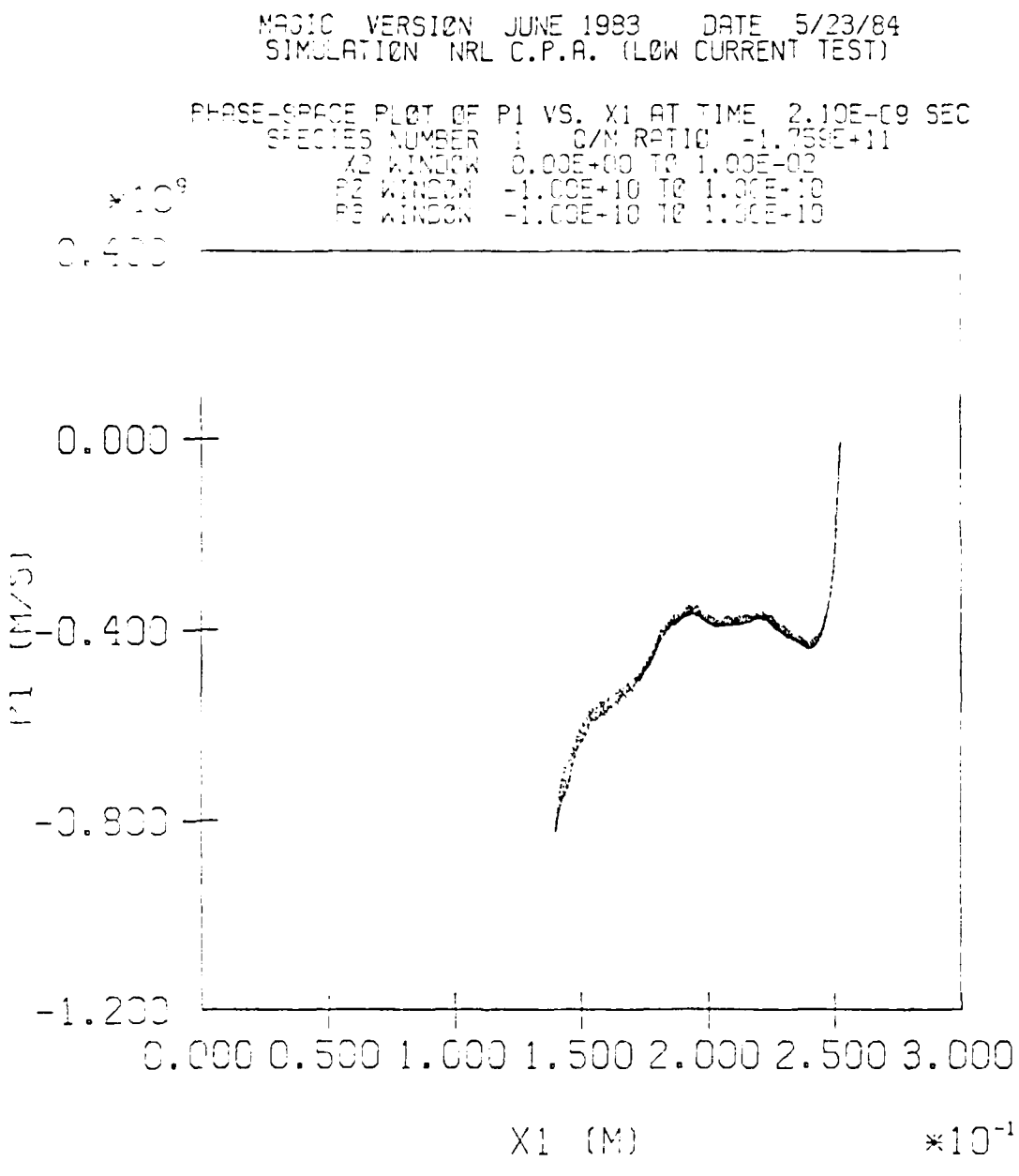

Figure 24. Phase-Space Plot of Central Beam Electrons for Low Current Test at t = 2.1 nsec.

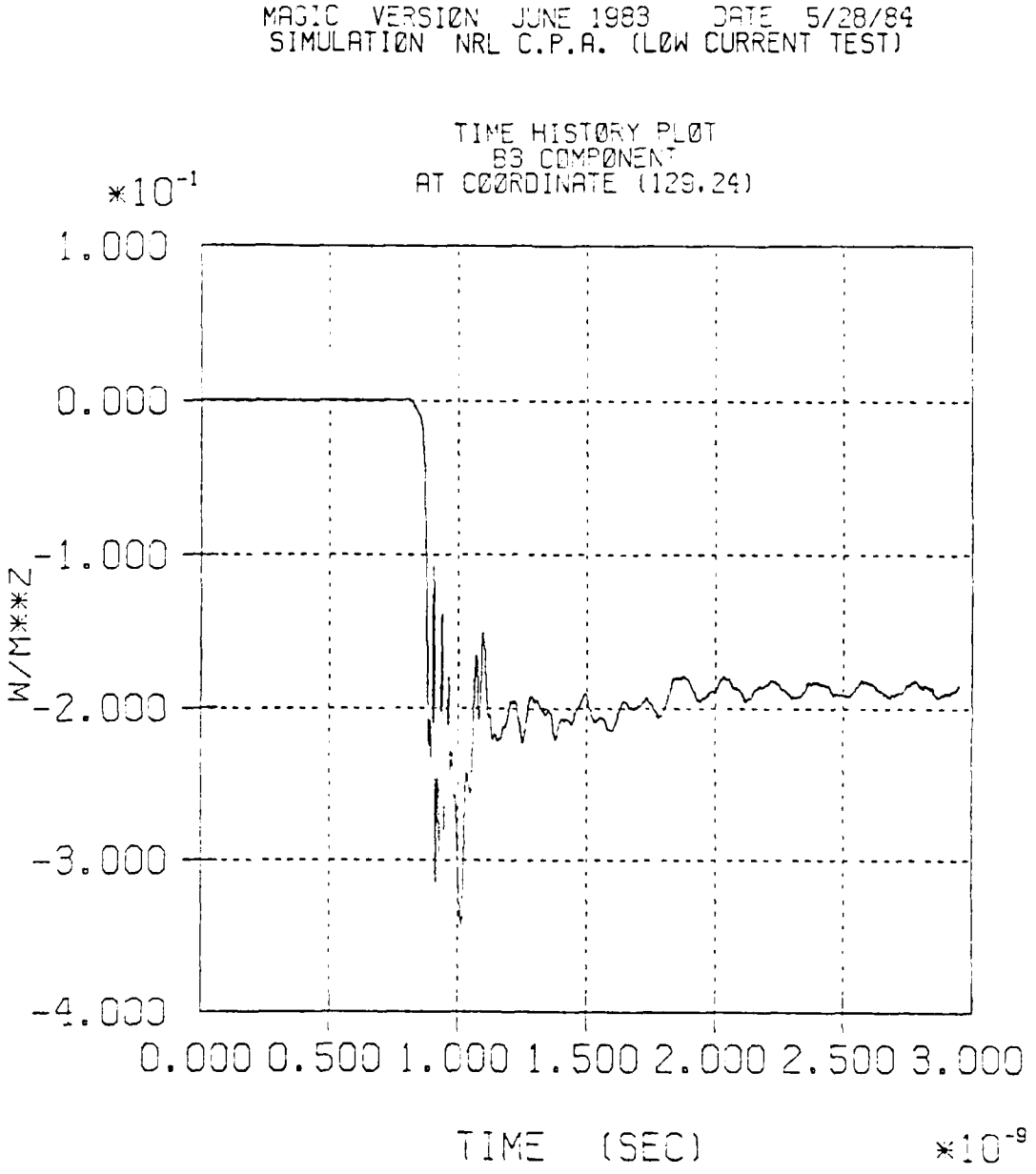

Figure 25. Time History of B_θ at a Radius of 2.345 cm for Low Current Test.

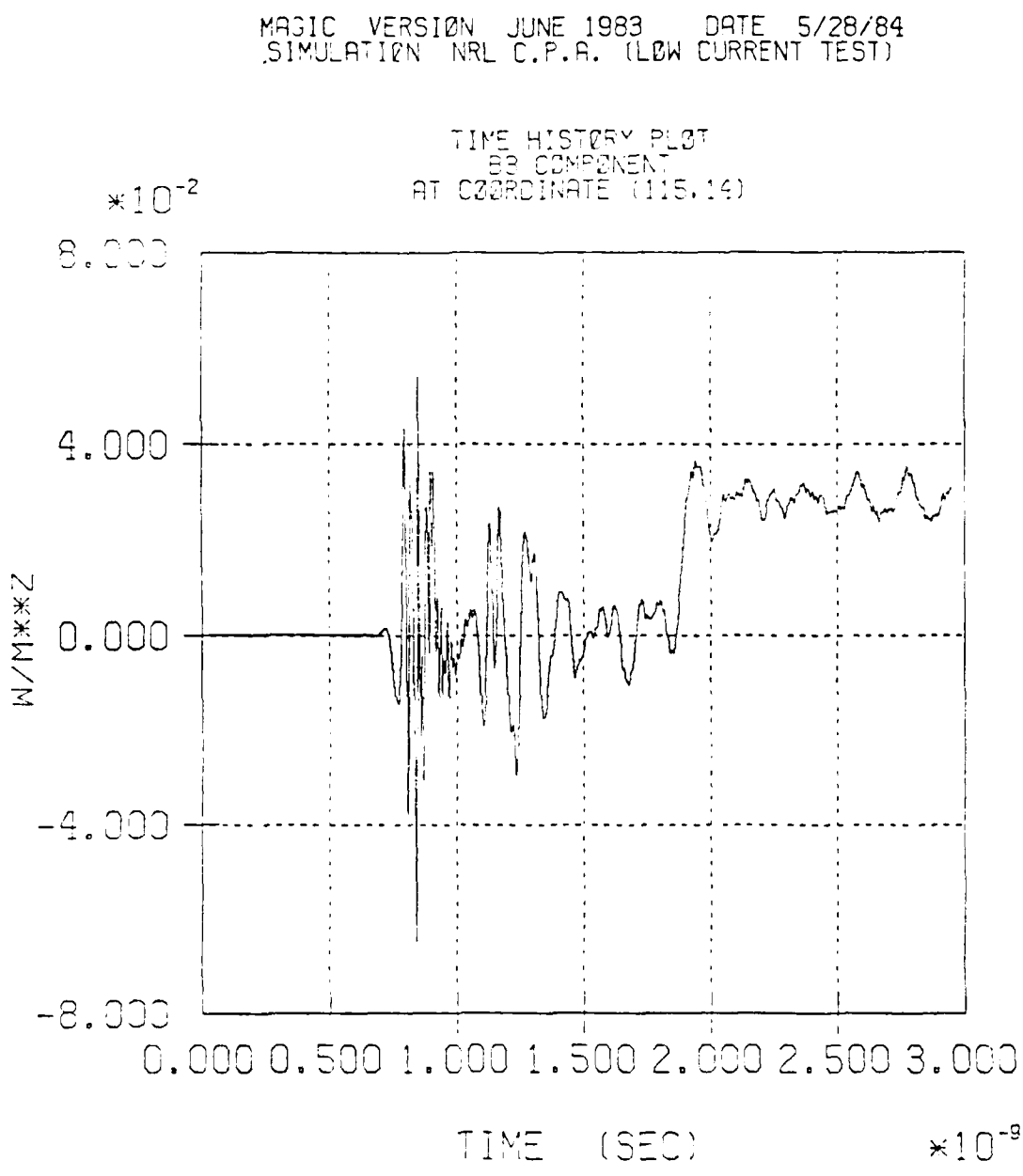

Figure 26. Time History of B_θ at a Radius of 1.413 cm for Low Current Test.

The major conclusion to be drawn from this simulation is clear; lowering the hollow beam current tends to raise the central beam current. By lowering the hollow beam current from 47 kA to 24 kA in order to more closely approximate the experiment, we doubled the central beam current from 1 kA to 2 kA.

Before leaving behind the previous numerical system model, two final test runs were conducted with it. The purpose of these final two runs was to evaluate the physical impact of substituting a numerically-applied, axial current density in place of the actual electron macroparticles being used to simulate the hollow beam. Two considerations motivated such a substitution. First, the physical dynamics of the hollow beam were not significantly effected by the central beam and, second, in transitioning to the half-meter-long model, it was desirable to save as much numerical data storage and numerical computation as possible. The elimination of discrete electrons from the hollow beam allowed the treatment of twice as many macroelectrons in the central beam (made necessary by the doubling of its length) without any increase in code running time.

The old simulation model was used to test the "pseudo-beam" concept in order to take advantage of the previous runs which were available to benchmark the results again. It was decided to rerun the two dual-beam cases with 47 kA and 24 kA in the hollow beam. The 1.5 MV pulse was applied in exactly the same fashion as before to the hollow cathode. Now, however, instead of allowing electrons to emerge from the hollow cathode tip, a uniform axial current density was applied to the data cells in the model which the actual beam had spanned. This current density was <u>not</u> simply "switched on" all across the entire axial length of the system at $t = 0$. Rather, a "pseudo-beam" front was allowed to propagate axially at a realistic beam velocity at the appropriate beam radius. The central beam continued to be treated exactly as it was before (i.e., with explicit electron macroparticles). The results of these two pseudo-beam test simulations were very satisfying. They agreed very closely with their real beam counterparts. This is shown in the summary Table 2.

TABLE 2

SUMMARY OF RESULTS USING OLD MODEL

	Hollow Beam Current (kA)	Y of Hollow Beam	Central Beam Current (kA)
Single (Central) Beam	0	N/A	2.40
Dual Beam (50 kA)	46.9	2.33	1.05
Dual Beam (25 kA)	24.0	3.0	2.12
Pseudo-Beam (50 kA)	47.5	2.4	1.13
Pseudo-Beam (25 kA)	24.4	2.4	1.94

Note: For all of the above, the axial guide B-field was kept constant at 25 kG and a voltage rise time of about 0.1 nsec was applied to the rod cathode.

4.3 SINGLE-BEAM BENCHMARK OF NEW MODEL

The remainder of this report deals with the three definitive simulations of the CPA which were conducted using the new, half-meter-long numerical model described in Section 3. In these runs, a pseudo-beam replaced the explicit hollow beam and the axial, guide B-field was reduced to a constant 15 kG. The obvious "first thing to do" was to benchmark the new model against the old model. To do this, we chose to run the single, central beam case.

The new model worked so predictably well that the run results were totally unremarkable. No voltage pulse was applied to the hollow cathode while the voltage pulse traced in Figure 27 was applied to the rod cathode. As in the runs with the old model, a rise time of about 0.1 nsec was chosen for convenience. In the absence of a hollow beam, the duration of this rise time is quite irrelevant. As desired, the voltage plateau is extremely close to 1.0 MV.

The magnitude of the azimuthal magnetic field at Z = 54.88 cm and R = 1.05 cm was monitored throughout this simulation and the resultant plot is shown in Figure 28. As the system relaxes to a steady state, the value of B_θ oscillates uniformly about a value of 0.44 kG. This indicates a central beam current of about 2.31 kA which compares very favorably with the 2.40 kA measured with the old model for the corresponding, single-beam case. The modest difference is understandable, given the slightly different plateau voltage, geometry, and axial B-field strength. These positive results encourage a high degree of confidence in the physical observations which will be drawn from the remaining two simulations.

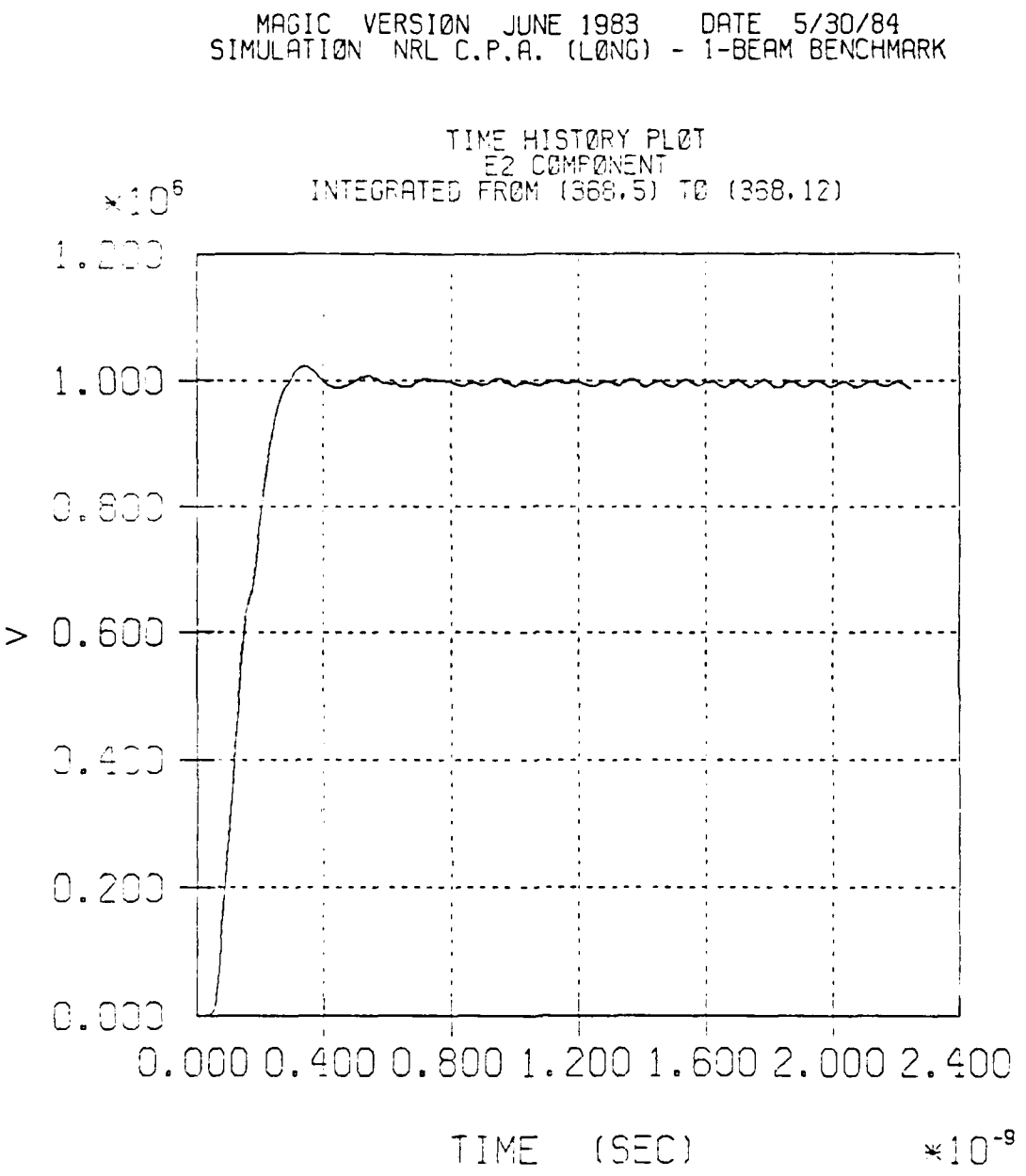

Figure 27. Temporal History of Voltage Pulse Applied to Rod Cathode for New Model Benchmark Case.

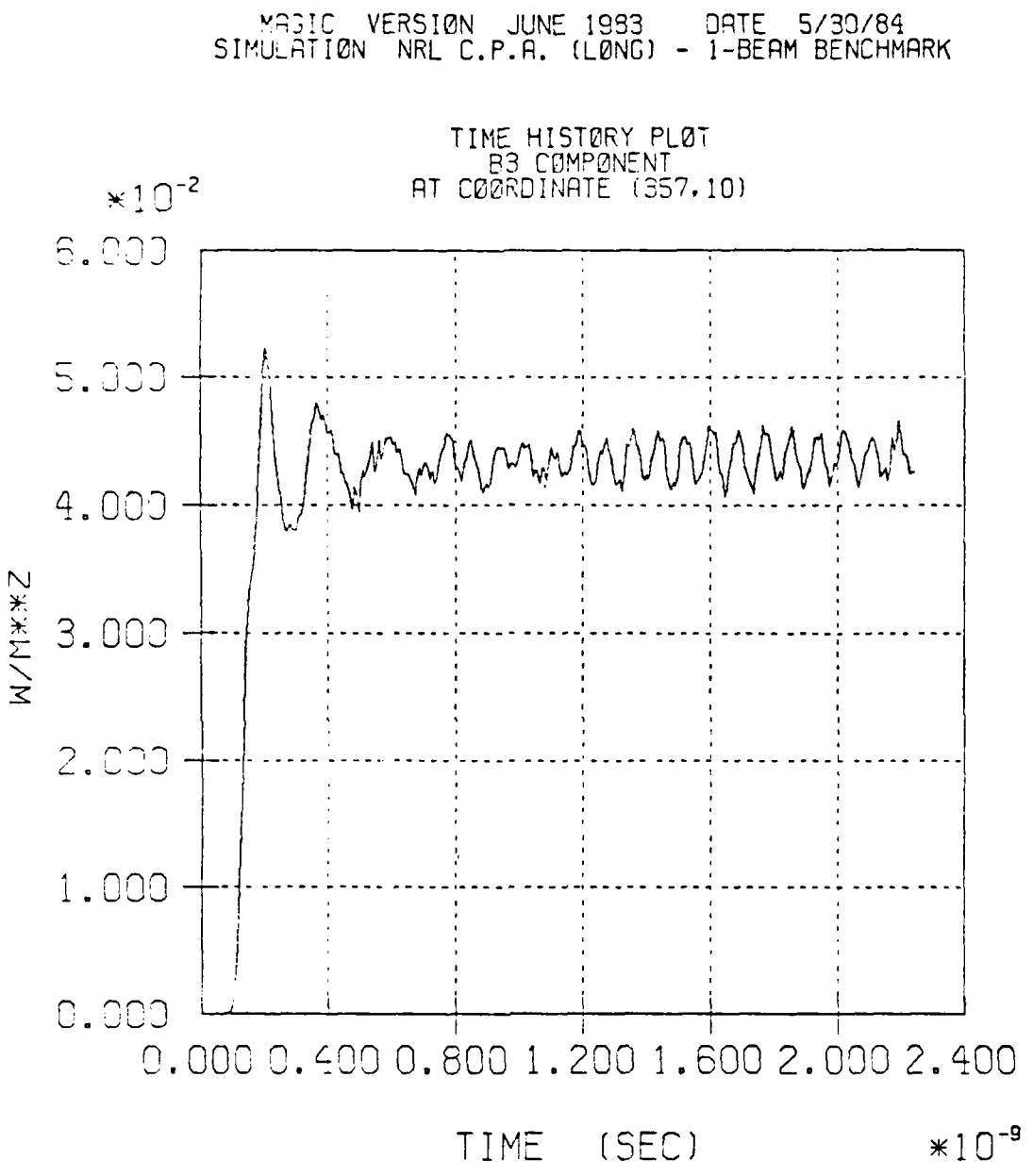

Figure 28. Temporal History of Azimuthal B-Field Strength at Z = 54.88 cm and R = 1.05 cm for the New Model Benchmark Run.

4.4 RUN WITH 1.5 NSEC RISE TIME

Having achieved a more experimentally accurate geometry, hollow beam current, and axial magnetic field strength, there remained only to examine the effects of a lengthened rise time on the performance of the CPA. A pseudo-beam of imposed, uniform, axial current density was used to mimic the presence of the hollow e-beam in both this and the following simulation. A short rise-time (~ 0.1 nsec) voltage pulse was applied to the hollow cathode as shown in Figure 29. This pulse plateaus at about 1.45 MV, which is acceptably close to the desired 1.50 MV. The corresponding voltage pulse which is applied to the rod cathode is shown in Figure 30. That pulse is not turned on until 3.0 nsec into the run. That delay allows time for the field structure in the drift tube to accommodate itself to the power influx from the hollow cathode diode. Thereafter, the voltage continues to rise linearly for another 1.5 nsec until leveling off at about 1.07 MV from t = 4.5 nsec for the duration of the run.

This new system, even with the much elongated rise time, behaved very smoothly. No evidence was found for the formation of the virtual cathode, which had significantly impeded the central beam current flow in the runs with the old model. The ease of central beam propagation is attested to by Figures 31 and 32, which present electron position plots for t = 5.25 and t = 5.60 nsec into the run. (Keep in mind that the hollow beam is present in the form of an imposed axial current density even though no particles are shown at that radius.) It appears that the beam may be divided into three distinct radial zones (corresponding to the three particle emission cells on the surface of the rod tip). The innermost zone is lightly populated. The outer two zones are densely populated. The electrons in the outermost zone are the only ones to experience significant radial oscillations.

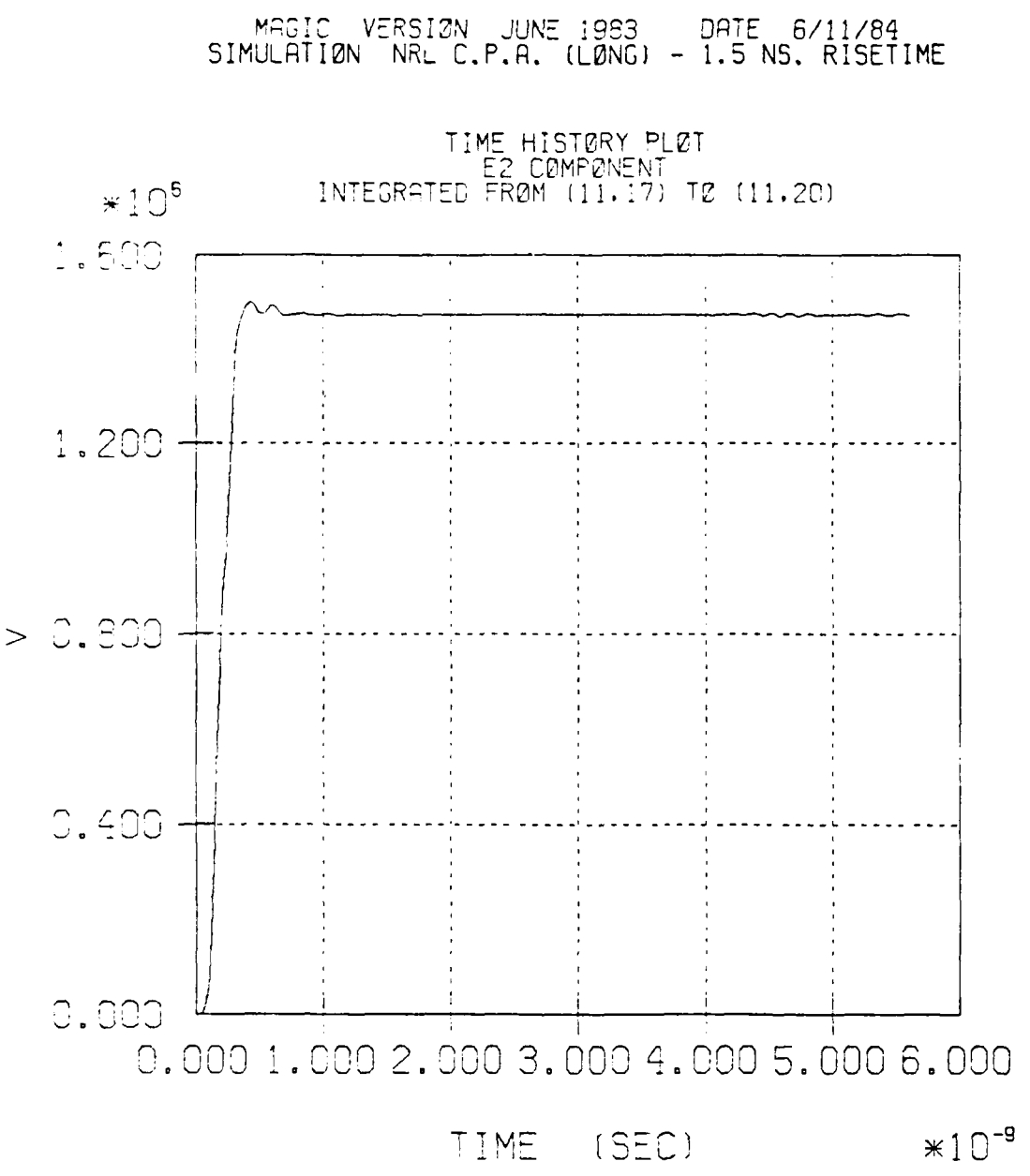

Figure 29. Hollow Cathode Voltage Pulse for the 1.5 nsec Rise-Time Run.

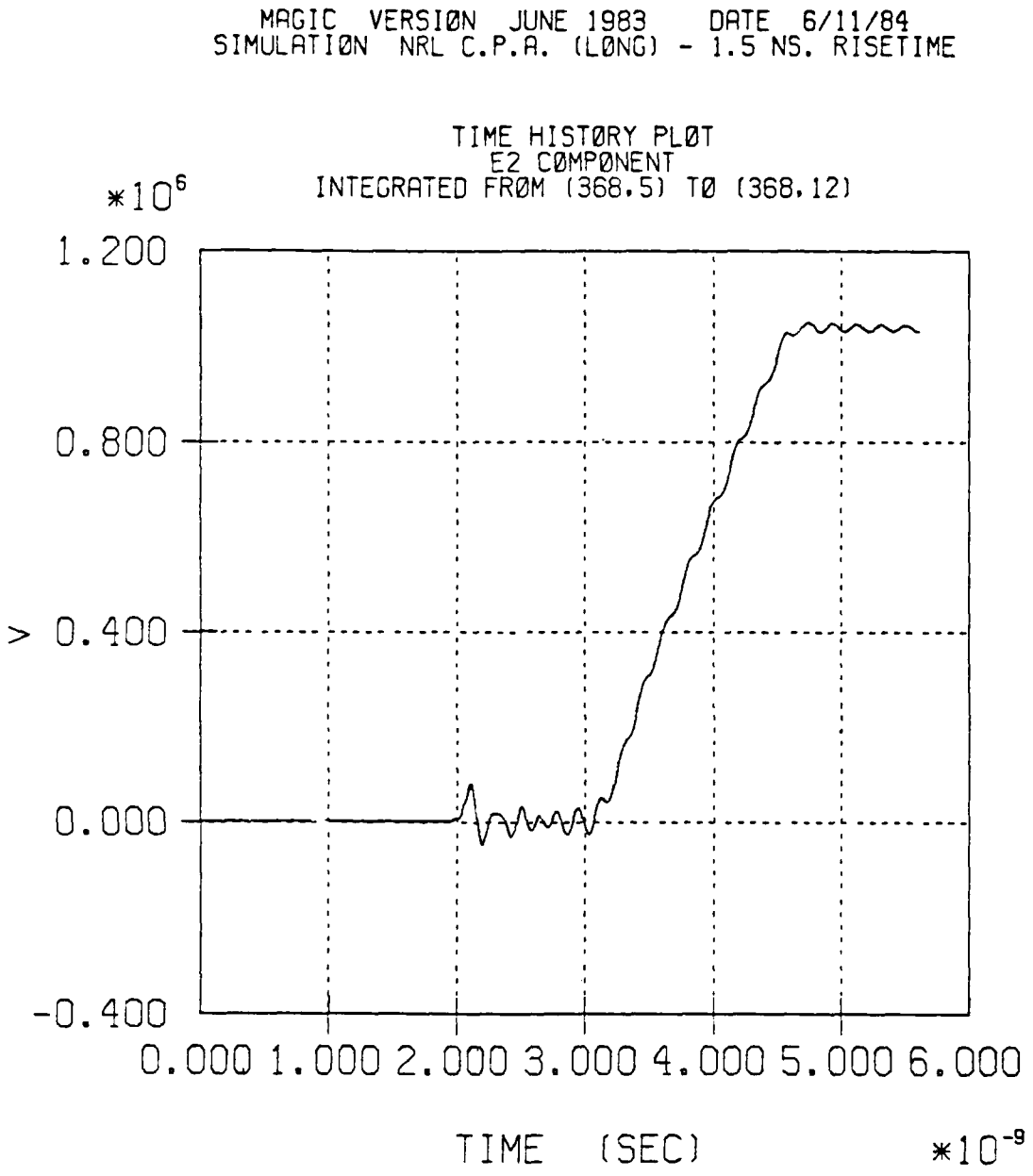

Figure 30. Rod Cathode Voltage Pulse for the 1.5 nsec Rise-Time Run.

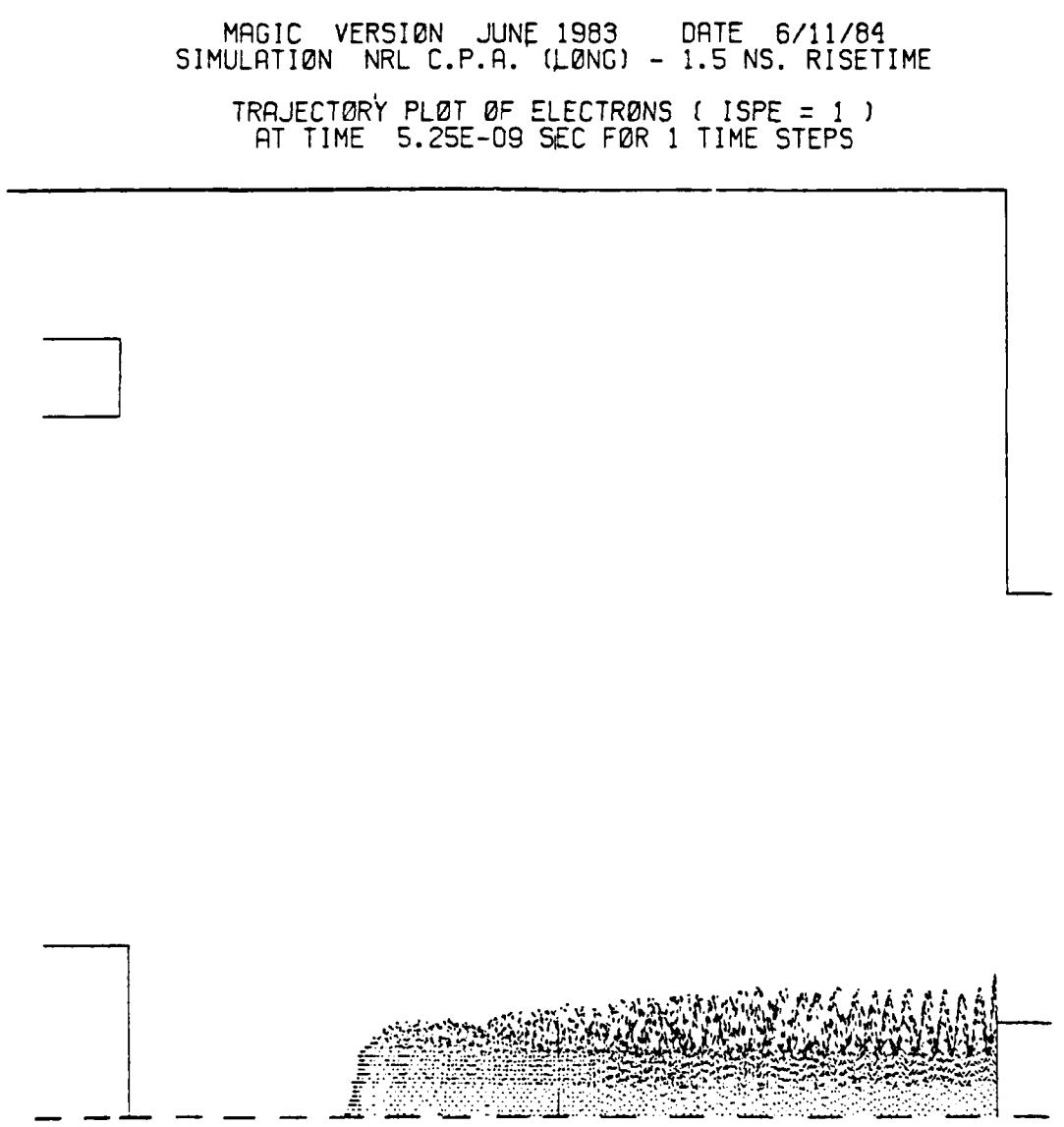

Figure 31. Electron Position Plot for 1.5 nsec Rise-Time Run at t = 5.25 nsec.

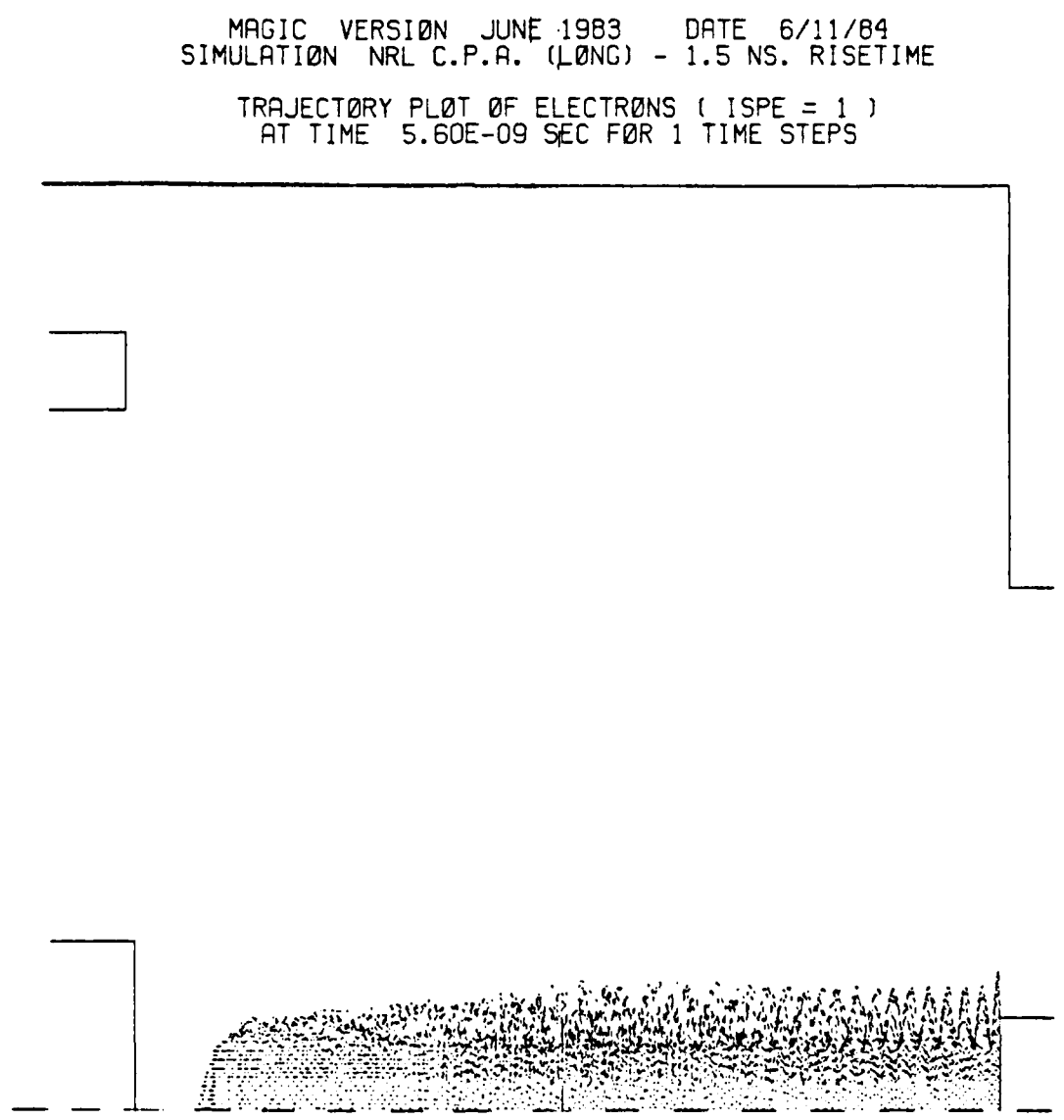

Figure 32. Electron Position Plot for 1.5 nsec Rise-Time Run at t = 5.60 nsec.

Once again, azimuthal magnetic field strength monitors were stationed at two separate radii, both inside and outside of the hollow beam. The one positioned outside the beam at R = 2.315 cm and at an axial position of 53.1 cm recorded a time dependency for B_θ as shown in Figure 33. The first plateau reading of about 2.6 kG indicates a hollow pseudo beam current of about 30 kA. The corresponding information for the central beam may be garnered from Figure 34. The readings there, taken at a radius of 1.05 cm, indicate a plateau B_θ-field strength of 0.36 kG. This determines the central beam current to be about 1.84 kA. Such a reading benchmarks quite favorably with the 2.12 kA and 1.94 kA currents measured using the previous model with a real and pseudo 24 kA hollow beam, respectively. The central beam is experiencing very little suppression due to the hollow beam in this configuration. This bodes well for the successful operation of the CPA experiment and reinforces the argument that perhaps a flaw in the experimental diagnostics failed to detect the central beam which actually <u>was propagating</u> down the 5-meter drift tube.

This simulation would have been the last in the series had it not been for two interesting points. First, it seemed possible that increasing the rise time even more (to approach the 5-10 nsec rise time in the experiment) might still further reduce the central beam current due to an increased number of low energy electrons during the start-up. Second, something very intriguing was observed in the central beam phase-space plots. An example is shown in Figure 35. Note the "bump" located at about Z = 30 cm. Was a virtual cathode being formed that might grow and travel backwards toward the rod cathode to suppress emission there? A clue to its origin could be found in the axial profiles of charge and current density given in Figure 36. The position of the "bump" seems to correspond roughly to the transition point between the voltage rise and plateau phase of the beam. In order to find out more, a 2.5 nsec rise-time run was conducted.

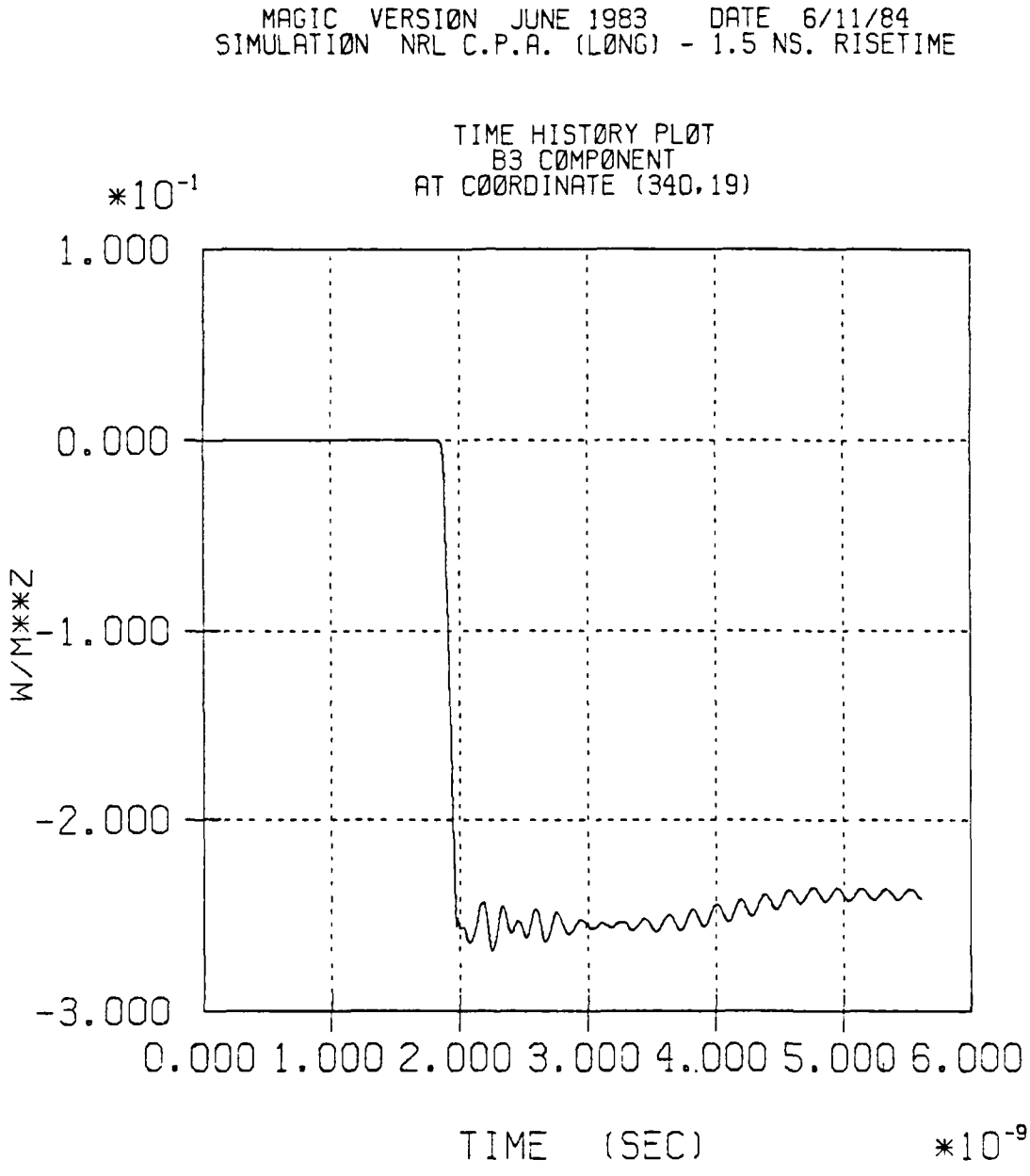

Figure 33. Time History of B_Θ at R = 2.315 cm and Z = 53.1 cm for the 1.5 nsec Rise-Time Run.

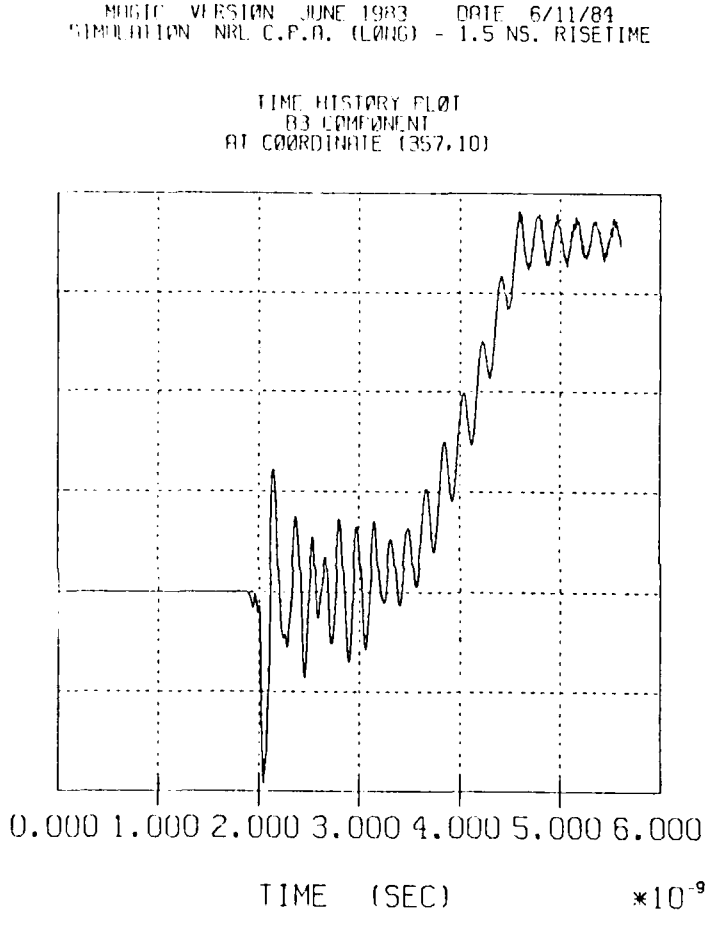

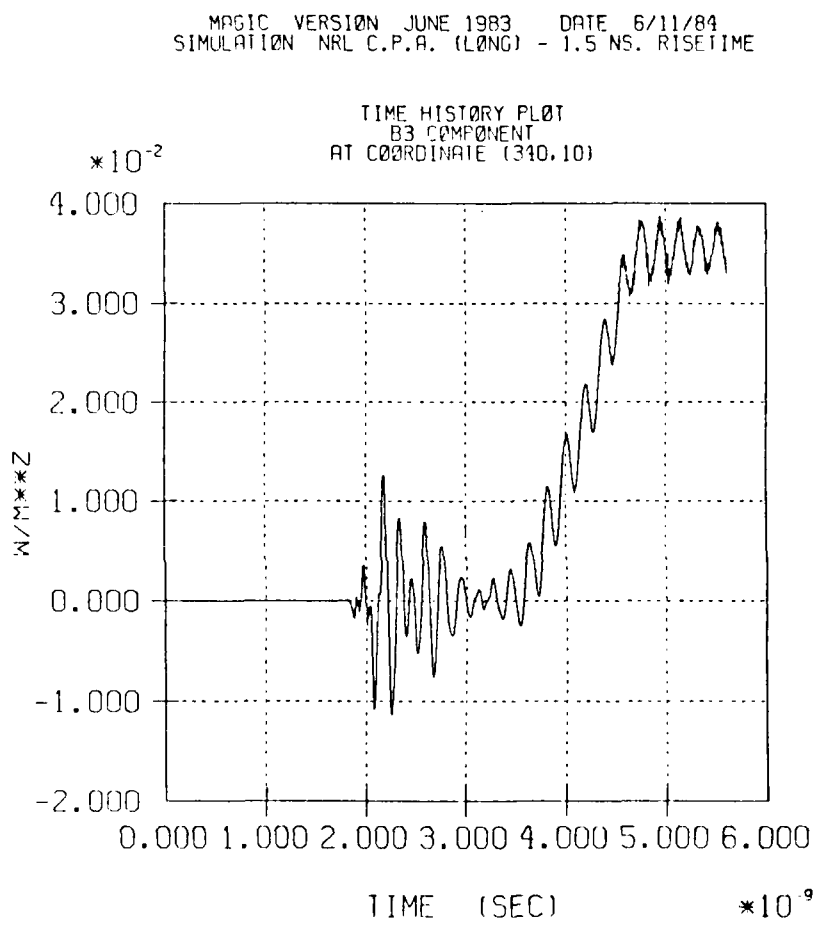

Figure 34. Time Histories of B_θ at R = 1.05 cm and Z = 54.88 cm (left) and Z = 53.1 cm (right) for the 1.5 nsec Rise-Time Run.

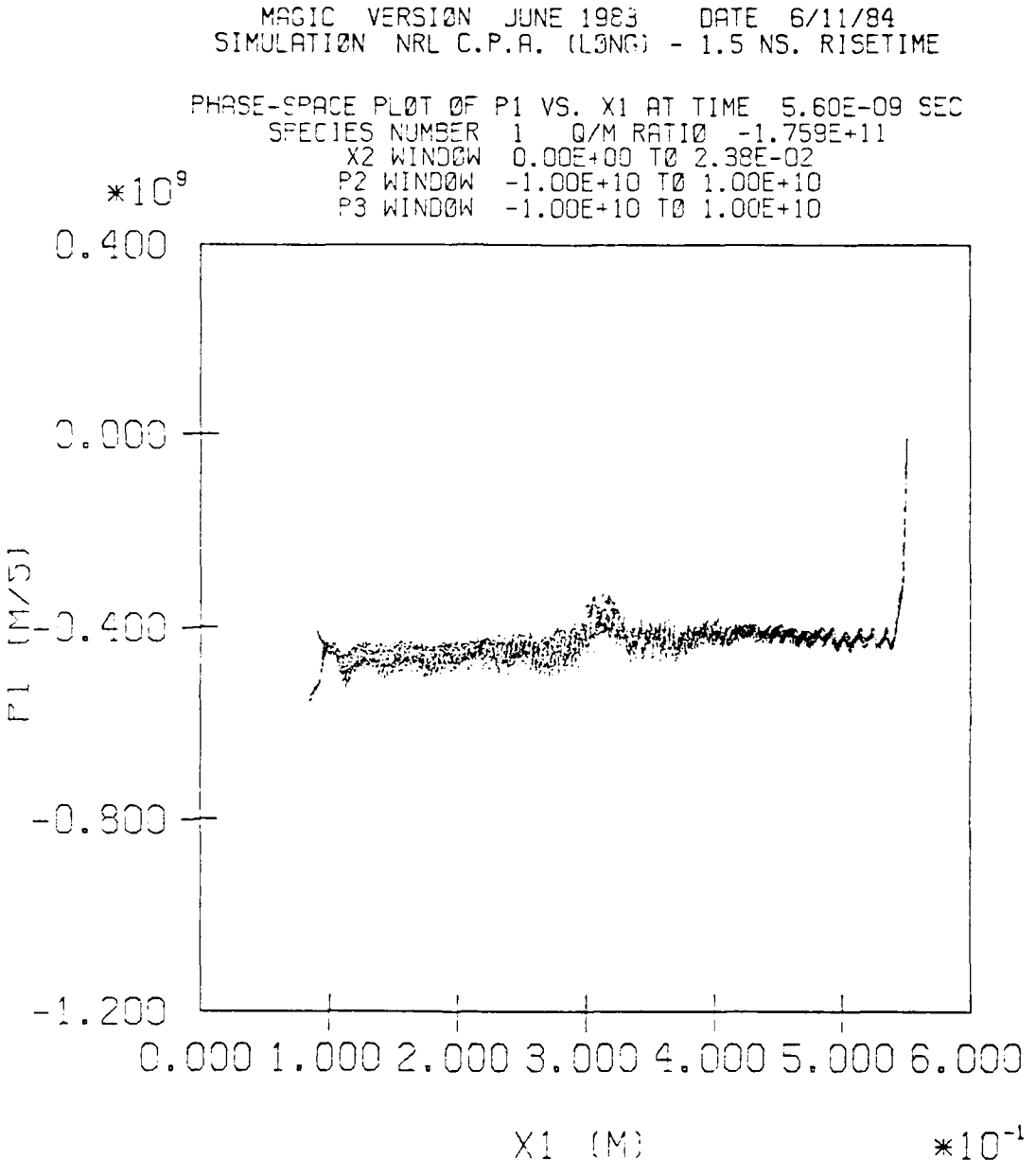

Figure 35. Phase-Space Plot for the Central Beam Electrons at t = 5.6 nsec in the 1.5 nsec Rise-Time Run.

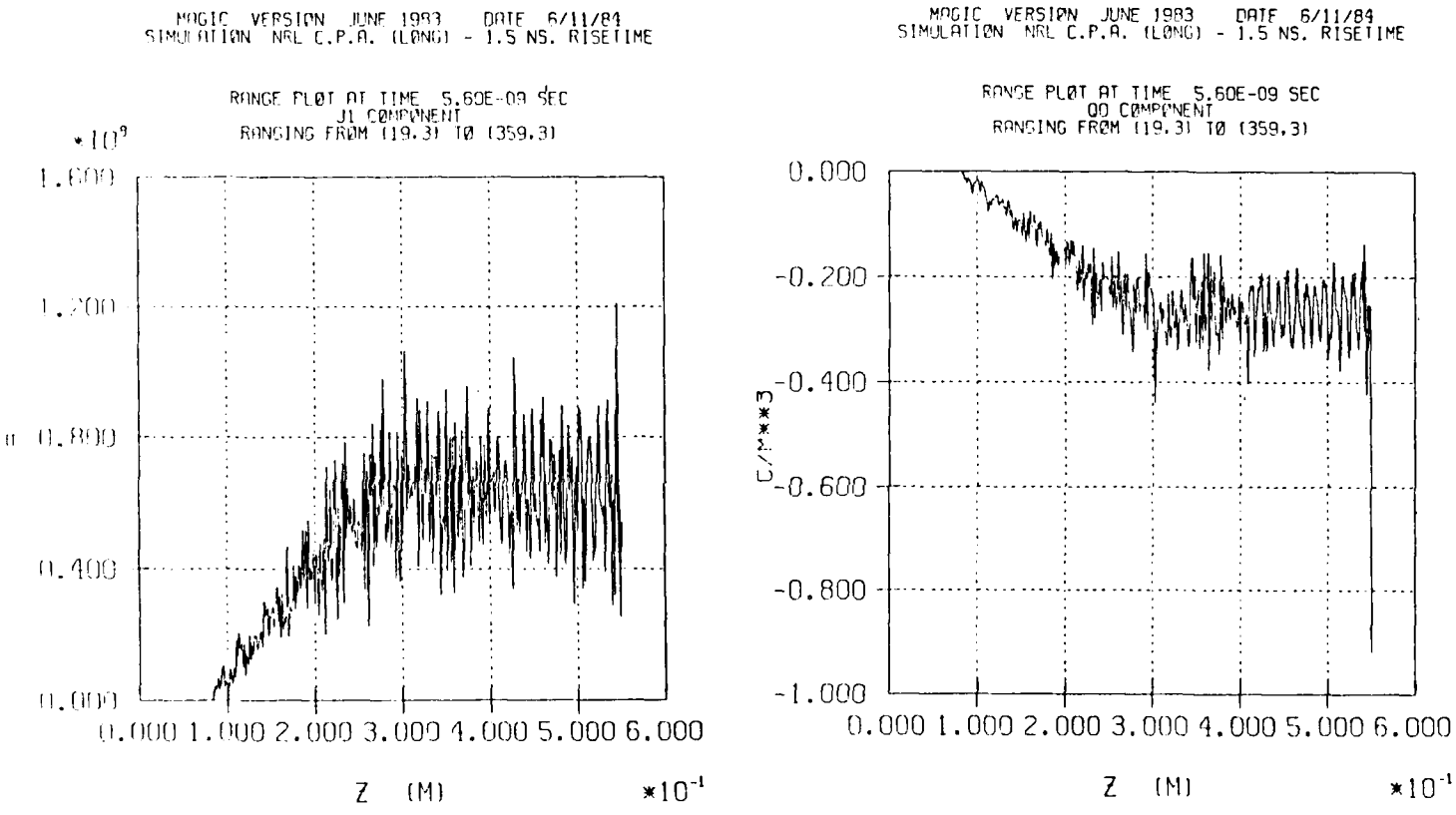

Figure 36. Axial Profiles of J_z and Charge Density at a Radius of 0.12 cm Inside the Central Beam at t = 5.6 nsec for the Rise-Time Run.

4.5 RUN WITH 2.5 NSEC RISE TIME

To execute this final simulation run in the present series, the voltages applied to the hollow and rod cathodes were changed to the temporal dependencies depicted in Figures 37 and 38, respectively. All other imposed conditions remained the same as those for the previous 1.5 nsec rise-time case. As can be seen from Figure 37, after a sharp rise, the hollow cathode voltage plateaus at approximately 1.47 MV. The rod cathode voltage of Figure 38 shows a turn on at t = 3.0 nsec into the run, followed by a linear rise for the next 2.5 nsec, followed by a plateau of about 1.07 MV. The total simulation run time was 7.0 nsec.

Lengthening the rod voltage rise time from 1.5 to 2.5 nsec had no noticeable effect on the propagation or current carrying capabilities of the central beam. Witness to this is borne by the azimuthal magnetic field strength temporal profiles presented in Figures 39 and 40. The measurements shown in Figure 39 were taken at a radius of 2.315 cm. They thus reflect the combined effects of both beams. The initial plateau of 2.55 kG represents a hollow pseudo-beam current of about 29.5 kA. After about τ = 4.0 nsec, the central beam makes its presence felt. To better gauge its magnitude, Figure 40 presents B_θ measurements taken at the same axial position but at a radius of 1.05 cm (i.e., inside the hollow pseudo-beam). The longer current rise time is clearly evident, leading to a plateau field strength of about 0.35 kG. This indicates an equilibrium current of about 1.85 kA for the central beam. This is virtually identical to the 1.84 kA measured for the 1.5 nsec rise-time run. These results are summarized in Table 3. Therefore, these simulations are consistent in their predictions of successful propagation of a significant central beam down the length of the drift tube in the preliminary CPA experiment.

The above results could hardly be described as exciting. A closer look at the detailed diagnostics, however, sheds significant new light on the nature of that phase-space "bump" observed in the 1.5 nsec

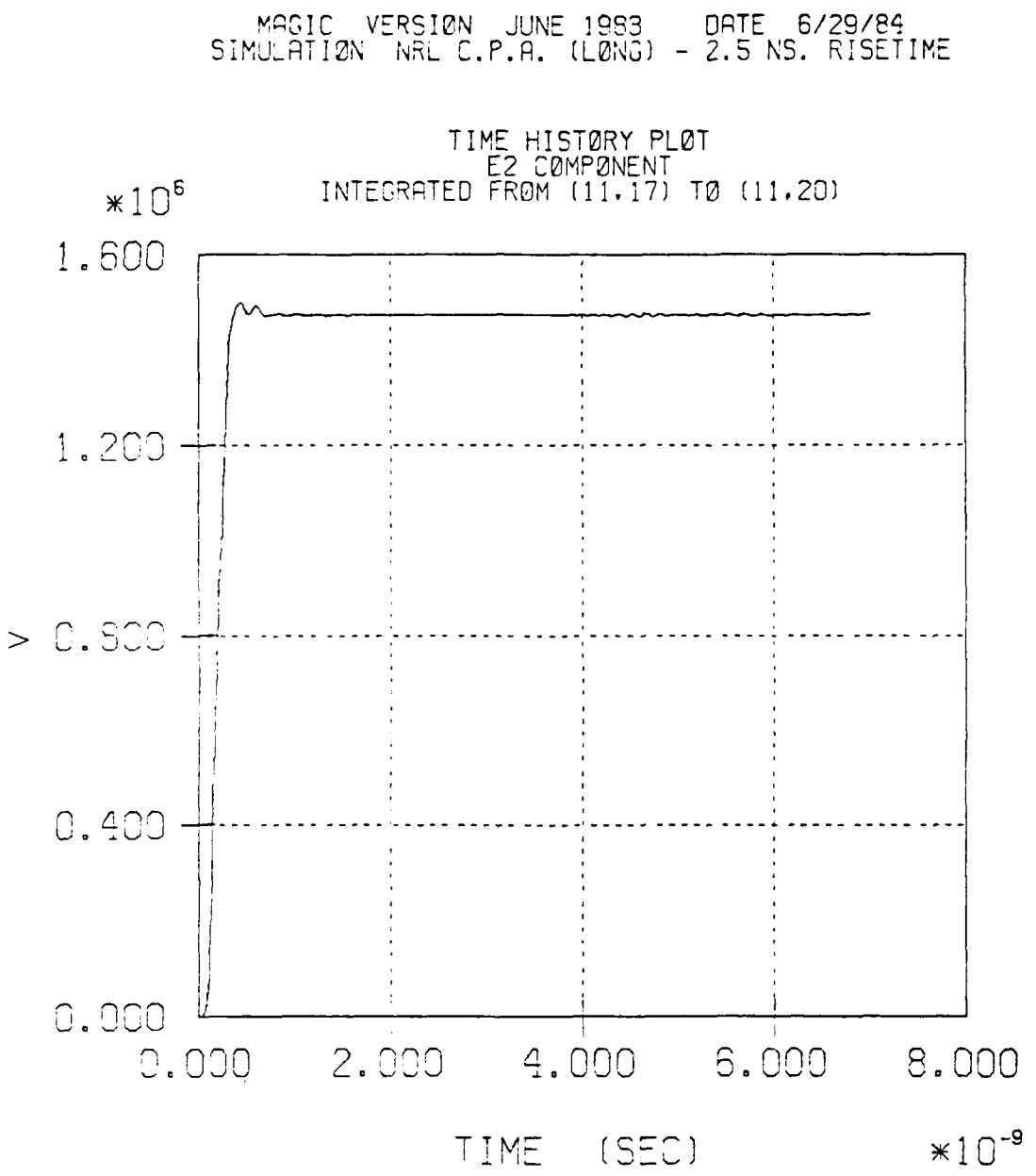

Figure 37. Time History of Hollow Cathode Voltage for the 2.5 nsec Rise-Time Run.

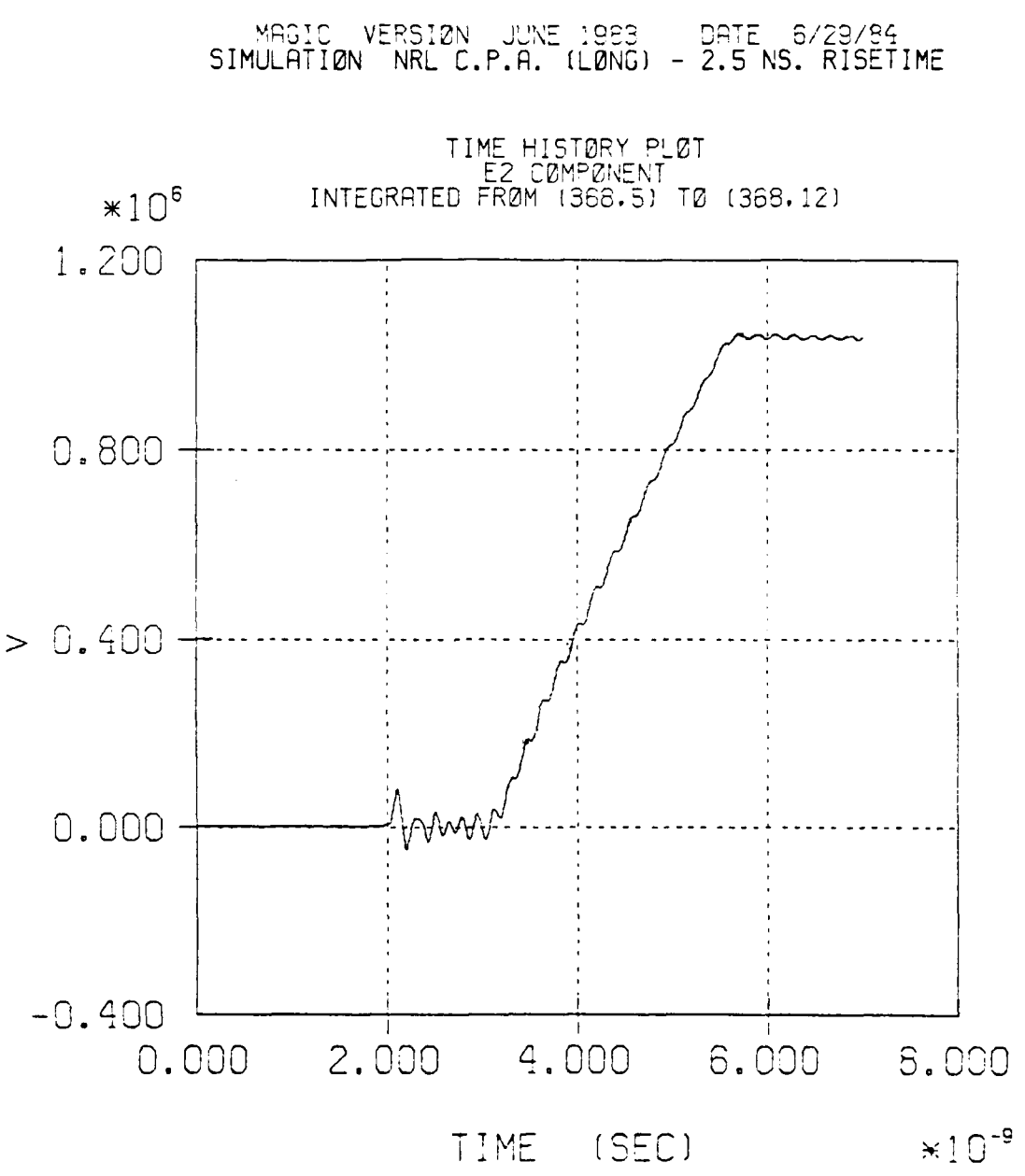

Figure 38. Time History of Rod Cathode Voltage for the 2.5 nsec Rise-Time Run.

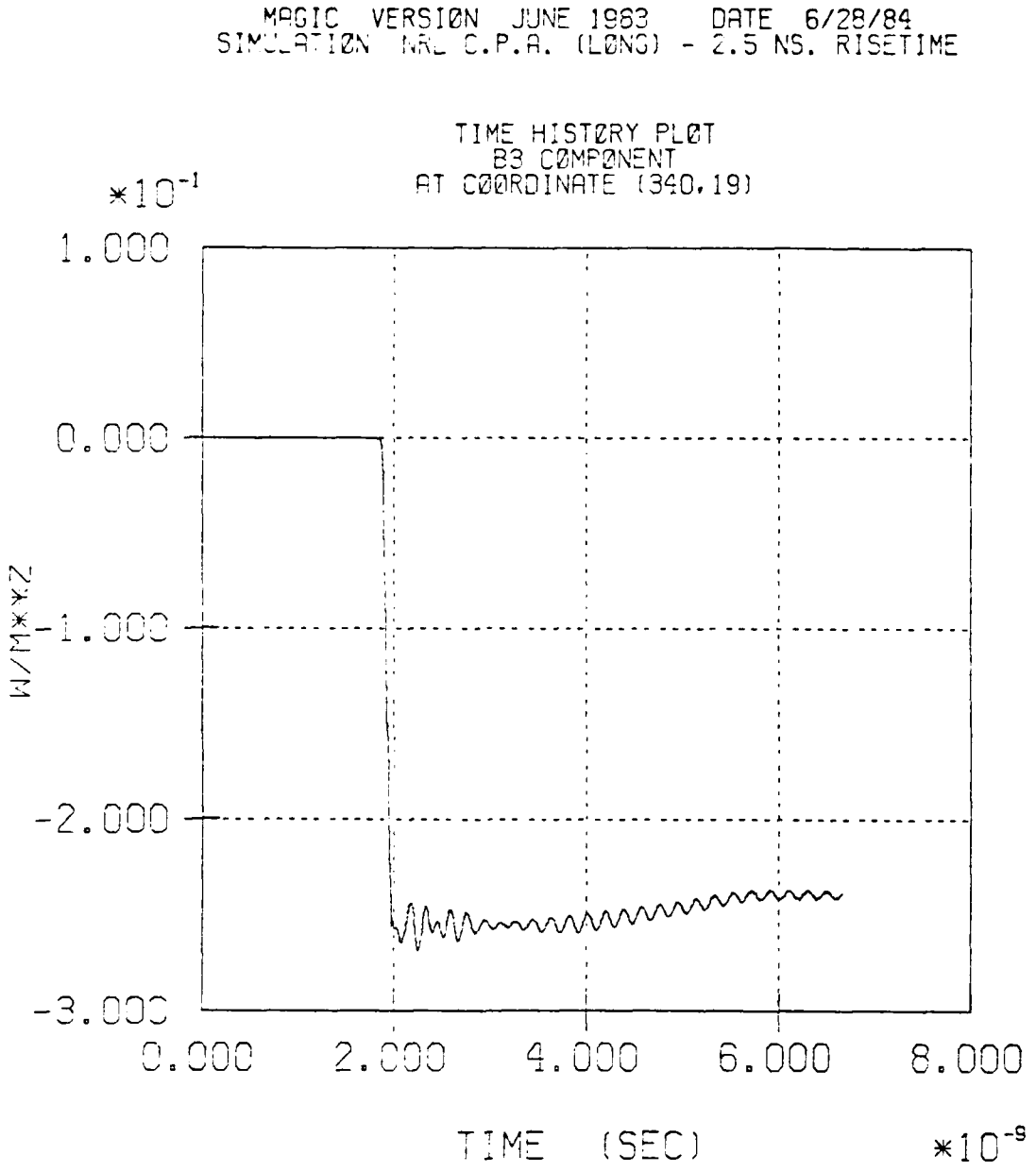

Figure 39. Time History of B_θ at R = 2.315 cm and Z = 53.1 cm for the 2.5 nsec Rise-Time Run.

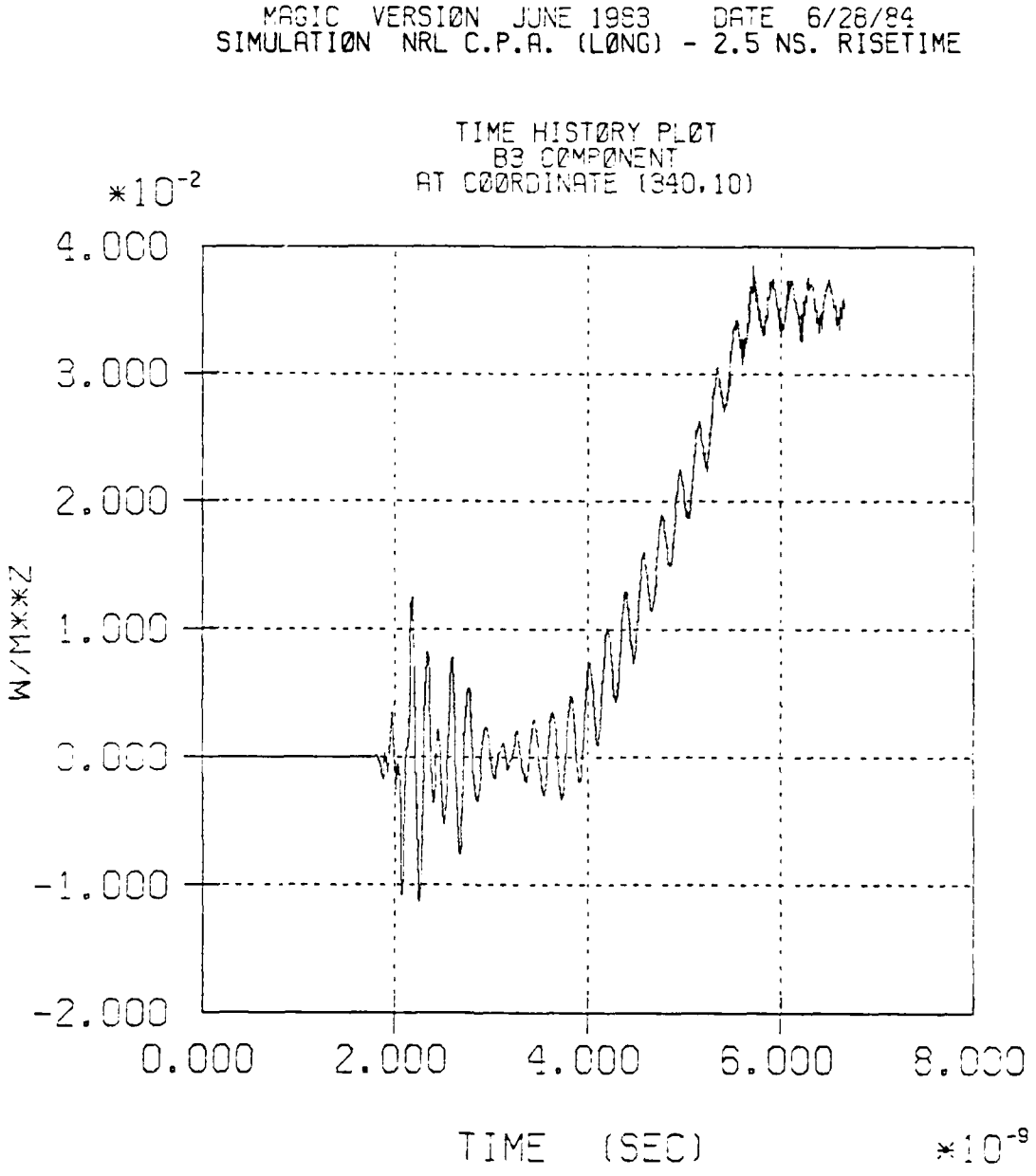

Figure 40. Time History of B_z at R = 1.05 cm and Z = 53.1 cm for the 2.5 nsec Rise-Time Run.

TABLE 3

SUMMARY OF RESULTS FROM THE NEW MODEL

	Hollow Beam Current (kA)	Rod Cathode Voltage Rise Time (nsec)	Central Beam Plateau Current (kA)
Central Beam Only	0	~ 0.1	2.31
1.5 nsec Rise Time	29.5	1.5	1.84
2.5 nsec Rise Time	29.5	2.5	1.85

Note: Only pseudo beams were used for the hollow beam, the hollow beam voltage rise time was always 0.1 nsec, and the imposed axial magnetic field was 15 kG throughout.

run. First, examine the series of sample electron position plots shown in Figures 41 through 45. These trajectory "snapshots" are temporally equispaced during the lifetime of the central beam. If studied carefully, they each reveal an axially narrow region of slightly enhanced electron number density. Following through from picture to picture, this density anomoly can be seen to move farther and farther to the left, although lagging significantly behind the head of the beam. The propagation of this structure is much more easily seen in the central beam electron phase-space plots of Figures 46 through 50. In these, the density anomoly stands out as a "bump" which slows down the electrons behind it and accelerates the electrons in front of it. From frame to frame, the bump moves steadily leftward. (Note that there exists a one-to-one correspondence between these phase-space "snapshots" and the previous set of position plots.) Just out of curiousity, the axial position of the peak of the bump was plotted as a function of time in Figure 51. It appears to show an initial phase of smooth acceleration which transitions at about t = 5.8 nsec into a constant velocity phase. The magnitude of that constant terminal velocity is approximately 1.17×10^{10} cm/sec.

The status of this phase-space "bump," as an axial density anomoly, is endorsed by the axial charge density profiles measured at a radius of 0.12 cm all down the drift tube at fixed points in time. These profiles are shown in Figures 52 through 54. (Note in viewing these plots that negative charge density is being measured. Thus, the zero point lies along the top border of the plot.) Unfortunately, these diagnostics were generated only half as frequently as were the particle position and phase-space plots. Still, they afford a more than adequate time sequence showing the formation, movement, and steady erosion of the density clump. For the same instants in time, the position of this density enhancement coincides precisely with the phase-space "bump." Yet another reference point for this phenomenon may be found in the axial electric field strength profiles. These were measured and plotted for the same instants in time as the charge density plots, but were accomplished at a uniform radius of 0.2 cm. They are shown in Figures 55 through 57. Once again, the positional correlation was exact.

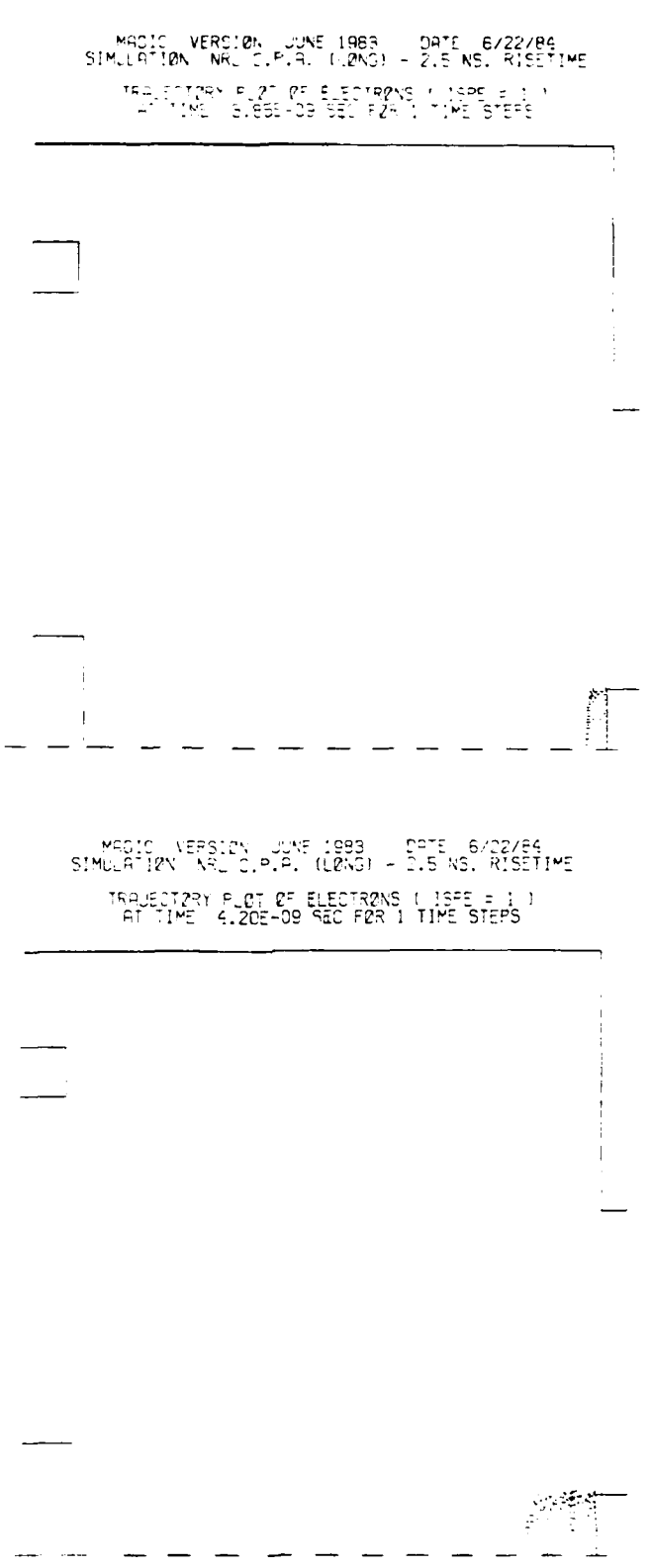

Figure 41. Sample Electron Position Plots at t = 3.95 nsec (top) and t = 4.20 nsec (bottom) for the 2.5 nsec Rise-Time Run.

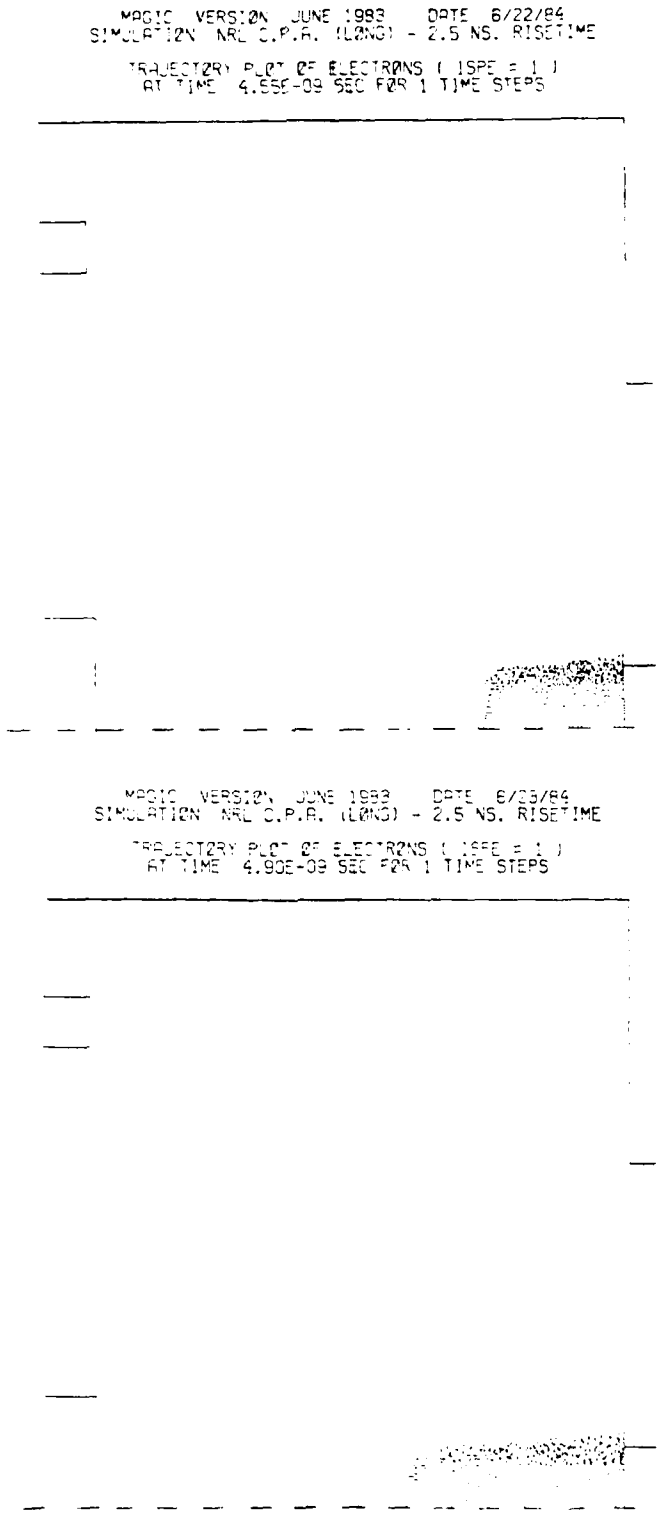

Figure 42. Sample Electron Position Plots at t = 4.55 nsec (top) and t = 4.90 nsec (bottom) for the 2.5 nsec Rise-Time Run.

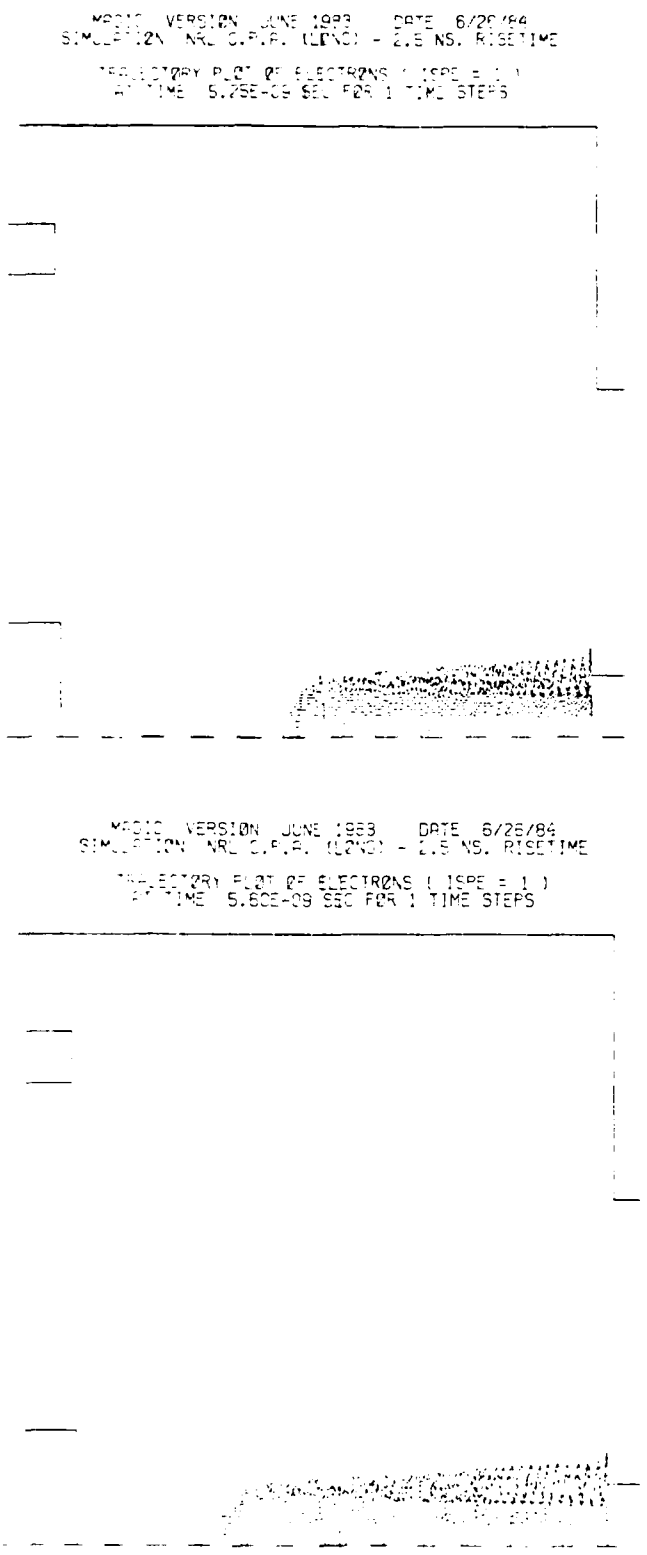

Figure 4-3. Sample Electron Position Plots at t = 5.25 nsec (top) and t = 5.60 nsec (bottom) for the 2.5 nsec Rise-Time Pulse.

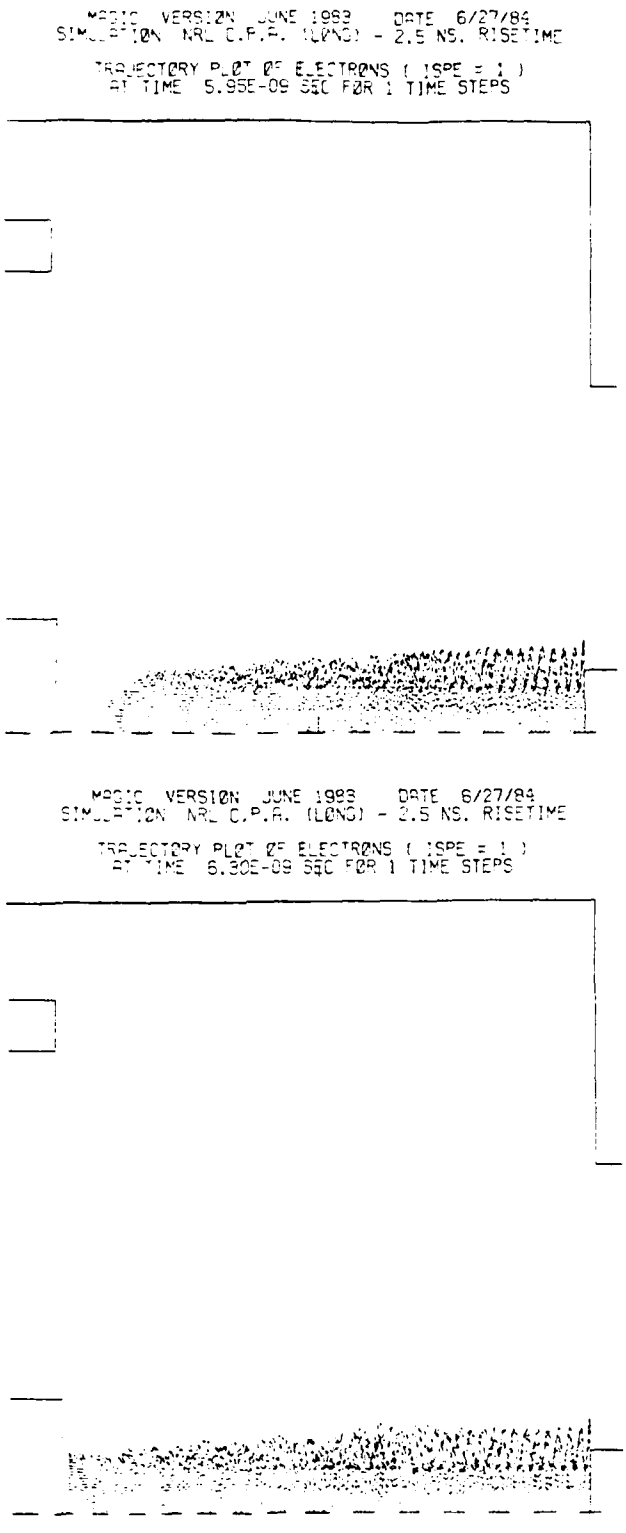

Figure 44. Sample Electron Position Plots at t = 5.95 nsec (top) and t = 6.30 nsec (bottom) for the 2.5 nsec Rise-Time Run.

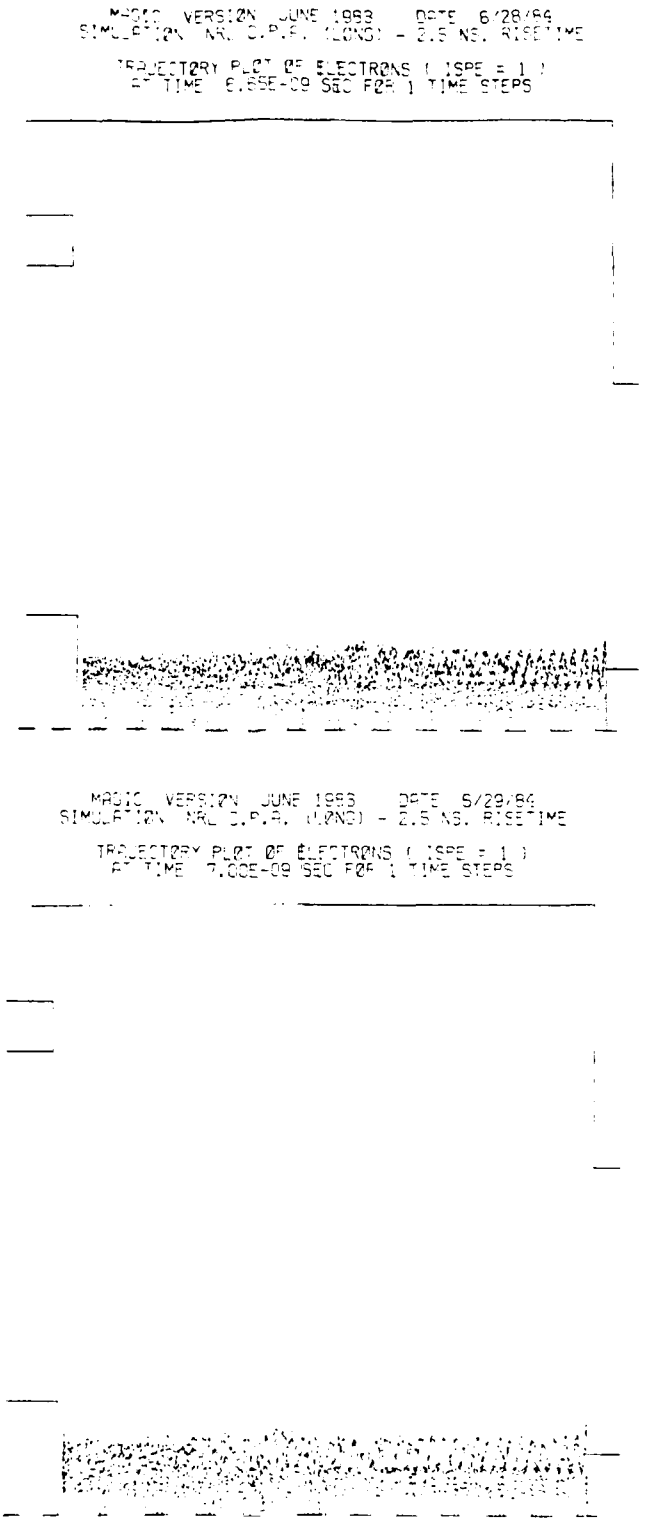

Figure 45. Sample Electron Position Plots at t = 6.65 nsec (top) and t = 7.00 nsec (bottom) for the 2.5 nsec Rise-Time Run.

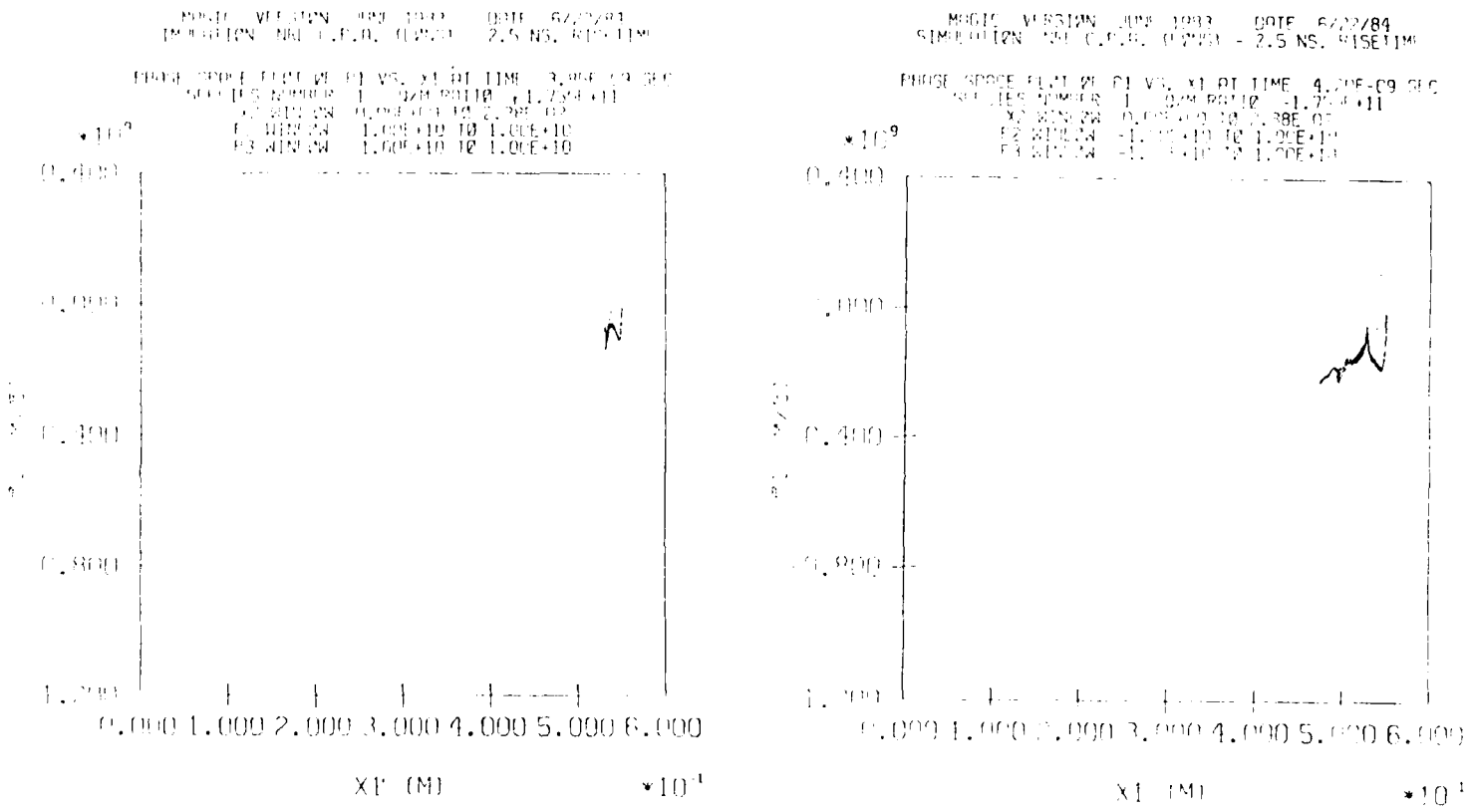

Figure 46. Electron Phase-Space Plots at t = 3.85 nsec (left) and t = 4.20 nsec (right) for the 2.5 nsec Rise-Time Run.

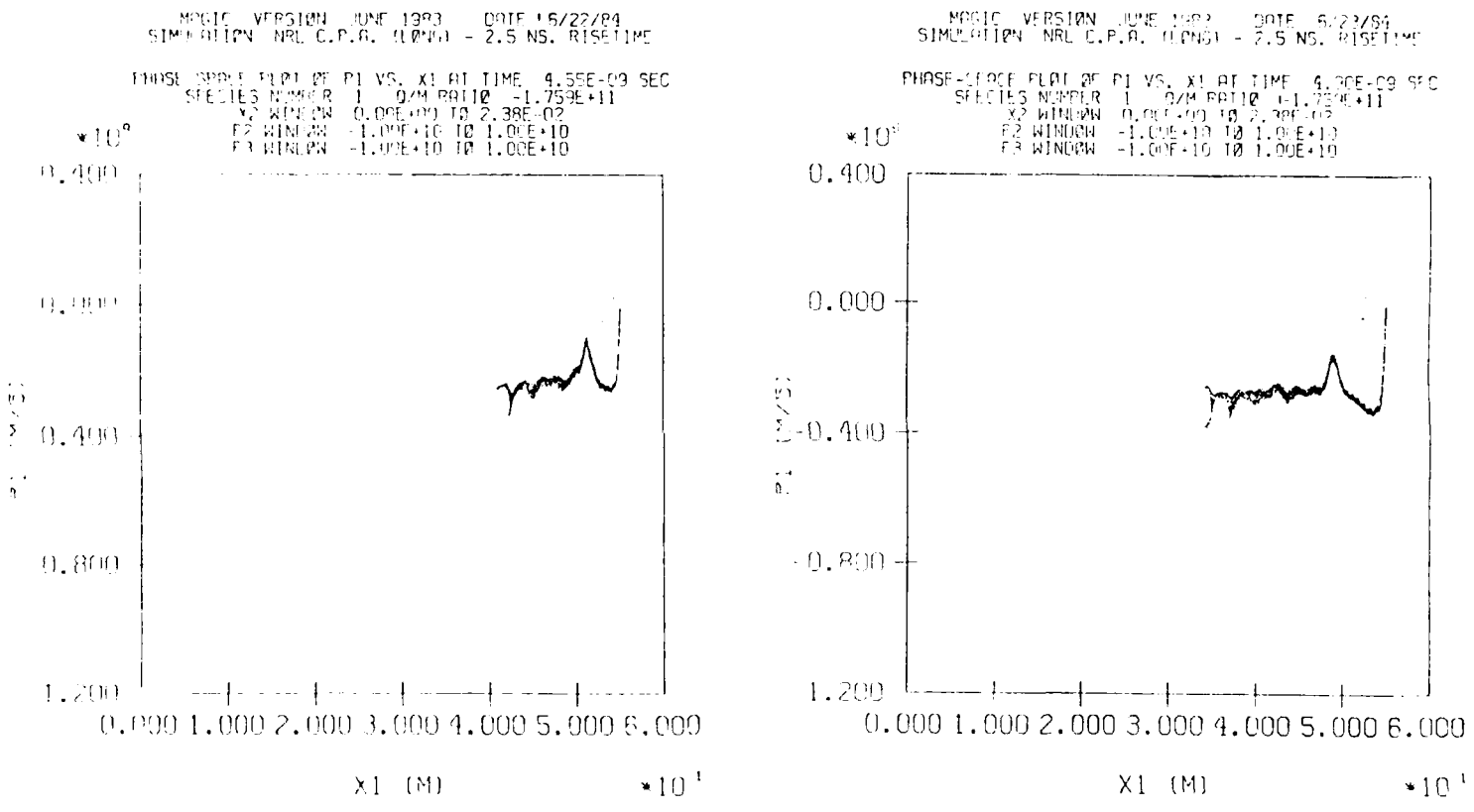

Figure 47. Electron Phase-Space Plots at t = 4.55 nsec (left) and t = 4.90 nsec (right) for the 2.5 nsec Rise-Time Run.

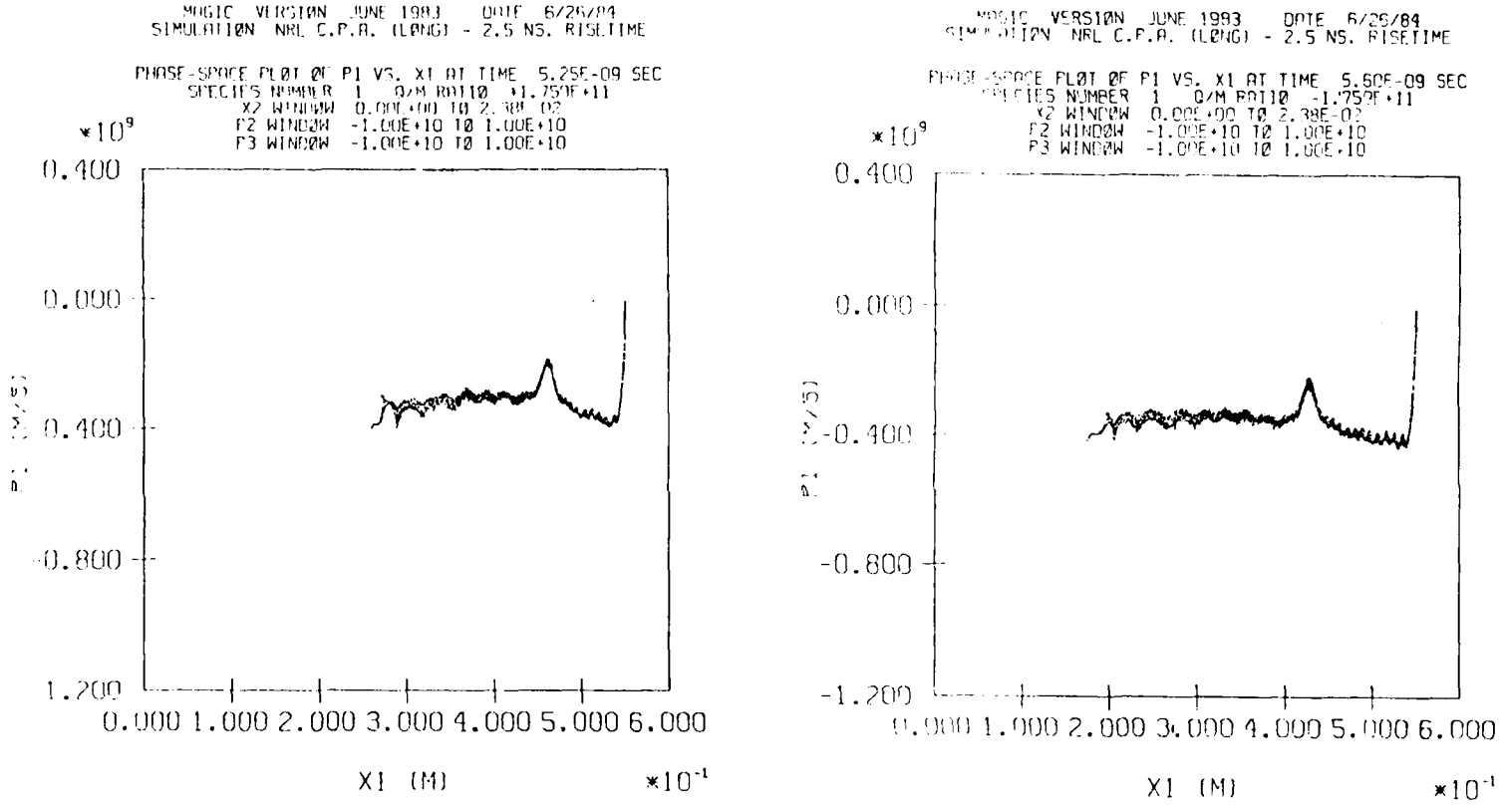

Figure 48. Electron Phase-Space Plots at t = 5.25 nsec (left) and t = 5.60 nsec (right) for the 2.5 nsec Rise-Time Run.

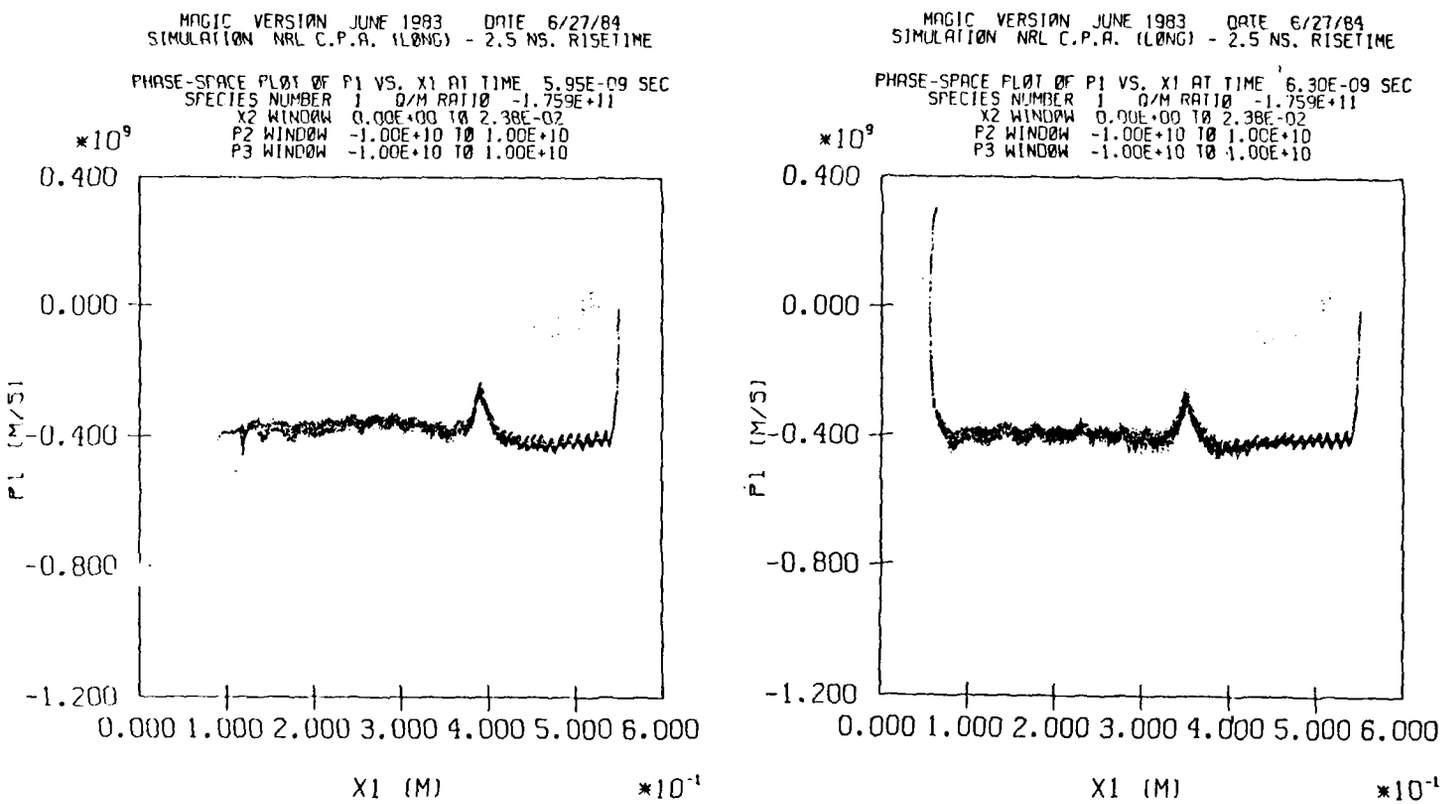

Figure 49. Electron Phase-Space Plots at t = 5.95 nsec (left) and t = 6.30 nsec (right) for the 2.5 nsec Rise-Time Run.

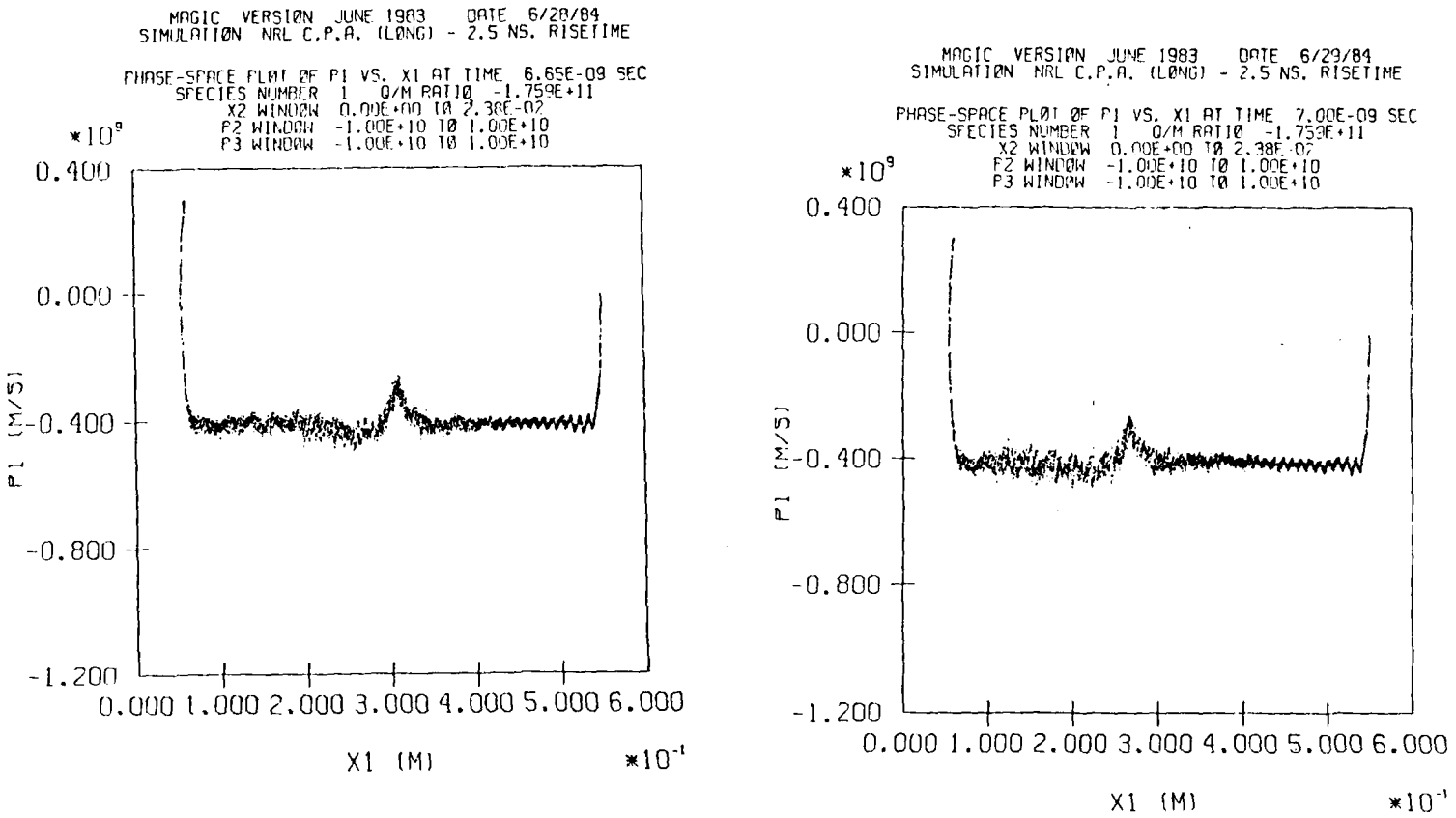

Figure 50. Electron Phase-Space Plots at t = 6.65 nsec (left) and t = 7.00 nsec (right) for the 2.5 nsec Rise-Time Run.

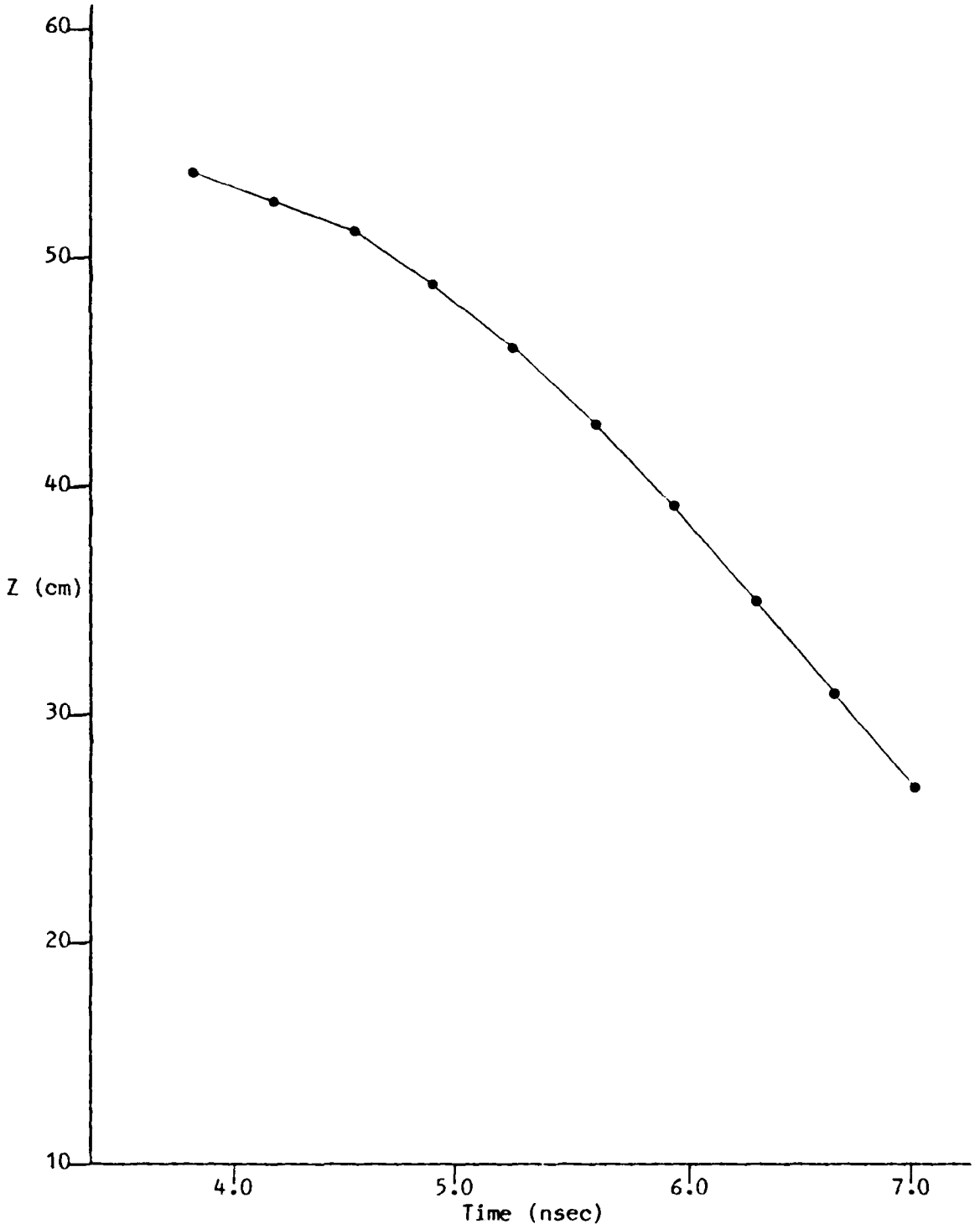

Figure 51. Plot of Axial Position of Peak of Phase-Space "Bump" as a Function of Time for the 2.5 nsec Rise-Time Run.

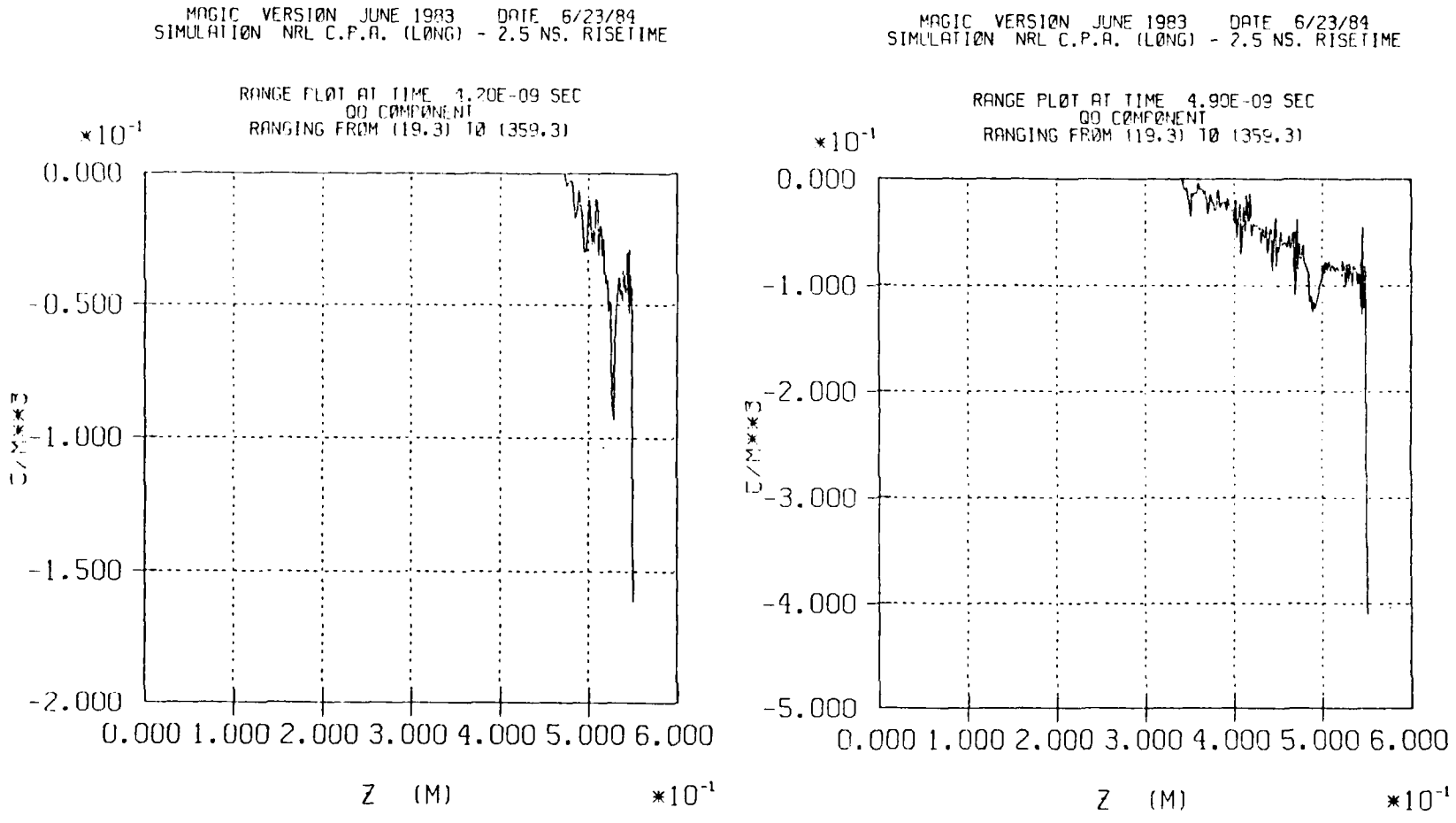

Figure 52. Axial Profiles of Electron Charge Density at a Radius of 0.12 cm at t = 4.2 nsec (left) and t = 4.9 nsec (right) for the 2.5 nsec Rise-Time Run.

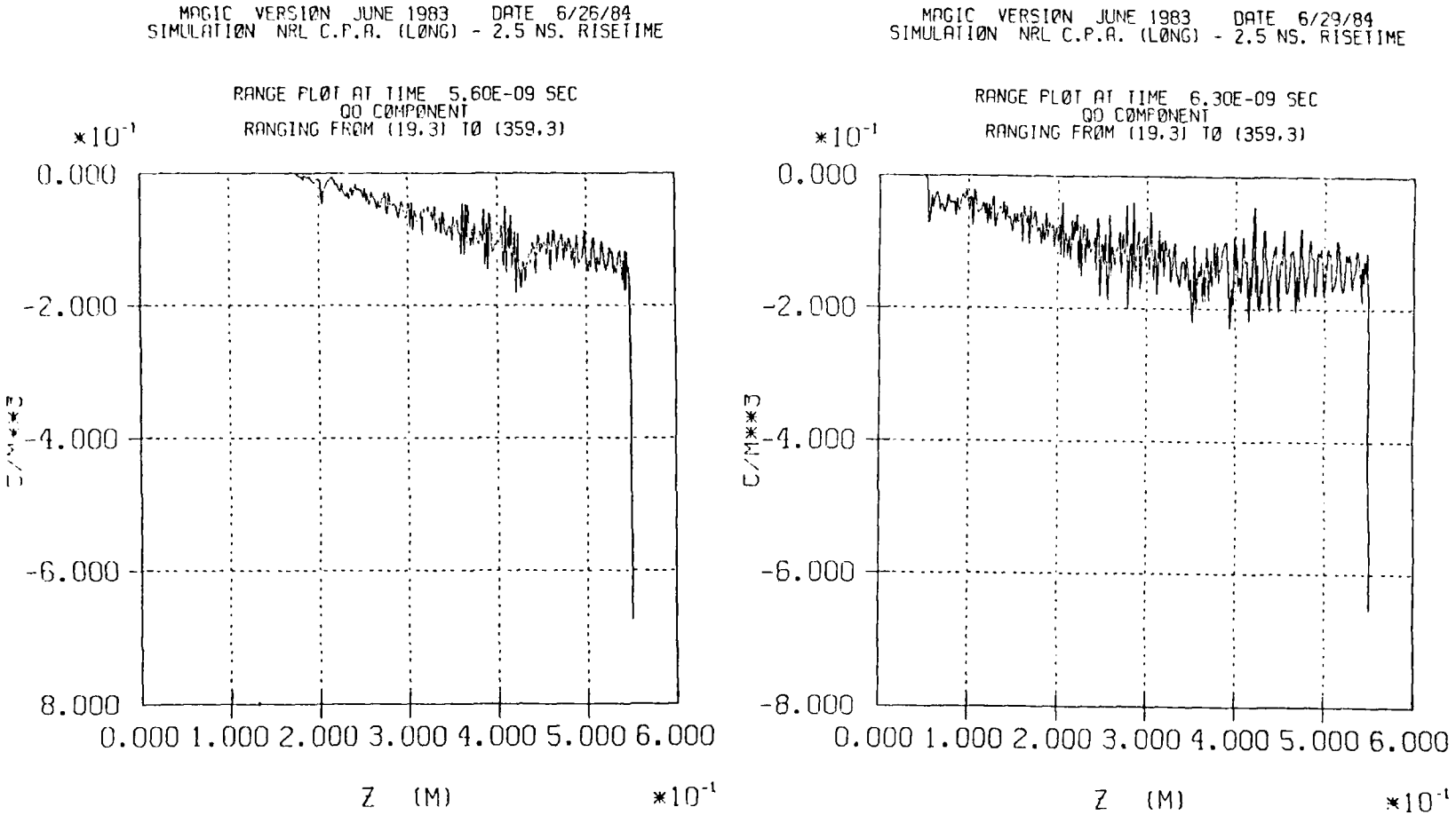

Figure 53. Axial Profiles of Electron Charge Density at a Radius of 0.12 cm at t = 5.6 nsec (left) and t = 6.3 nsec (right) for the 2.5 nsec Rise-Time Run.

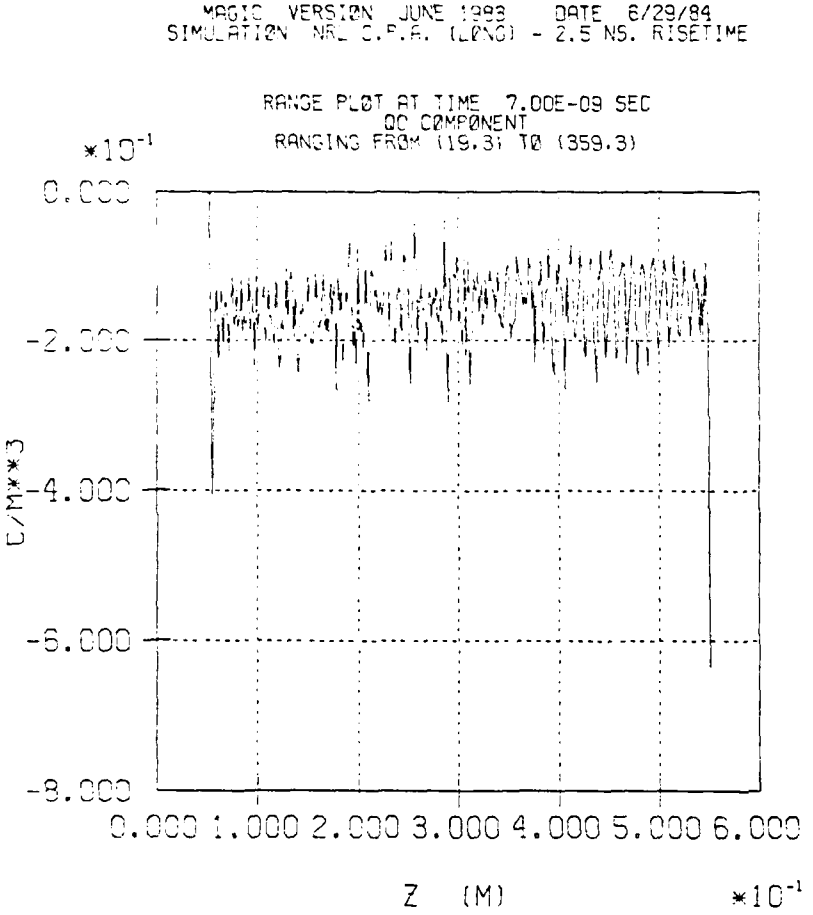

Figure 54. Axial Profile of Electron Charge Density at a Radius of 0.12 cm at t = 7.0 nsec for the 2.5 nsec Rise-Time Run.

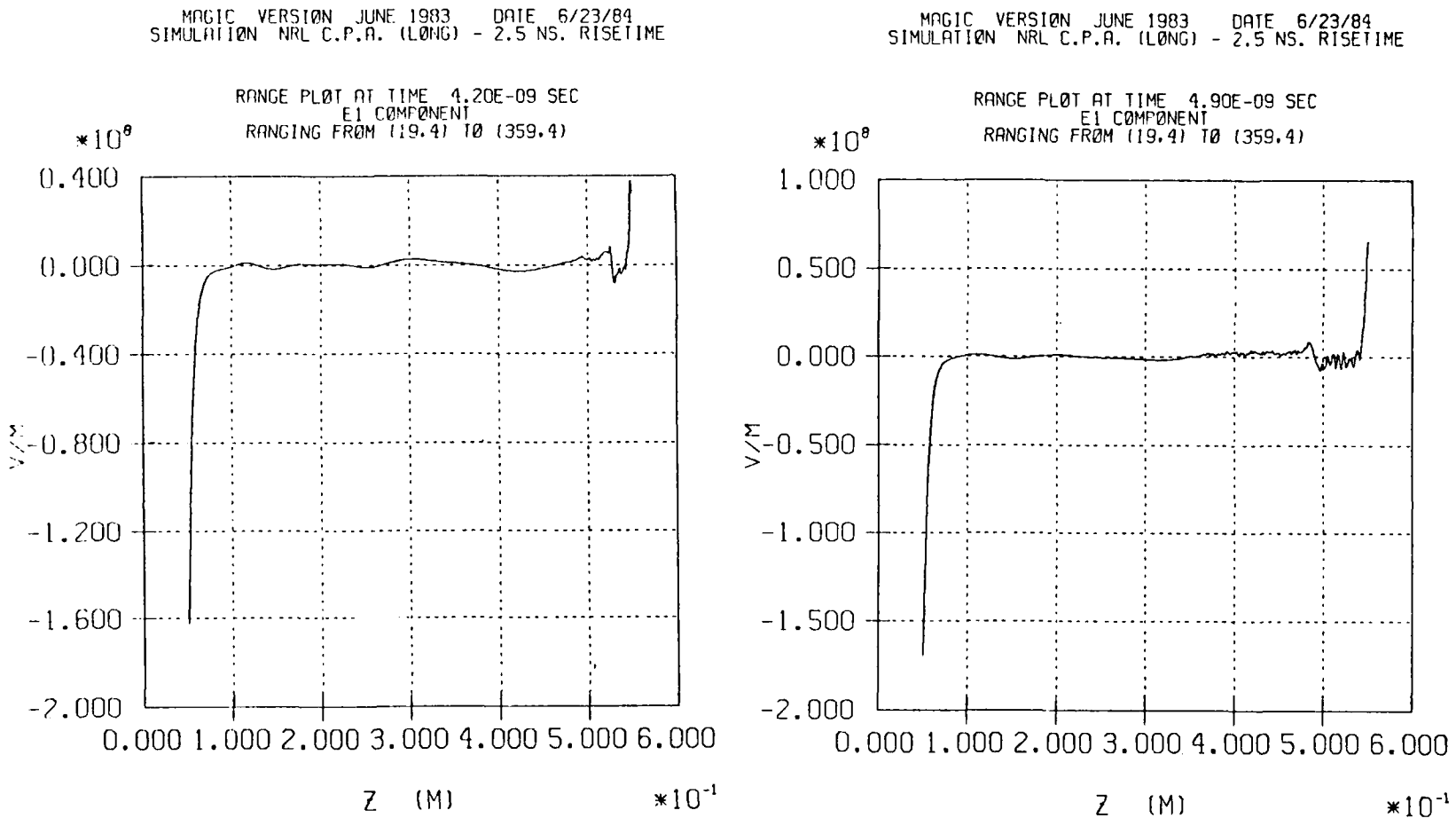

Figure 55. Axial Profiles of E_z at a Radius of 0.2 cm at t = 4.2 nsec (left) and t = 4.9 nsec (right) for the 2.5 nsec Rise-Time Run.

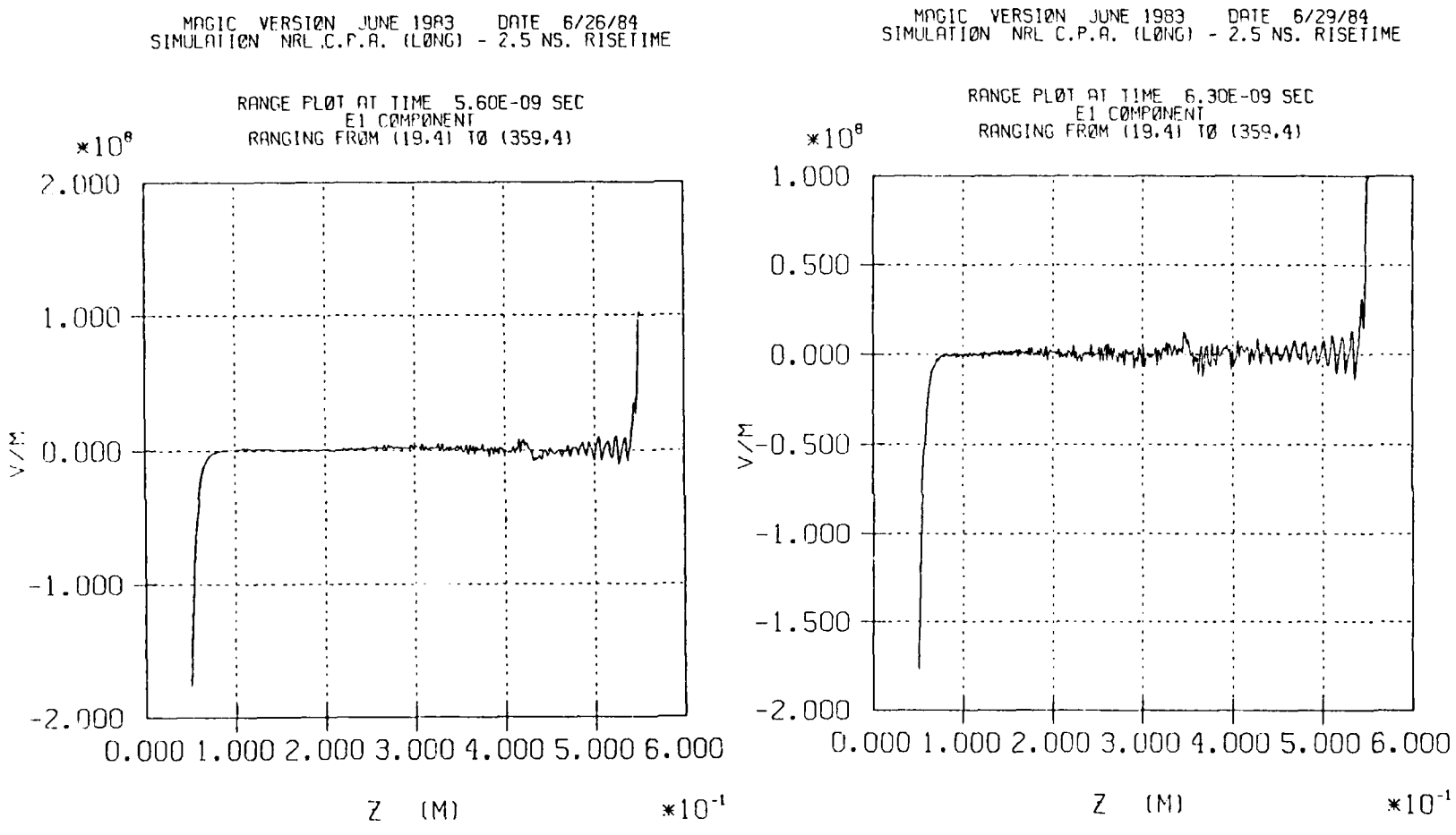

Figure 56. Axial Profiles of E_z at a Radius of 0.2 cm at t = 5.6 nsec (left) and t = 6.3 nsec (right) for the 2.5 nsec Rise-Time Run.

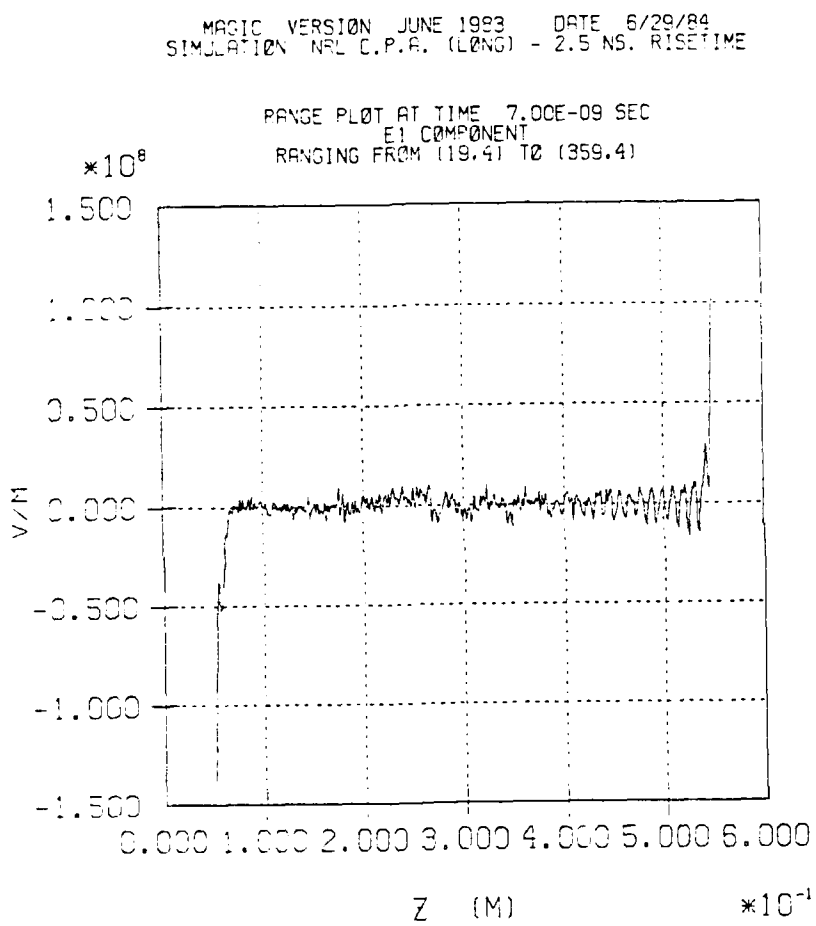

Figure 57. Axial Profile of E_z at a Radius of 0.2 cm at t = 7.0 nsec for the 2.5 nsec Rise-Time Run.

A detailed study of this soliton behavior would be a fascinating topic by itself. Unfortunately, it lies beyond the scope of this present work.

SECTION 5

CONCLUSIONS

With this last series of long rise-time runs in an improved geometry, this simulation effort in support of the NRL CPA assessment program comes to an end. The code results have delivered a consistent message that the central beam of the CPA test device should propagate almost the entire length of the drift tube with a reduced, but still healthy 1 to 2 kA of current. Charge density anomalies may develop within the body of the beam, but these never threaten to shut the beam off.

The curious electron density clamp which was observed to form and then propagate within the central beam in the 2.5 nsec rise-time run seems to merit further study on its own.

SECTION 6

REFERENCES

1. Moshe Friedman, "A New Collective Particle Accelerator," NRL Memorandum Report 3724, February 1978.

2. Moshe Friedman, "The C.P.A.," IEEE Transactions on Nuclear Science, NS-26, No. 3, June 1979.

3. Robert J. Barker, "Numerical Simulations of the NRL Collective Particle Accelerator," Mission Research Corporation Report MRC/WDC-R-073, November 1983.

4. Moshe Friedman, private communication.

5. B. Goplen, R. E. Clark, and J. McDonald, "Users' Manual for MAGIC/ Version - July 1981," Mission Research Corporation Report, MRC/WDC-R016, July 1981.

6. B. Goplen, "Boundary Conditions for MAGIC," Mission Research Corporation Report, MRC/WDC-R-019, presented at the 23rd Annual APS Plasma Physics Division Meeting of 12-16 October 1981.

7. B. B. Godfrey and B. Goplen, "Practical Evaluation of Time-Biased Electromagnetic Field Algorithms for Plasma Simulations," AMRC-N-146, presented at the 22nd Annual APS Plasma Physics Division Meeting of 10-14 November 1980.

8 B. Goplen, R. E. Clark, and S. J. Flint, "Geometrical Effects in Magnetically Insulated Power Transmission Lines," Mission Research Corporation Report, MRC/WDC-R-001, April 1979.

9. W. A. Seidler, B. Goplen, and W. Thomas, "Investigation of Enhanced Electron Current Transport in a Dielectric Lined Cavity," IEEE Transactions of Nuclear Science, NS-26, No. 6, December 1979.

10. D. B. Seidel, B. Goplen, and J. P. VanDevender, "Simulation of Power Flow in Magnetically Insulated Convolutes for Pulsed Modular Accelerators," presented at the 14th Pulse Power Modulator Symposium, 3-5 June 1980.

11. B. B. Godfrey, Proceedings of the Ninth Conference on Numerical Simulation of Plasmas, Paper OD-4, 1980.

12. B. Goplen, "Boundary Conditions for MAGIC," Mission Research Corporation Report, MRC/WDC-R-019, October 1981.

13. Sandia Report SAND82-0192, February 1982.

14. R. E. Clark, W. M. Bollen, J. McDonald, and B. Goplen, "Simulation of Microwave Devices Using MAGIC," Mission Research Corporation Report, MRC/WDC-R-040, November 1982.

AD-A153 583 FURTHER STUDIES OF THE NRL COLLECTIVE PARTICLE ACCELERATOR VIA NUMERICAL..(U) MISSION RESEARCH CORP ALEXANDRIA VA R J BARKER AUG 84 MRC/WDC-R-086 2/2

UNCLASSIFIED N00014-84-C-2136 F/G 9/2 NL

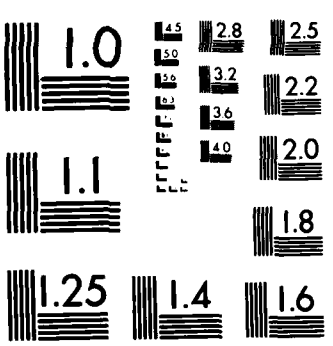

APPENDIX

THE MAGIC SIMULATION CODE

MAGIC (MAGnetic Insulation Code) is a computer code designed to simulate self-consistent (nonlinear) processes typically associated with pulsed power systems. Examples include power transport, beam propagation, magnetic insulation, diode operation, microwave tube design, etc. MAGIC is an intermediate size code (about 20,000 statements), and is highly optimized both for user efficiency and computational efficiency. It was developed by MRC under contract to Sandia National Laboratories for use in their light ion and electron fusion program. MAGIC is now entering the fifth year of development as a production code. There is an active user group, supported by an extensive User's Manual and active consultation with the authors. The code is available on Cyber 176, Cray-1, and VAX-780 computers. The code has been documented extensively (References 5-7) and many results have been published (e.g., References 8-10); the discussion which follows will deal with the code's options and features which are crucial to successful simulation of relativistic electron beam devices.

Conducting surfaces can be imposed arbitrarily to exactly duplicate structural geometry in any of four coordinate systems (cartesian, cylindrical R-Z, cylindrical R-θ, and spherical). Periodic and mirror symmetry conditions, which apply to both fields and particles, can be imposed on the ends of a computational region. MAGIC has the capability of linking one-dimensional transmission lines to the two-dimensional simulation; this provides the means to model the interior structure of devices, which are plasma free. Such lines can be truncated with a "lookback" model which allows reflected waves to escape from the system.

Externally applied (static) magnetic fields can be imposed in any direction and can be a function of the spatial coordinates. (The dynamic magnetic field adds linearly to the static field to affect particle motion.) The functional form of electric fields from a static voltage can be determined initially from the solution of Poisson's

equation. These fields can be imposed by means of an external circuit to represent a power pulse propagating in the third dimension. Either the steady-state or the time dependent case can be represented. In either case, the dynamic fields again add linearly to the static fields to affect particle motion.

The emission of electrons or ions can be simulated over arbitrary predetermined conductor surfaces by application of Poisson's equation to surface cells, i.e., cells immediately adjacent to the electrode surface. The external normal electric field and charge existing within the cell are used to determine the surface normal field. To obey Child-Langmuir physics, this field should vanish. In MAGIC, enough charge is created near the surface to force this field to vanish (if the field has the wrong sign, no charge is created). This charge is normally broken up into a small number of macroparticles, which are then distributed randomly along the cell surface. A small spatial distribution in the normal direction provides effective temporal separation. The surface force algorithm is also altered to take actual surface charge into account.

This very simple model has seen effective use in a variety of applications. It has been validated by comparison with one-dimensional Child-Langmuir analysis. The primary requirement to achieve accuracy is fine normal spacing near the surface, and this is easily attained in MAGIC using the nonuniform spacing option. Finally, MAGIC has the capability to simultaneously model up to 10 particle species, which may be useful if positive ions are believed to play any role.

Two standard explicit (centered-difference and time-symmetric) and one novel implicit (time-biased) electromagnetic field solving algorithms are available as user options in the code. Particular mention should be made of the implicit solver since this is the one actually employed in these simulations. The basic idea behind this algorithm is very similar to the notion behind predictor-corrector. That is, spatial gradients of a magnetic field at several points in time are used to

estimate the time rate of change of the electric field. If these several points in time include advanced (unknown) magnetic fields, then the algorithm is implicit. In MAGIC, the implicit equations are solved by repetition for a single time step, making use of relaxation coefficients to improve convergence. This algorithm was originally developed by B. Godfrey of MRC (Reference 11), and has been extensively tested by use (e.g., Reference 7) in applications involving magnetic insulation.

The primary advantages of the time-biased over standard centered difference methods are that (1) high frequency noise is greatly reduced, (2) certain numerical instabilities are damped, and (3) the Courant criterion is usually relaxed. On this last point, the penalty of iterative solution outweighs the advantage of larger time steps. That is, the time-biased algorithm is always more expensive computationally. However, use of this algorithm (along with temporal filtering of magnetic forces) has virtually eliminated the debilitating wave trapping normally encountered in magnetic insulation type problems (see Reference 8 for a discussion of wave trapping).

Local charge conservation is another algorithm which is essential to a good representation of intense particle beam devices. The majority of PIC codes conserve charge only in the global sense - that is, system charge equals charge created minus charge destroyed. In many applications, the fluctuations in individual cell fields (due to various charge weighting schemes) are small compared with fields themselves. In such applications, the global conservation schemes are adequate. In beam-diode problems, however, the accumulated charge creation and destruction typically greatly exceed the system charge. In this case, the field fluctuations can exceed the magnitude of the fields themselves. This proceeds linearly with time in a simulation, culminating in obviously catastrophic results.

This effect is eliminated if charge conservation is ensured locally (cell-by-cell). There are several approaches possible to achieve this.

For example, some electromagnetic PIC codes periodically during the simulation (say, every 50 time steps) will solve Poisson's equation, and use the results to "correct" the local conservation directly through the current density algorithm. By contrast, MAGIC relies on consideration of multiple, orthogonal motions of particles and exact enforcement of the continuity equation in the direction of motion. Thus, local conservation is provided automatically by the current density algorithm in MAGIC, eliminating the need for subsequent, periodic "corrections".

MAGIC has been used to simulate too many devices to conveniently list them all here. Still, it is useful to mention several examples which illustrate the power and feasibility of the code. The first is explained in Reference 12. MAGIC was there used to simulate the effect on electron beam transmission of adding a dielectric liner to the cylindrical outer wall of an experimental drift tube cavity. The second example relates to an extensive series of foilless diode simulations conducted with MAGIC by Sandia National Laboratories (Reference 13). Some 22,000 macroelectrons were used in these runs which tested the effects of different values of an applied, uniform, axial magnetic field, B_0. The final example presented in Reference 14 looked at the problem of electron leakage in the NRL hybrid-inverted coaxial magnetron.

END

FILMED

6-85

DTIC